
# The alumino-magnesiothermic production of NiB master alloy in a D.C. arc furnace

Motshele Mansell Mafiri

A dissertation submitted to the Faculty of Engineering and the Built Environment, University of the Witwatersrand, in fulfilment for the degree of Master of Science in Engineering.

Johannesburg, 2015

# Contents

## DECLARATION

I declare that this dissertation is my own unaided work. It is being submitted to the Degree of Master of Science to the University of the Witwatersrand, Johannesburg. It has not been submitted before any degree or examination to any other University.

……..

(Signature of Candidate)

……day of ……year…….

# ABSTRACT

The investigation of Nickel Boron (NiB) alloy production was undertaken in a D.C. arc furnace in an attempt to yield an alloy containing a minimum of 15% boron (B). The aluminothermic, magnesiothermic and the dual reduction with aluminium and magnesium (alumino-magnesiothermic) reduction of boron oxide ($B_2O_3$) production methods were investigated. The impact of varying the reductant mass was investigated. The alloys produced by the aluminothermic, magnesiothermic and alumino-magnesiothermic production methods were analyzed in comparison to NiB master alloy B specification. The maximum B content of the aluminothermic reduction process was found to be 7.59 %. This result was obtained from the reaction which reached a maximum process temperature of 1666°C. The input $B_2O_3$ in the feed was at 15% excess over stoichiometry. The aluminothermic runs were solely fluxed with lime (CaO). In the magnesiothermic experiments, excess input $B_2O_3$ was used as flux. The maximum B content obtained for this production method was found to be 11.82%, where 15% excess reductant magnesium was used. Moreover the maximum recorded operating temperature reached was 1779°C. The alumina-magnesiothermic production method yielded a maximum of 10.88% B content in the alloy; at a peak operating temperature of 1796°C and 15% excess input $B_2O_3$. The process was fluxed with silica ($SiO_2$).

It was also found that excess $B_2O_3$ increased the B yield.

The alloys produced by the aluminothermic and alumino-magnesiothermic processes were contaminated with aluminium and silicon, respectively.

Further research is required to determine the thermodynamic interaction of the species in the liquid systems investigated.

# ACKNOWLEDGEMENTS

I acknowledge Dr P. Holmes for the financial assistance and facilities for this work, Messrs' I. Ball and F. van Der Berg for the technical assistance. I am grateful for Messrs' D. Munzhelele and F. Dhladhla for assisting in operating the furnace. Prof. Kucukkaragoz for supervision. I acknowledge Dave Onderstall for supplying the furnace refractory.

# LIST OF FIGURES

# LIST OF TABLES

# LIST OF SYMBOLS

| | |
|---|---|
| $\Delta G$ | Gibbs Free Energy Change (kJ/mol) |
| $\Delta H°_{298}$ | Standard enthalpy Change at 25℃ or 298K |
| *M* | Reductant Metal |
| *M'O* | Metal/metalloid oxide |
| NiMg | Magnesium-Nickel alloy |
| $a_{(m)}$ | Thermodynamic activity of species m |
| p° | vapour pressure of pure component |
| p | vapour pressure |
| *x,y,z* | Stoichiometric co-efficients |

# NOMENCLATURE

- NiB: Nickel Boron alloy of boron content greater than 15 weight%.
- Aluminothermic: utilization of aluminium (Al) as a reductant.
- Magnesiothermic: use of magnesium (Mg) as a reductant
- Alumino-magnesiothermic: use of aluminium (Al) and magnesium (Mg) simultaneously
- Passivate(d): minimization of reactivity of generally reactive materials.
- %stoichiometry: level of excess or lean over the stoichiometric requirement
- Autothermic: phenomenon of a reaction to self-propagate without additional external heat input, post ignition.
- Yield: recovery of element to the alloy
- Reaction Booster: generally a highly oxidic and reactive compound which when reduced releases large quantity of heat energy that can provide addition heat to the main reactions.

# 1 INTRODUCTION

Nickel Boron (NiB) alloy for the welding and hardfacing industry is produced by mainly two methods, the carbothermic and aluminothermic processes. The carbothermic production of NiB alloy results in large volumes of $CO_2$ emissions. The aluminothermic process can cause considerable aluminium (Al) contamination of the final alloy produced. Magnesium (Mg) from NiMg alloy fines can be used to improve the thermodynamics of the aluminothermic process. According to the Ellingham Diagram, the standard Gibbs free energy values of the magnesiothermic reduction of Boron Oxide ($B_2O_3$) are more thermodynamically favourable than the aluminothermic reduction of $B_2O_3$.

In industry NiB and NiMg are used as master alloys. Master alloys are alloys used as additives in the preparation of complex alloys. These alloys generally contain a carrier element and other elements which may be incongruous to direct melt addition. Thus in the case of NiB and NiMg master alloys, nickel (Ni) is a carrier element for boron (B) and Mg.

NiB master alloy should typically contain 15-20% B, 80-85% Ni and the balance of permissible contaminants. Hardfacing alloys contain 3-6% B, Ni and other elements. Hardfacing alloys are normally produced by using master alloys of higher B content.

NiB master alloy is primarily used in these alloys for the preparation of complex hardfacing alloys. The B in hardfacing alloys serves to increases the hardness of the final alloy.

The conventional method of producing hardfacing alloys is by melting the low melting point master alloy and alloying it with other requisite elements. The relatively low melting point of NiB (between 1000-1200℃) assists in the production of such alloys**.** The addition of pure B directly into the melt was not considered due to the following limiting factors; i. cost and ii. reactivity.

i. The cost of 90% pure B is approximately US$ 100/kg and higher purity B costs in excess of US$ 1000/kg. Comparatively, the average cost of $B_2O_3$ is US$ 600/tonne.
ii. Furthermore; B is unstable at high temperatures reached in furnaces under normal practice. The melting point of NiB is 500℃ higher than the ignition temperature of pure B. B burns in air to form $B_2O_3$ at approximately 500℃. Such oxidation of B would result in excessive losses of expensive B to the slag.

It is evident from these aforementioned limitations that $B_2O_3$ is a cheaper and more stable source of B units for the production of NiB master alloy.

The alloying of B with Ni results in two beneficial properties:

1. The reduction of the alloy melting point as can be seen on the B-Ni phase diagram (Figure 1).
2. The carrying and stabilizing of the hardener element (B) from oxidation.

These properties assist in lowering the practical furnace operating temperature and improve B yields to the melt.

## 1.1 Industrial Production Methods of NiB Master Alloy

There are two current industrial production methods of NiB, [1] the Carbothermic and [2] Aluminothermic reduction of $B_2O_3$ or $H_3BO_3$ in the presence of Ni and or NiO in an electric furnace.

Baudis and Fichte in *Boron and Boron Alloys* showed that the carbothermic process requires high temperatures and is therefore undertaken in electric arc furnace. Table 1 shows the typical chemical composition of the NiB alloy produced in industry (1).

**Table 1: Typical chemical composition of NiB produced by the carbothermic process**

| Elements | Content (%) |
|---|---|
| Ni | Balance |
| B | 15-18 |
| C | 0.15 max |
| Al | 0.20 max |

With the increased environmental concerns, primarily on carbon emissions, the carbothermic process with its high energy input is increasingly becoming an unfavourable/ non-preferable production method.

The alternative industrial production method uses Al as a reducing agent. This process is known as the aluminothermic production of NiB. Unlike the carbothermic reduction of $B_2O_3$, the aluminothermic reduction of $B_2O_3$ is exothermic. Albeit this process is exothermic, it is

not autothermic/self-propagating. Therefore, the process is undertaken in an electric arc furnace in order to supplement the energy requirement for good slag metal separation (1). The use of recycled Al in this production method has the potential of reducing the environmental impact of the reaction procedure. However, utilizing recycled Al risks the introduction of inherent contaminants to the final alloy.

The benefit of the exothermic nature of the aluminothermic process results is lower power consumption as compared to the carbothermic processing route. However, the major disadvantage of the aluminothermic process is that it can cause high Al contamination in the final NiB alloy. Al is a deleterious element in hardfacing applications. High Al content alloys would thus require subsequent refining. This generally increases production costs as well as process complexity.

## 1.2 Investigation of Practical use of Mg in NiB Production

The aluminothermic process previously mentioned is an industrial NiB production method. This production method was compared with the possibility of replacing all or a fraction of Al reductant with Mg. These processes are termed the magnesiothermic and the alumino-magnesiothermic processes. The processes were investigated using NiMg master alloy fines. Supplementary Mg was investigated in the magnesiothermic process.

NiMg master alloys which are used in the iron and steel foundry industry generally contain 5-20% Mg. These alloys are used for ductile iron treatment where NiMg is used to promote graphite nodularization. Due to the reactivity of dissolved Mg, the NiMg alloys are introduced to specialized steel melts as sulphur and oxygen scavengers.

A problem of using pure Mg is that, Mg has the propensity to flare or burn in air at high temperatures. This limitation is overcome by using stable NiMg fines. The availability of NiMg master alloy fines and the passive nature of the associated Mg motivated the investigation of the alumino-magnesiothermic production route.

## 1.3 Report Structure

1. Chapter 1 is an introductory statement that details the purpose of this report.

2. The research objectives are shown in Chapter 2.

3 .Information of the literature survey undertaken for current NiB production methods is discussed in Chapter 3. In this chapter the theoretical principles obtained from literature are presented. This includes the thermochemical and thermodynamic properties of the production processes investigated.

4. Chapter 4 details the experimental apparatus and procedure followed. In addition, the input amounts of the stoichiometric charges are presented in this chapter.

5. The results of the various experiments undertaken are presented and discussed in this chapter.

6. The results of the experiments are discussed with respect to slag metal equilibria in Chapter 6. Moreover practical considerations of this work are presented in this chapter.

7. The conclusions derived from the results of this research work are mentioned in Chapter 7.

8. Recommendations regarding further experimentation are purported in Chapter 8.

9. A list of references cited in this work is attached in Chapter 9.

10. The additional information regarding the raw materials used is appended.

# 2 RESEARCH OBJECTIVES

## 2.1 To investigate the thermodynamics of the system for the aluminothermic, magnesiothermic and alumino-magnesiothermic:

- Generating an Ellingham Diagram reflecting the Al, Mg and other reductants with respect to the $B_2O_3$ formation line.
- Calculating the heat requirement for reaction self-propagation.

## 2.2 To determine the possible pyrometallurgical processing route by pilot plant scale experiments by:

- Comparing the results of the NiB production experiments with particular respect to B and Ni recovery.

## 2.3 Research Limitations

The investigation was undertaken in pyrometallurgical pilot plant environment not in controlled laboratory conditions. The research does not give experimental data about the reaction kinetics of the processes investigated rather, the possibility of NiB production with regard to thermodynamic aspects. Raw materials used were of metallurgical grade. The specification of the reagents used is presented in the Appendix.

# 3 LITERATURE REVIEW

The annual world usage market for NiB master alloy for the welding and hardfacing industry is reported to be approximately 800 tonnes per annum (Private Communication). The world NiB market is supplied by various companies which have not publicly disclosed detailed production procedures and or parameters.

The relevant information about the nature of NiB production process was compiled from previous applicable works available in literature. It was determined that the carbothermic and aluminothermic reduction of boron oxide ($B_2O_3$)and boric acid ($H_3BO_3$) is mainly used to produce NiB with a B content ranging from 15-20% in a D.C. arc furnace (1). Information pertaining strictly to the NiB production process is scant although the relevant Ferroboron (FeB) production methods are detailed in literature. In Ullmann's Encyclopaedia of Industrial Chemistry, Baudis and Fichte report comprehensively on the carbothermic and aluminothermic FeB production methods.

The carbothermic production of FeB from pig iron swarf and boric acid ($H_3BO_3$) to produce an alloy containing 16-18% B, 0.03-0.06%C and 0.03-0.06%Al after a final oxygen blow is reported to have a B recovery between 60-65%. Evidently, the final oxygen blow refines the alloy and concomitantly adding complexity to the production process. Additionally, this production process is energy intensive at reported power consumption of 16500kWh/tonne alloy produced (1).

The aluminothermic production of FeB as reported by Baudis and Fichte is undertaken by two distinct batch wise methods: the autothermic and the electro-aluminothermic processes. In the autothermic processes, batches of $Fe_2O_3$, $B_2O_3$ /$H_3BO_3$ and Al are mixed, ignited and reacted in a refractory lined pot. The electro-aluminothermic processes replace the $Fe_2O_3$ with iron ore of unknown chemical specification and use similar reagents and CaO as flux. This method is up to 10 times less energy intensive as the carbothermic process. The reported power consumption of the electro-aluminothermic process ranges from 940-1800kWh/tonne of FeB produced.

In the same work, it was reported that the metallothermic principles for the production of FeB and NiB are similar. The variations between the aluminothermic FeB and NiB processes is the form of Ni and Fe used. Ni in these aluminothermic processes is normally charged as pure

Ni not NiO in an attempt to minimize Al consumption. The use of NiO as a source for Ni units would require additional Al that would NiO to Ni.

The Ni-B binary phase diagram, Figure 1 (2), shows that the 15-20% B range is selected for the relatively low liquidus temperature range. This low melting temperature allows for uncomplicated preparation for hardfacing alloys. Additionally, FeB melts at a similar temperature as NiB master alloy. But, in general FeB is used as master alloy in the steel industry and NiB is used as master alloy in the hardfacing and welding industry where Ni is a requisite element.

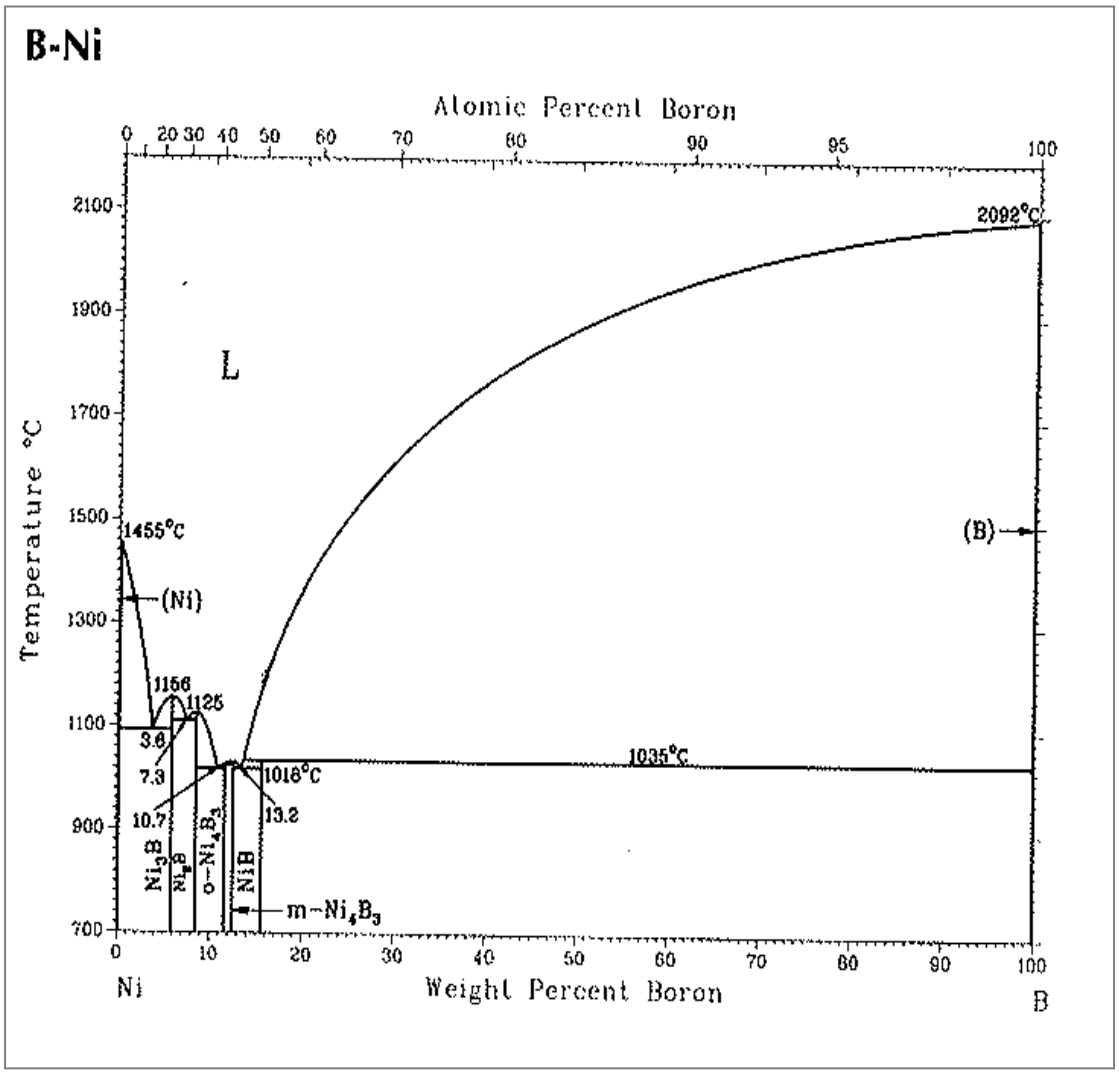


**Figure 1: Ni-B Phase Diagram**

## 3.1 Carbothermic Production

The carbothermic reduction of metal oxides is generally the production method for metals and their alloys. Alloys such as ferrosilicon, ferromanganese and high carbon ferrochrome are typically produced by the carbothermic process. Specialist alloys such as ferroboron (FeB) and NiB are also commercially produced by the carbothermic process. The carbothermic reduction of metal oxides is commonly undertaken by the CO that forms when carbon is oxidized at sufficiently high temperatures.

### 3.1.1 Basic Thermodynamics of Carbothermic Reduction

The Ellingham Diagram presented in Figure 2 is a plot of the standard free energy change (ΔG°) with temperature for common metal oxides. The Gibbs free energy of a reaction is a measure of the thermodynamic driving force that makes a reaction occurs. A positive ΔG indicates that the reaction cannot proceed spontaneously without external inputs, while a negative ΔG shows that spontaneous reaction may occur (3). Ellingham Diagrams may also be constructed for chlorides, sulphides and halides. As may be seen on the Ellingham Diagram of common oxides, most of the lines slope upwards. The reason for this trend is that the standard Gibbs free energy change is related to the standard entropy (randomness) change (ΔS°) of the reaction as depicted in the equation:

$$\Delta G^\circ = \Delta H^\circ{}_T - T\Delta S^\circ{}_T$$

A similar equation may be presented for non-standard states and the terms thereof do not contain the ° superscript. The reaction of a solid (ordered state) with oxygen gas ($O_2$) to form an oxide produces the standard heat of reaction (ΔH°).If the oxide formed is in the condensed phase, either liquid or solid, the standard entropy change is normally minimal (ΔS°≈0). The standard entropy change is positive and very large (ΔS° >>0) when the same reaction liberates a gas phase which is highly disordered or random (3). Thus, the reaction of 1 mol $O_2$ gas with solid carbon (C) generates 2 mol of carbon monoxide therefore resulting in a large positive entropy change. This results in the downward slope of the CO formation reaction as depicted on the Ellingham Diagram (Figure 2).

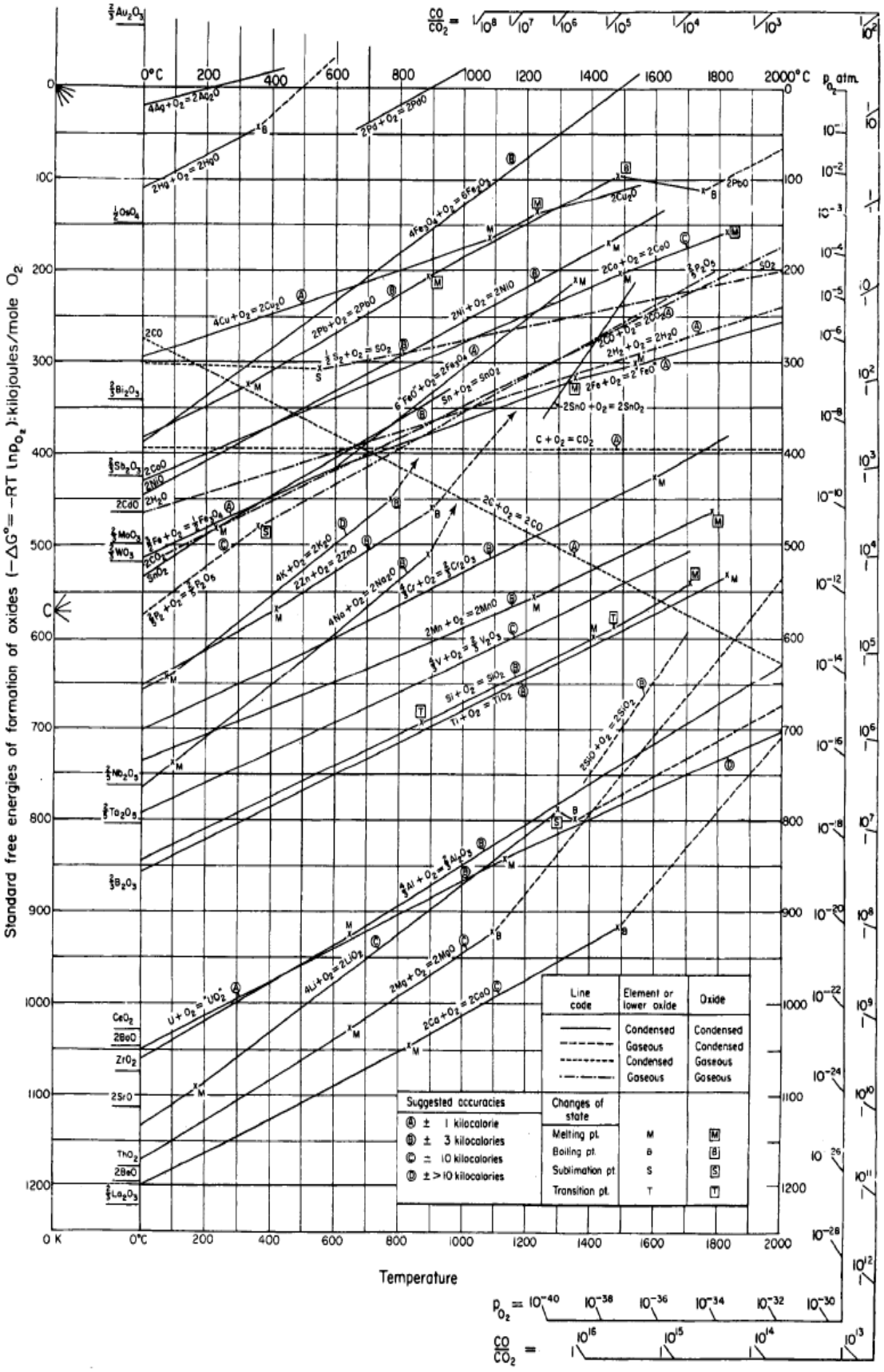


**Figure 2: The Ellingham diagram for metallurgically important oxides**

The CO formation line shows that the stability of CO increases proportionally to temperature. Therefore, once the CO line intersects and goes below the target oxide line, the carbothermic reduction of such oxide may occur. As can be seen on the Ellingham Diagram, most metal oxides can be reduced by carbon provided that adequate temperatures are reached. Moreover carbon reductant may be in the form of inexpensive and readily available coal, coke or low cost wood chips.

### 3.1.2 Heat Energy Requirement

The carbothermic reduction of oxides is typically an endothermic reaction. Therefore, additional heat input is required to promote the reduction reaction. This necessitates either the use of fuels or blowing with air as is the case in the production of iron in blast furnaces. Electric energy is typically used in the carbothermic production of metals and alloys. The electrical energy is converted to heat energy by the use of different plant equipment. Electric arc furnaces, whether of A.C. or D.C configuration, are commonly used for the production of commodity alloys. The carbothermic production of NiB in a D.C. arc furnace has been reported to be commercialized in Europe (4).

### 3.1.3 Furnace Practice and Emissions

Submerged arc smelting is common practice for the carbothermic reduction of metal oxides. A typical A.C. arc furnace operation contains three carbon electrodes submerged into the burden. The electrical energy is converted into heat during arcing. The carbon in the furnace burden reacts with the oxygen in the metal oxide to produce the metal and CO. A classic three- electrode A.C. arc furnace is depicted in Figure 3 (5). D.C. arc furnaces are of similar construction and design however they commonly contain one electrode.

Submerged arc smelting is generally preferred as it minimizes radiant heat losses. Additionally, the rising CO gas pre-reduces the burden above the smelting zone. However, the rising gas may carry particulate matter out of the furnace. It is common practice to control the furnace emissions by implementing dust extraction equipment (5)

The produced metal and slag are removed/ tapped in their respective tapholes. Tapping may be continuous or intermittent depending on production process although; it is more common to tap either slag or metal at predetermined times. (5)

The carbothermic process produces significant CO which is a greenhouse gas. The environmental concerns about $CO_2$ emissions have resulted in increased scrutiny on $CO_2$ generating industries such as pyrometallurgical operations. Increasingly stringent air quality and emissions legislations have resulted in the installation of sophisticated air quality monitoring equipment. The capital expenditure of installing such equipment can result in the closing or relocation of pyrometallurgical plants to areas or countries with less stringent emissions regulations.

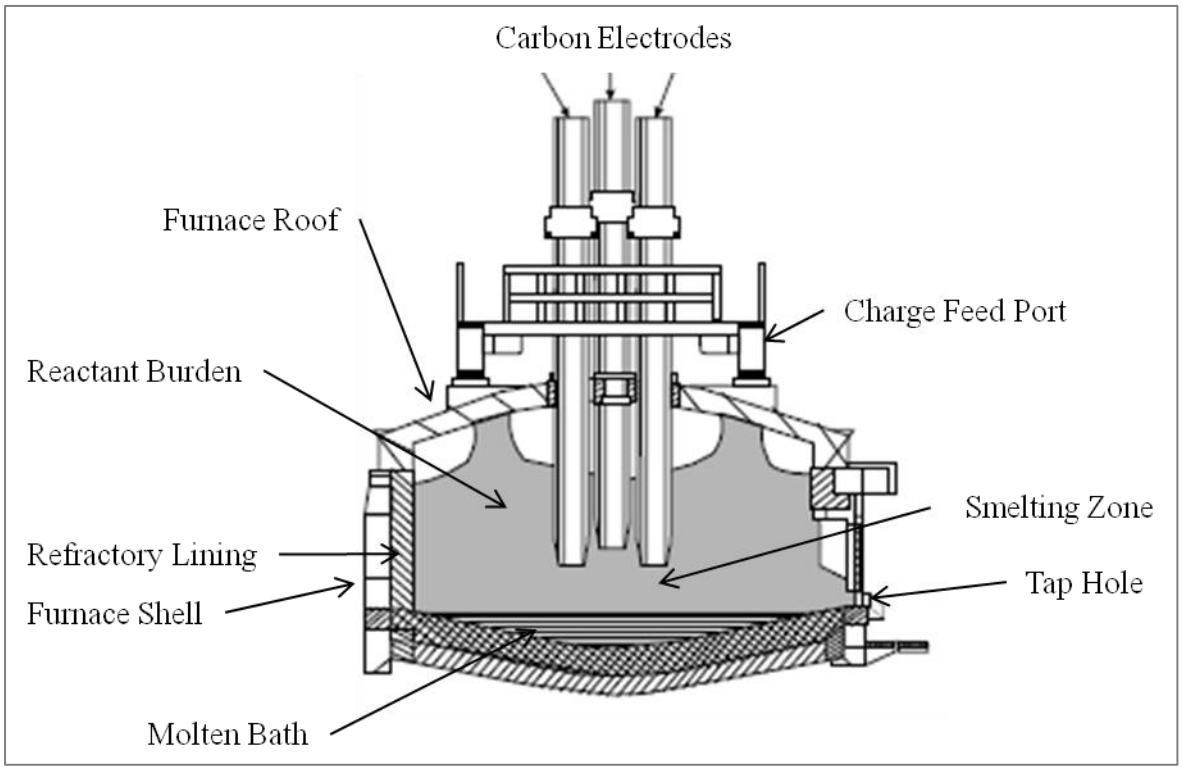


**Figure 3: Typical arc furnace design**

### 3.1.4 Carbide Formation

Under certain conditions, the carbothermic production of metals may produce stable carbides. The refractory carbides may precipitate and build up at the furnace bottom. Silicon carbide (SiC) is commonly produced during the production of ferrosilicon (6). In this process, SiC is further oxidized to eventually produce silicon as depicted in the following reaction:

$$2SiC(s) + SiO_2 = 3Si(l) + 2CO(g)$$

However, it was showed that the above reaction is feasible at 1830°C (6). Therefore high smelting temperatures would be required to dissolve the precipitated carbides. Thus it is important that furnace practice should avoid the formation of carbides.

The carbothermic production of NiB from $B_2O_3$ may form boron carbide ($B_4C$). Nevertheless it has been reported that $B_4C$ oxidizes above 700°C in air (7).This may suggest that in the production of NiB, $B_4C$ formation may not present a significant smelting challenge.

## 3.2 Carbothermic Production of NiB

The industrial carbothermic production of NiB uses $B_2O_3/H_3BO_3$, Ni and carbonaceous materials as input reagents. It is not known what physical form the Ni charged into the furnace is, although it has been indicated that $B_2O_3/H_3BO_3$ is charged as powder and, the carbonaceous material is mainly wood chips (1).

Tasyurek, Alkan and Yucel investigated the carbothermic production of NiB in a small scale 270kVA D.C. arc furnace. The raw materials used were $H_3BO_3$ (99.50% purity), NiO (99.0% purity), and carbon in the form of charcoal and sawdust. The fixed carbon content of the charcoal and sawdust was 65.18% and 10.16%, respectively. The $H_3BO_3$: NiO ratio was fixed at 1.11:1.The charcoal addition was experimented from 12.80-17.80% of the total mass of input charge. The input amount was fixed at 60kg. The mixed charge was loaded and reacted in an open arc furnace. The reaction time was fixed at 1hour and maximum casting temperature achieved was 1182 °C.

The chemical analysis of the produced alloys showed that increasing the fixed carbon in the raw materials yielded high B content of the final alloy (Table 2). Conversely, the recovery of metal/alloy decreased with increasing initial fixed carbon. The minimum and maximum fixed charcoal content of the initial charge were the only reported results, that is the 12.80% and 17.80% fixed carbon of total charge. It is evident that the target 15-20% B content alloy was not attained in the reported experiments. However, it was further reported that an alloy of 18.40% B was recovered. This alloy met the chemical specification but information pertaining to its production was not reported (8).

Tasyurek et al also report that the power consumption of the process was 11.62kWh/kg alloy produced. The power consumption is similar to reported values in industrial FeB production.

This work also highlights the common characteristic of low Al levels in NiB produced by the carbothermic process.

**Table 2: Chemical analysis of alloys (8)**

| | | Composition (wt. %) | | | | | | |
|---|---|---|---|---|---|---|---|---|
| Exp. No | Charcoal/Total Mixture Ratio (%) | Ni | B | Al | S | Si | Fe | C |
| 1 | 12.80 | 90.06 | 9.13 | 0.007 | 0.006 | 0.35 | 0.26 | 0.07 |
| 2 | 17.80 | 85.25 | 13.76 | 0.280 | 0.003 | 0.23 | 0.33 | 0.06 |

Tasyurek et al further determined the composition profile of the alloys produced. The B content of the alloys was reported with respect to furnace depth. The most probable chemical reactions were deduced from the results of the alloy composition profile. Alloy samples were taken from different sections of the furnace at 20cm intervals from the top down.

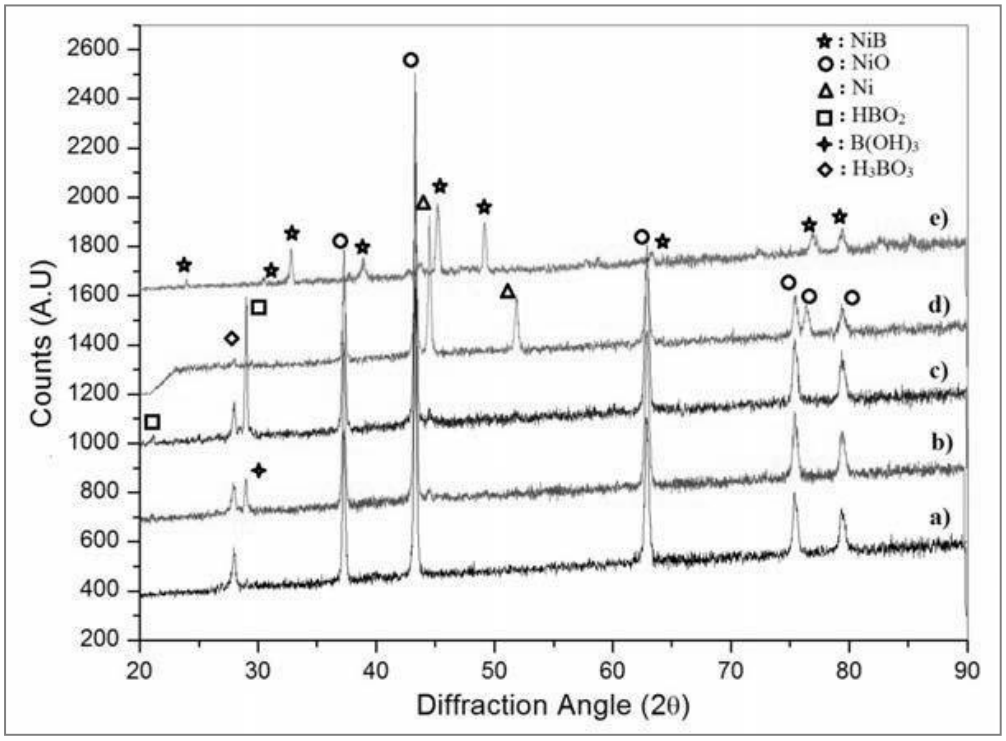


**Figure 4: Comparative XRD graphs of the samples taken from a) 20cm depth) 40cm depth, c) 60cm depth, d)80cm depth, e)at the bottom of the furnace (8).**

The bottom of the furnace reported the maximum prevalence of NiB as presented in Figure 4. The upper sections of the furnace showed minimal NiB and increased levels of unreduced

and partially reduced $H_3BO_3$. Tasyurek et al concluded that NiB formation reaction occurred predominately at the electrode tip.

Similar work undertaken by Yucel, Addemir, Cinar (9) corroborated the findings reported by Tasyurek et al. Yucel et al similarly reported a concentration profile for B content in the furnace. Yucel et al attempted to produce FeB from a mixture of boric acid ($H_3BO_3$), hematite ($Fe_2O_3$), charcoal and wood chips in a 100kVA single electrode D.C. arc furnace.

The effect of charge composition was investigated by varying the ratio of $H_3BO_3$ and $Fe_2O_3$ between 0.44 and 1.12 and the charcoal addition between 5-25% of the charge by weight. Of interest are the results of the samples taken from the different sections of the furnace as in the work done by Tasyurek et al. The samples were taken at different sections of the electric arc furnace and were analyzed by X-ray diffraction and were tabulated (Table 3). Yucel et al proposed that at the upper sections of the furnace, dehydration of boric acid ($H_3BO_3$) and pre-reduction of hematite ($Fe_2O_3$) occurred. Moreover, it was reported that the iron-borates were simultaneously reduced at the electrode tip near the furnace bottom. The reduction of iron-borates with C and CO formed FeB.

**Table 3: XRD results of the compounds formed at different sectors in furnace under optimum production conditions of ferroboron (9).**

| Compounds | | Sectors | | | | | | | | |
|---|---|---|---|---|---|---|---|---|---|---|
| | | **1** | **2** | **3** | **4** | **5** | **6** | **7** | **8** | **9** |
| $H_3BO_3$ | | ◊ | ◊ | ◊ | | | | | | |
| $B_2O_3$ | | | ◊ | ◊ | ◊ | ◊ | ◊ | | | |
| $Fe_2O_3$ | | ◊ | ◊ | ◊ | ◊ | ◊ | ◊ | | | |
| $Fe_3O_4$ | | | ◊ | ◊ | ◊ | ◊ | ◊ | | | |
| C | | ◊ | ◊ | ◊ | ◊ | ◊ | ◊ | ◊ | | |
| $FeB_2O_4$ | | | ◊ | ◊ | ◊ | ◊ | ◊ | ◊ | | |
| $FeB_4O_7$ | | | ◊ | ◊ | ◊ | ◊ | ◊ | ◊ | | |
| Glassy Phase | | | | | | | | | ◊ | |
| FeB | | | | | | | | | ◊ | ◊ |
| Analysis (wt. %) | B | 9.6 | 8.9 | 9.0 | 8.5 | 9.7 | 9.8 | 9.8 | 20.9 | 17.9 |
| | C | 12.8 | 22.0 | 24.8 | 23.7 | 23.7 | 14.9 | 14.9 | 4.9 | 0.1 |

◊: Detected by XRD

The different sectors corresponded with the level in the furnace which samples were taken. Sectors 1-9 represented the upper to the lower sections of the furnace as depicted in Figure 5.

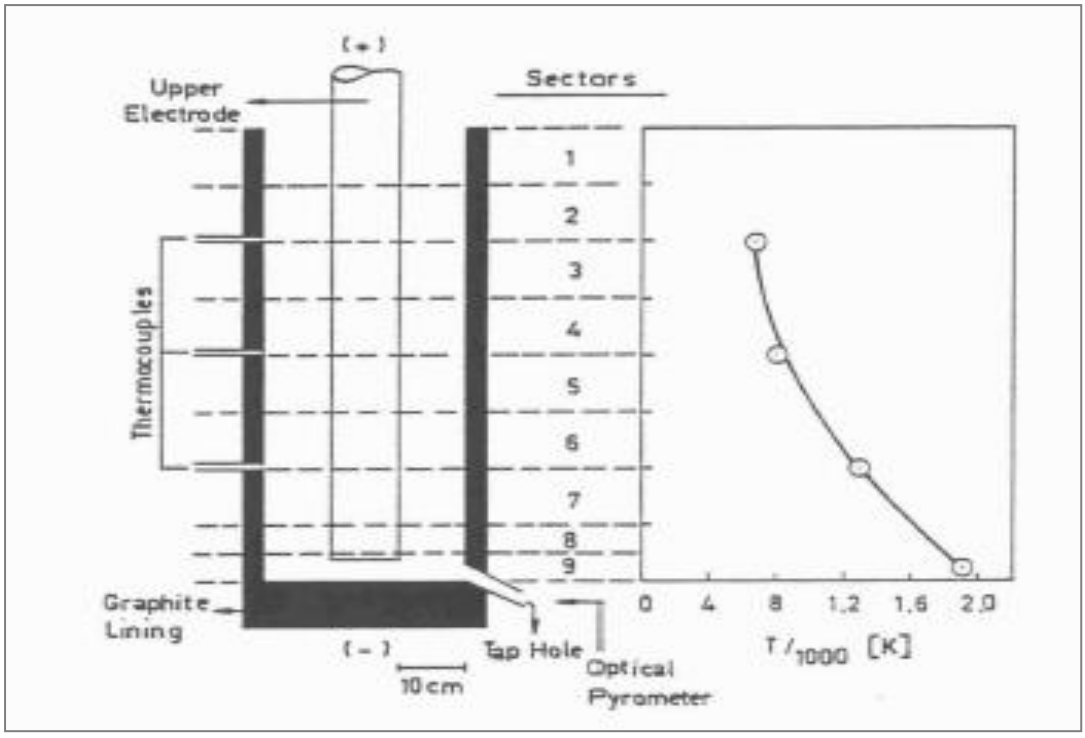


**Figure 5: Sectors in the furnace from which samples were taken and their temperatures**

The results reported by Tasyurek et al and Yucel et al showed that the B content of the alloy peaked at the furnace bottom. Thus, recovering the entire alloy from the furnace may dilute the overall B content of the tapped/final alloy.

### 3.2.1 Furnace Design and Emissions

The corroborative results reported by Yucel et al and Tasyurek et al pose significant furnace design challenges. The resultant B concentration profile may necessitate optimally designed furnace body along Blast Furnace design principles. Similarly shaped D.C .arc furnaces may possibly maximize B production from the rising CO gas.

Moreover, Tasyurek et al reported that the production furnace was lined with graphite. Several authors have described the interaction of C in Ni-B melts under different conditions. Yukinobu, Ogawa and Goto (10) investigated the activity of B in Ni-B-C melts saturated with C under Argon atmosphere. A key finding from this work was that the solubility of C in the Ni-B melt exhibited almost no dependency on temperature. They also found that the C content of the resultant alloy rapidly increased with decreasing B content as depicted in Figure 6.

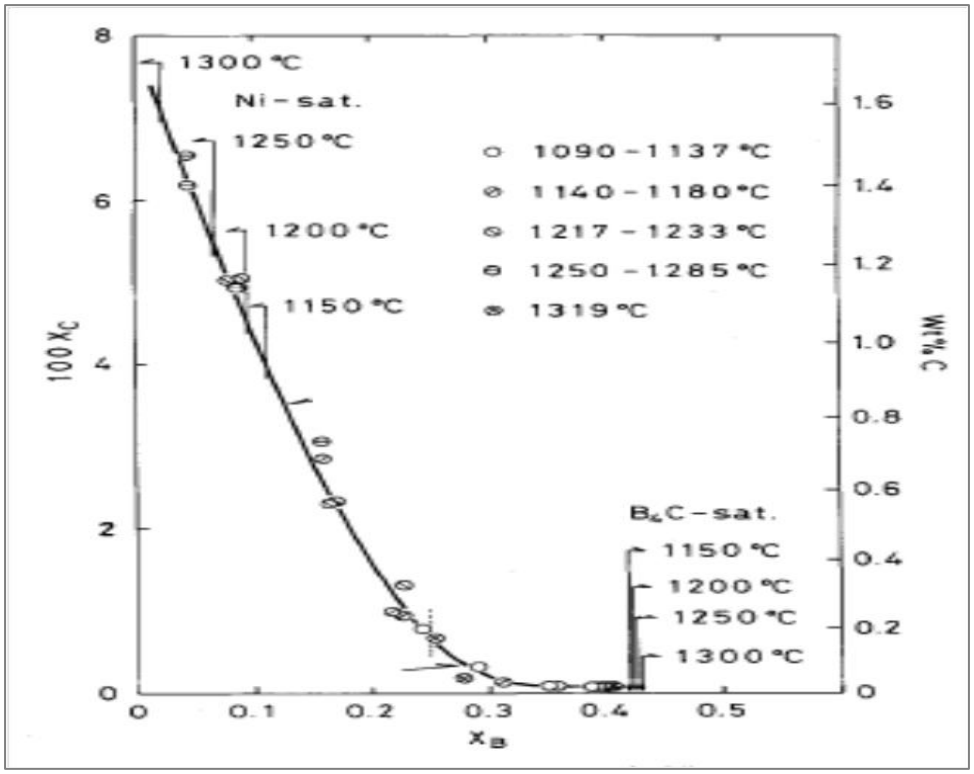


**Figure 6: Saturation concentration of carbon in Ni-B-C melts (10)**

Yukinobu et al reported that Omori and Hashimoto have estimated the B activity in Ni-B-C melts formed in the presence of $B_2O_3$ (l) and C(s) under about 1 atm of CO. The author of the present work failed to obtain this reference. However, Yukinobu et al compared their own findings with the results of other authors. Yukinobu et al concluded that due to the different experimental conditions, their findings were not necessarily conclusive. Furthermore the work done by Omori and Hashimoto could be utilised to determine the interactions of Ni-B-C particularly under CO atmosphere present in carbothermic production of NiB.

Carbothermic reduction of oxides typically generates reducing atmospheres which may be attributable to the formation of CO gas. Yucel et al observed that the vapour pressure of $B_2O_3$ at the smelting temperature (1900K) was 10mm Hg. A relevant study investigating the high temperature vaporization behaviour of oxides corroborated this observation. It was determined that under reducing conditions vaporization primarily takes place by evolution of $B_2O_3$ (g) except that $B_2O_2$ (g) becomes more important at higher temperatures as shown in Figure 7 (11) .

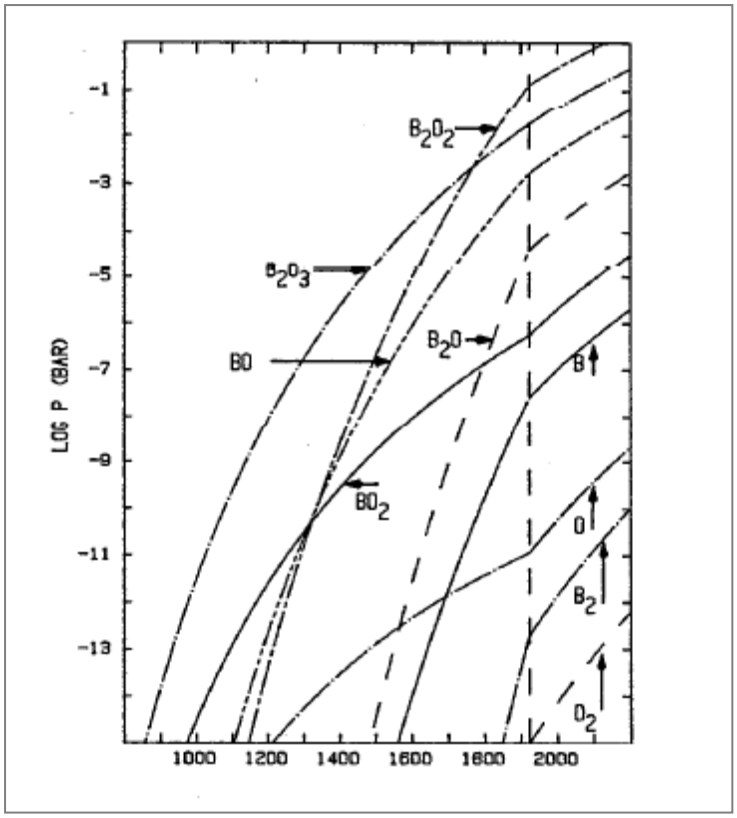


**Figure 7: $B_2O_3$ vaporization in $10^{-15}$ bar $O_2$ below 1923K and vaporization of B-$B_2O_3$ mixture above 1923K (11)**

This would suggest minimal $B_2O_3/B_2O_2$ fume generation. In any event the generation of $B_2O_3/B_2O_2$ fume and CO gas would therefore require gas and fume handling equipment. Installing such equipment may possibly result in higher capital costs.

### 3.2.2 Disadvantages of Carbothermic Production of NiB

Charcoal or wood chips, and other carbonaceous materials used as reductants for the production of NiB obviously present a competitive price advantage over common metallic reductants such as Al, Mg, Ca and Si. Notwithstanding the low Al content of the final alloys produced by the carbothermic process, it is evident that the slags formed are predominantly ash type slags inherent of carbothermic reduction processes.

The endothermic nature of the carbothermic process requires high power usage per Kg alloy produced. This may necessitate extended production times when the furnace power input is limited as was the case with the 270kVA furnace used by Tasyurek et al. Tasyurek et al

reported that the carbothermic smelting time of a 60kg NiB producing charge was 1 hour. It was deduced from the fact that samples were taken at different sections of the furnace that not all of the charge was completely smelted. Extended production times may cause excessive heat build-up at the anode resulting in anode melt-down, if a metallic anode is used. Alternatively, in an attempt to reduce smelting times it may be necessary to smelt with furnaces with a high power rating. High power rating furnaces (above 1MVA) are typically associated with high costs which may be offset by high production volumes. The NiB market of approximately 800tonnes per annum is possibly insufficient for such furnaces.

## 3.3 Metallothermy

Metallothermy is the metallurgical practice of reduction smelting of metal ores or oxides with reactive metals such as Aluminium (Al), Calcium (Ca), Magnesium (Mg) and Silicon (Si).Where the reduction process is termed aluminothermic, calciothermic, magnesiothermic and silicothermic, this is with reference to reductant Al, Ca, Mg and Si, respectively.

The metallothermic reduction of metal oxides to form metals and alloys is an alternative process to the carbothermic reduction smelting. The metallothermic reduction of oxides is generally an exothermic process unlike the carbothermic process. Ferro-alloys such as Ferro-Manganese (FeMn), Ferro-Chromium (FeCr) and Ferro-Silicon (FeSi) are and some Nickel based alloys such as NiB are commercially produced by the reduction smelting of their metal oxides with carbon, either as coke or charcoal, in an electric arc furnace. The carbothermic reduction reactions are generally endothermic and therefore require large thermal energy input when producing liquid products (6).The exothermic nature of metallothermic processes is commonly managed to reduce the thermal energy input.

### 3.3.1 Thermal Energy Requirement and Management

The thermal energy requirements of carbothermic process necessitate high power rating furnaces as previously mentioned. High Power rating furnaces require proportionally high capital expenditure. In contrast, some metallothermic reductions are sufficiently exothermic to be autothermic. That is, the reaction generates adequate heat energy to propagate to completion without any external heat input post ignition. In general, autothermic reactions reach high temperatures that yield well separated metal and slag. Dautzenberg presented a comparison of non-self-sustaining (non-autothermic) and self-sustaining (autothermic)

aluminothermic and silicothermic reduction reactions of metal oxides (12). It is noteworthy that all the reactions presented in Tables 4 and 5 are exothermic.

The major advantage of self-sustaining reactions is that the capital expenditure can be kept at a minimum. For instance, the production of Ferro-Vanadium (FeV) and Vanadium from $V_2O_5$ can be carried in a simple refractory lined reactor. Krishnamurthy and Gupta reported that the commercial production of Vanadium from $V_2O_5$ was carried out in closed bomb such as depicted in Figure 8 (13). The power source depicted in Figure 8 is used to provide activation energy to result in ignition of reactants.

**Table 4: Self and non-self-sustaining aluminothermic reactions**

| Aluminothermic Reaction | Reaction Enthalpy($-\Delta H°_{298}$) in kcal/g-mol Al | |
|---|---|---|
| $\frac{3}{4}SiO_2 + Al = \frac{3}{4}SiO_2 + \frac{1}{2}Al_2O_3$ | 37.9 | Not self-sustaining |
| $\frac{1}{2}B_2O_3 + Al = B + \frac{1}{2}Al_2O_3$ | 46.9 | |
| $\frac{1}{2}V_2O_3 + Al = V + \frac{1}{2}Al_2O_3$ | 58.0 | |
| $\frac{3}{2}MnO + Al = \frac{3}{2}Mn + \frac{1}{2}Al_2O_3$ | 62.0 | |
| $\frac{1}{2}Nb_2O_5 + Al = \frac{3}{5}Nb + \frac{1}{2}Al_2O_3$ | 63.8 | |
| $\frac{1}{2}Cr_2O_3 + Al = Cr + \frac{1}{2}Al_2O_3$ | 65.0 | |
| $\frac{1}{2}Mn_3O_4 + Al = \frac{9}{8}Mn + \frac{1}{2}Al_2O_3$ | 75.6 | Self-sustaining |
| $\frac{1}{2}Mn_2O_3 + Al = Mn + \frac{1}{2}Al_2O_3$ | 85.3 | |
| $\frac{3}{10}V_2O_5 + Al = \frac{3}{5}V + \frac{1}{2}Al_2O_3$ | 88.5 | |
| $\frac{3}{4}MoO_2 + Al = \frac{3}{4}Mo + \frac{1}{2}Al_2O_3$ | 95.6 | |
| $\frac{1}{2}Fe_2O_3 + Al = Fe + \frac{1}{2}Al_2O_3$ | 101.8 | |

**Table 5: Self and non-self-sustaining silicothermic reactions**

| Silicothermic Reactions | Reaction Enthalpy($-\Delta H°_{298}$) in kcal/g-mol Si | |
|---|---|---|
| $\frac{2}{3}B_2O_3 + Si = \frac{4}{3}B + SiO_2$ | 12.0 | Not self-sustaining |
| $\frac{2}{3}V_2O_3 + Si = \frac{4}{3}V + SiO_2$ | 20.8 | |
| $2MnO + Si = 2Mn + SiO_2$ | 22.1 | |
| $\frac{2}{5}Nb_2O_5 + Si = \frac{4}{5}Nb + SiO_2$ | 34.1 | |
| $\frac{2}{3}Cr_2O_3 + Si = \frac{4}{3}Cr + SiO_2$ | 36.1 | |
| $\frac{1}{2}Mn_3O_4 + Si = \frac{3}{2}Mn + SiO_2$ | 50.4 | |
| $\frac{2}{3}Mn_2O_3 + Si = \frac{4}{3}Mn + SiO_2$ | 63.6 | |
| $\frac{2}{5}V_2O_5 + Si = \frac{4}{5}V + SiO_2$ | 67.5 | |
| $MoO_2 + Si = Mo + SiO_2$ | 76.1 | |
| $\frac{2}{3}Fe_2O_3 + Si = \frac{4}{3}Fe + SiO_2$ | 85.2 | Self-sustaining |

#### *3.3.1.1 Alternative Heat Input*

The additional energy required to promote self-propagation of metallothermic reaction can be obtained through several methods. In certain cases, the reactants are preheated to the relevant temperature to effect self-propagation/autothermicity. In other instances the use of highly oxidic compounds which are simultaneously reduced with the charge are introduced to the bulk charge. These oxidic compounds are commonly termed reaction boosters as they generate high energy per mol reductant and therefore boost the overall reaction enthalpy. In both these cases, the equipment used may require minimal modifications. It is noteworthy that $V_2O_5$ can be used as a reaction booster for the aluminothermic production of FeV from $V_2O_3$ (13).

The use of electric arc furnaces for the metallothermic production of metals and alloys is also implemented in cases where charge preheating or use of reaction boosters is deemed unnecessary or unsafe. Moreover, preheating of charge may cause pre-ignition of reactants which may pose significant safety risks. Nelson reported that some reactions boosters such as Potassium Chromate can form toxic compounds (14) . In any event, the metallothermic reactions generally require less heat input than carbothermic reactions and hence may reduce the overall energy costs.

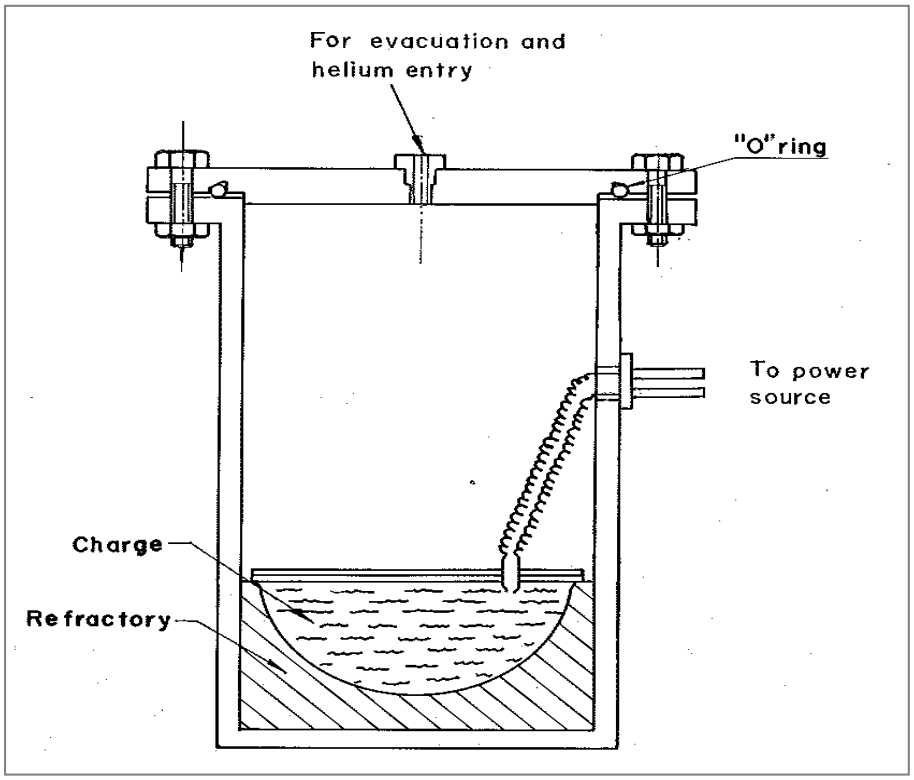


**Figure 8: Closed bomb reactor for large scale aluminothermic reduction of $V_2O_5$**

### 3.3.2 Low Carbon Alloys

The metallothermic reduction of metal oxides is commonly implemented in an attempt to produce low carbon content metals or alloys. In certain instances, the carbon specification of an alloy commonly produced by the carbothermic process is lower than can be economically achieved through the exact process. As an example; Eissa, El-Fawakhry, and Mishreky (15) reported that the production of extra low carbon FeCr (containing less than 0.02%C) can be successfully produced through the metallothermic process and in particular, the aluminothermic process.

### 3.3.3 Fume and Off-gas

Typical metal extraction through the pyrometallurgical processing route results in fumes or dust generation. It is common practice that pyrometallurgical reactors are connected to dust collecting and gas cleaning equipment. These units control the quality of off-gas and particulate matter that is discharged into the atmosphere in accordance to the prescribed legislations. Air quality legislation has been promulgated in most of the developed and developing world. Furthermore breach of these regulations may result in severe punitive measures let alone the health risks. Therefore it is very important for processes to control off-gas streams.

Metallothermic are generally tailored to produce liquid or solid products. The high temperatures (above 1000 °C) achieved in metallothermic processes may result in the boiling of reactants or formation of gaseous products. In certain instances some reductants such as Mg and Ca have a relatively low boiling point, 1090°C and 1494°C respectively (13). Other reaction species may volatilize or boil at reaction temperatures. It was shown that $B_2O_3$ has a wide volatilization range. Under 0.2 partial pressure of $O_2$ (conditions similar to normal atmosphere) Lamoreaux et al (11) showed that $B_2O_3$ vaporization occurs from the melting point of 450°C as can be seen in in Figure 9.

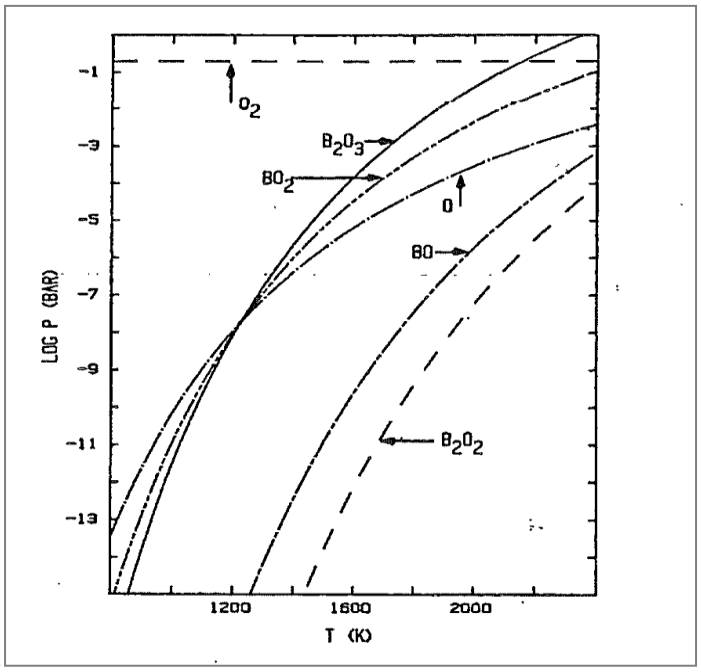


**Figure 9: $B_2O_3$ volatilization in 0.2bar $O_2$**

However, the principle behind metallothermic reactions is to utilize solid or liquid reductants contrary to the primary use of CO gas in the carbothermic process.

Mindful of $CO_2$ emissions regulations, carbothermic processes may be seen to be a major contributor to greenhouse gases. Nonetheless, some carbothermic processes may have a lower overall $CO_2$ footprint, because many commercial processes reuse the produced CO. Regardless, most metallothermic reactions may require less capital intensive gas cleaning equipment due to the inherent state of final reaction products.

### 3.3.4 Liquid Products

The formation of liquid products presents some disadvantages. In typical metallothermic reactions the liquid products are slag and metal. The interaction between the liquid products, slag and metal, has been and continues to be a subject of research. The reductant used may also readily dissolve in the liquid metal phase if the main reaction is incomplete. This can result in contamination of the alloy. Increasing the metal reductant may yield higher metal recovery at the risk of contaminating the final alloy. Furthermore, Alcock (16) showed that the co-produced impurity metals may dissolve more readily in the liquid metal produced by the primary reduction reaction as compared to the generation of solid products. This can reduce the quality of the final alloy and result in the addition of further treatment processes. It is not uncommon for metals/alloys to undergo subsequent refining. The desulfurization and dephosphorization of steel melts is a common method of refining steel.

### 3.3.5 Slag Disposal

The nature of metallothermic reduction of metal oxides is that the production of slag is inevitable. If the slag is a high temperature phase then the addition of materials that reduce the melting point of the slag (fluxes) will naturally increase slag volumes. High slag volumes present the challenge of slag disposal if the slag cannot be recycled in a different process. Aluminothermic reduction of metal oxides produces Alumina ($Al_2O_3$) which may be used in refractories depending on the quality of alumina slag produced. But, in many instances the slag is dumped in designated areas.

## 3.4 Typical Aluminothermic and Alumino-magnesiothermic Production of NiB

### 3.4.1 Metallothermic Reduction Principles

Gupta and Krishnamurthy (13) simplified the metallothermic reduction reaction as represented by the equation:

$$zM + M'_xO_y = zMO_{y/z} + xM' \quad \text{(eq. 1)}$$

- The *x,y,z* represent the stoichiometric co-efficients.
- *M, M'* and *O* are reductant metal, metal/metalloid (in this case, Boron) produced and Oxygen, respectively.

The feasibility of this reaction is based on the Gibbs free energies of formation (G) of the species of the above reaction. Therefore; as a rule, the difference between the free energy of formation for the compound products and the compound reactants free energy should be less than zero for the reaction to be feasible. This general rule can be represented by the equation:

$$\Delta G\left(MO_{\frac{y}{z}}\right) - \Delta G(M'_xO_y) < 0 \quad \text{(eq. 2)}$$

The Gibbs free energy rule does not serve as a basis for determining the reaction kinetics. As other properties such as reaction temperature, melting point, boiling point, vapour pressure, density, chemical reactivity and alloying behaviour can have a significant impact on the practicality or kinetics of a reaction (13). The thermodynamic assessment of the metallothermic production of NiB is presented in the results section of this work. Due to limited practical thermodynamic properties pertaining to this study, most of the thermodynamic properties are assumed in standard state unless otherwise stipulated.

The common challenge faced in the aluminothermic production of NiB is the contamination of the alloy with Al. The aluminothermic reduction process is generally operated with excess Al to improve the extent of the reduction reaction. For hardfacing applications, NiB alloys have Al levels less than 0.5%. It is unavoidable that Al contamination will occur due to the necessity for high B recoveries. Zhan-Gou and Chang-ye (17) have investigated methods to produce low Al content aluminothermic NiB alloy. This was done by reacting $B_2O_3$ with Al contained in the spent NiAl catalyst (containing 48% Ni and 50% Al and the balance Fe, Si, S

and P) in a graphite lined induction furnace at 1600̊ C as represented by the following chemical reaction:

$$B_2O_3 + 2NiAl = Al_2O_3 + 2NiB$$

The standard Gibbs free energy change with respect to temperature for the reaction was calculated to be:

$$\Delta G° = -533700 + 77.4T \ (J/mol)$$

The reaction temperature was set at 1600°C and the Gibbs free energy was computed to be -388729.8 J/mol. The very negative free energy change suggested that the production of NiB from spent NiAl catalyst would be possible. The alloy produced from spent NiAl catalyst contained 14.55% B and 0.016% Al.

Sourcing NiAl catalyst presented a challenge during our investigations. Consecutively, melting pure Ni and alloying it with Al to produce a chemically equivalent NiAl would have increased production/experimentation costs. The chemically equivalent NiAl would not only need to be re-melted during the NiB production process (increasing melting costs), but also would have required size reduction of the alloy to increase the surface area and therefore promote the reaction kinetics. The use of NiAl was hence not investigated.

Zhang-Guo and Chang-ye further studied the effects of Mg addition on the chemical composition of the alloy. In an effort to reduce the Al content of the NiB alloy, Chang-ye and Zhang-Guo used an Mg-Al alloy containing 20% Mg and 80% Al by weight. The addition of Mg to the process displaced the Al therefore reducing Al available in the system. However, the authors of this work did not disclose the results of this experiment. The authors only suggested that the MgO formed from the reduction of $B_2O_3$ would lower the slag viscosity. Notably, the graphite crucible used in these experiments was deemed passive to chemical attack as indicated by the low carbon content of the alloy (reported to be less than 0.001%).

Batch-wise aluminothermic production of NiB is exothermic. Exothermic metallothermic reactions do not necessarily produce fluid metal and slag. The heat generated from the batch-wise aluminothermic production of NiB is not sufficient to raise the slag and metal to an adequate slag and metal fusion temperature. If the slag and metal melt or fuse, the metal phase (generally of higher density than slag) sinks and the slag with the lower density floats.

Along with the density difference, viscosity plays a role in metal slag separation. Density difference promotes good metal and slag separation when the relative viscosities of the metal and slag are low. If the slag and or metal are not molten by the reaction heat, poor slag metal disengagement is observed despite the relative density differences. This can occur when highly viscous slag entrains the formed metal particles and as a result; a congealed mass of metal and slag with dispersed metal droplets is formed. Poor metal slag separation results in loss of metal to the slag. Operating the furnace at a high temperature for fluid metal and slag can improve metal slag separation. However; such an operating regime can result in an overall increase in power consumption.

Thus, in an effort to maximize metal recoveries without increasing furnace or reaction temperatures, Chang-ye and Zhang-Guo used CaO as flux for the slag formed. Calcium Carbonate ($CaCO_3$) containing 85% CaO was calcined and mixed with the raw materials. It was reported that the lime addition of 1.4% total charge weight lowered the slag liquidus temperature. Moreover, increasing CaO above the 1.4% total charge weight further decreased the slag liquidus. Unfortunately details of these experiments were not disclosed.

Metal or Ni recovery reported by Chang-ye and Zhan-Guo was 80%. Due to the inherent value of NiB, the recovery of the alloy is important. One of the tools of increasing metal recoveries is by reclaiming metal entrained in the slag. This can be realized by selectively dissolving the slag in appropriate solvents such as acids and recovering the insoluble metal.

Andrieux, Grenoble and Peffen (18) patented a method to develop acid soluble process slags. The patent reported that these acid soluble slags were by-products of the aluminothermic reduction of $B_2O_3$ to form various boron containing compounds and alloys.

The information from this patent can be utilized when assessing the aluminothermic production of NiB. Process slags of various $Al_2O_3$, CaO and $B_2O_3$ compositions presented in Table 6 were purported as soluble in hydrochloric and nitric acid albeit at undisclosed acid concentrations. Insufficient information regarding the acid concentrations and or type of acid used for a particular slag limited the potential application of these acid soluble slags in attempting to produce NiB master alloy.

**Table 6: Composition of acid soluble slags (expressed in mol %)**

| **Slag** | $Al_2O_3$ | CaO | $B_2O_3$ |
|---|---|---|---|
| **A** | 45.0 | 47.5 | 7.5 |
| **B** | 8.5 | 84.0 | 7.5 |
| **C** | 8.5 | 36.5 | 55.0 |
| **D** | 23.0 | 22.0 | 55.0 |
| **E** | 23.5 | 47.5 | 29.0 |

As mentioned previously, in the aluminothermic process, Al is the sole reductant and in the alumino-magnesiothermic method, a fraction of the Al is replaced by Mg in NiMg alloy fines.

There is no detailed information about the precise alumino-magnesiothermic production of NiB. However, relevant phase diagrams of aluminothermic and alumino-magnesiothermic components have been compiled. In the aluminothermic and alumino-magnesiothermic production of NiB, Ni-Al-(Mg)-B-O are the primary components of the systems, with the obvious exception of Mg in the aluminothermic system.

The interaction between these components in either metal or slag phase can be deduced from the respective phase diagrams. Such information may include melting temperature, inter-solubility of the components with regard to composition.

### 3.4.2 Metal Phase Systems

The Ni-B phase diagram presents information of the final expected alloy (Figure 1). However it is intrinsic in metallothermic processes that contamination of the final alloy by the system's components may occur. Therefore, the interactions of the reductant metals with the carrier metal (Ni). This is significant because reaction extent in metallothermic reactions is generally determined post reaction. That is, the extent of Al and Mg consumption in the process is commonly calculated after the reaction. If the reduction reaction is incomplete or there is excess reductant, the unreacted Al and Mg would possibly report to the metal phase. Hence the solubility of the reductants in Ni and B needs to be determined.

*Aluminothermic Metal Phase*

The metal phase of the aluminothermic system can be categorized as formed by the Ni-Al-B-O quaternary system. Comprehensive information discussing this aforementioned quaternary system is inadequately discussed in literature. However, the relevant Ni-Al, B-Al and Ni-O and B-O binary systems have been compiled and are discussed with regard to the NiB production processes.

Al-Ni System

It can be deduced from the Al-Ni system purported by Nash, Singleton and Murray (19) that excess or unreacted Al can be dissolved in the Ni matrix. It can be seen from the phase diagram that at temperatures above 1638℃ Al is completely soluble in Ni across the composition range (Figure 2).

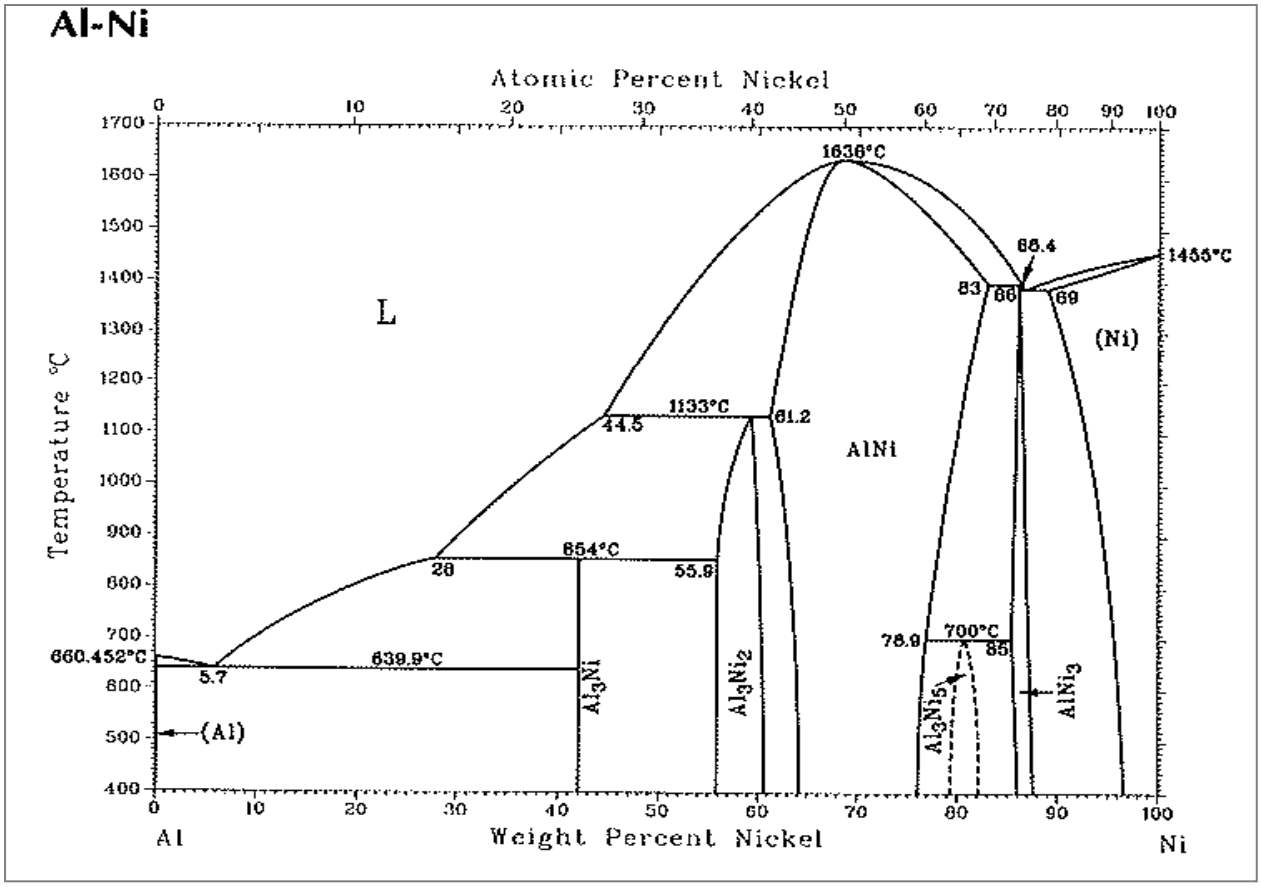


**Figure 10: Al-Ni phase piagram**

The limitation of the Al-Ni binary phase diagram is that the interaction of the produced B with Al and Ni cannot be accurately deduced. In spite of this factor, it is possible that the

produced B is not immediately collected by the Ni carrier. This may cause Al to dissolve in the Ni. This can potentially result in contamination of the final alloy if the dissolved Al is not oxidized.

Al-B System

The Al-B system obtained from the Factsage database (20) shows that Al reduces the melting point of B (Figure 3). Therefore, any formed B can alloy with available Al to form a lower melting temperature species. It can be assumed that given the relatively good solubility of Al in Ni and B, the final alloy may suffer Al contamination, hence the investigation of Al refining undertaken by Zhan-Gou and Chang-ye.

Obviously, the co-interaction of these components is more complex than the binary phase diagrams suggest. The ternary and quaternary systems would remove suppositions inherent when using binary phase diagrams to determine multi-component systems.

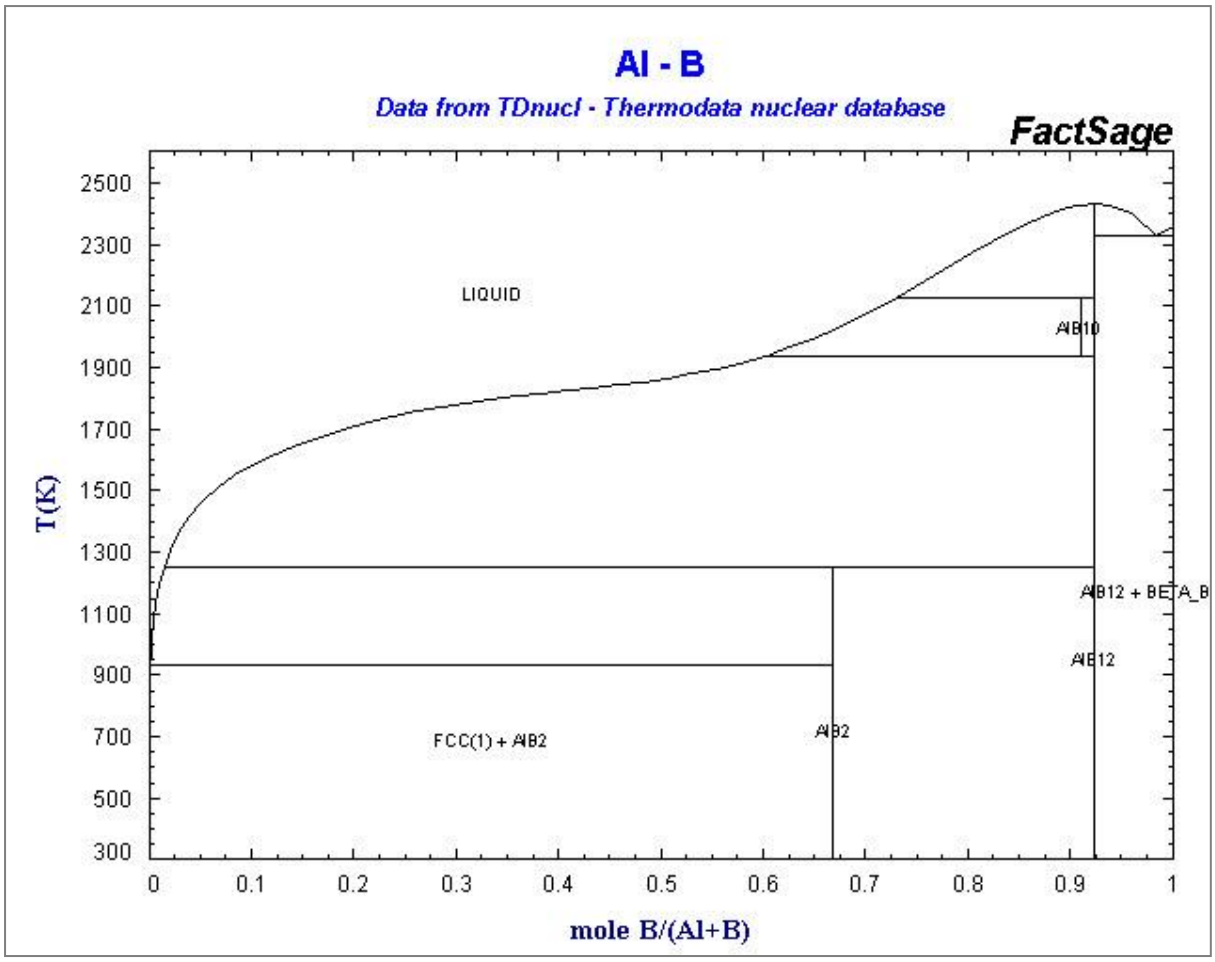


**Figure 11: Al-B phase diagram**

*Alumino-magnesiothermic Systems*

The information discussed pertaining to the interaction of the metal phase components in the aluminothermic process is applicable to the alumino-magnesiothermic metal phase. However, the alumino-magnesiothermic metal phase contains an additional component Mg. The additional binary systems therefore are Mg-Ni, Al-Mg and B-Mg.

Mg-Ni System

The Mg-Ni phase diagram compiled by Nayeb-Hashemi and Clark (21) shows that the melting temperature of NiMg (15-17.5% Mg) alloy used as raw material is approximately 1150℃ (Figure 4). This temperature is approximately 550℃ higher than the melting point of pure magnesium and about 100℃ above the boiling point of pure Mg. The Mg in solution with Ni is therefore passivated in the NiMg alloy. This can potentially increase the efficiency of $B_2O_3$ reduction by Mg.

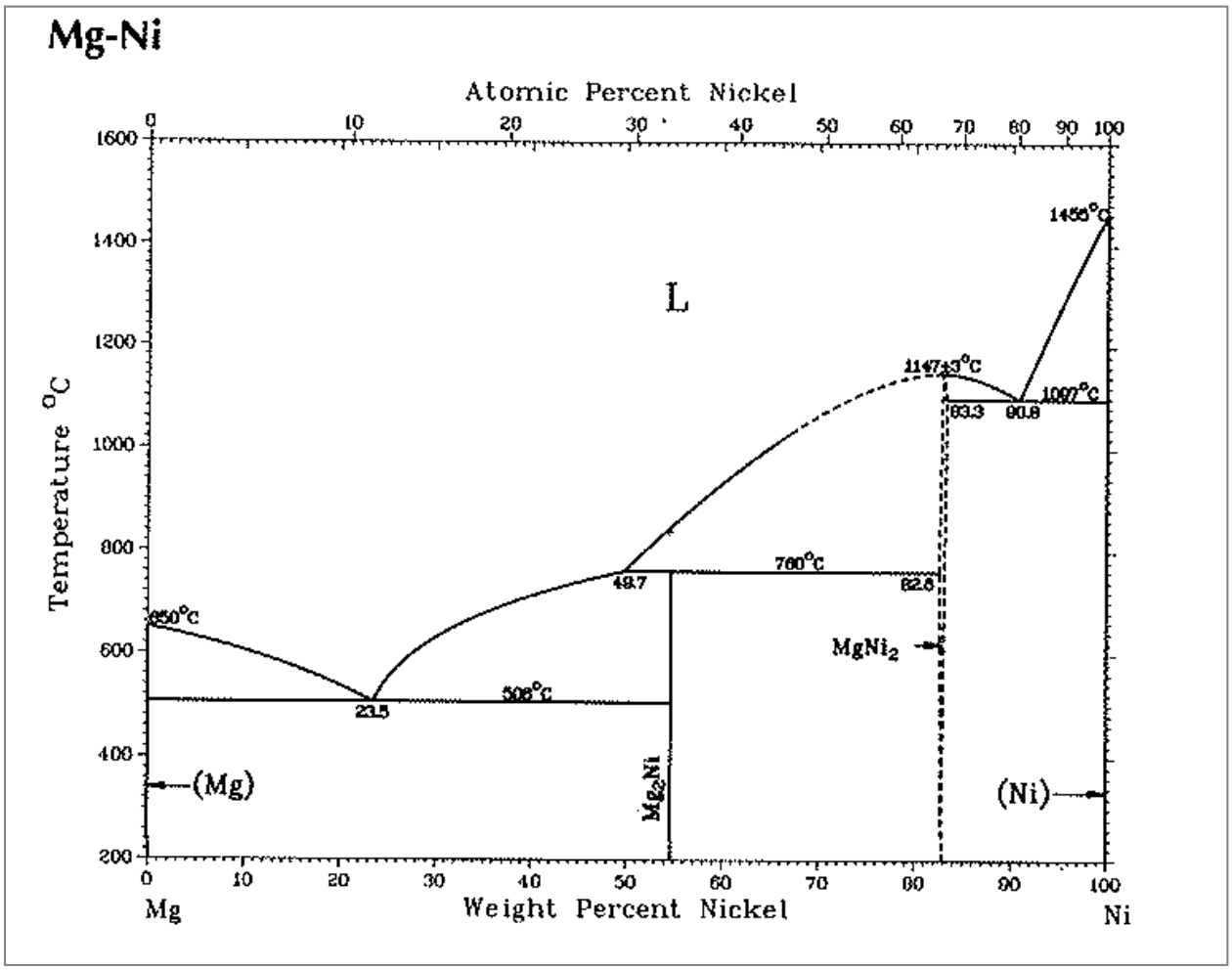


**Figure 12: Mg-Ni phase diagram**

Pure Mg has the propensity to flare off the furnace air atmosphere at elevated temperatures at which metallothermic reactions are carried out. Al has a similar the passivating effect on Mg as Ni.

Al-Mg System

The melting points of Al and Mg shown on the Al-Mg binary phase diagram compiled by Murray (22) are relatively low at 660℃ and 650℃, respectively (Figure 5).

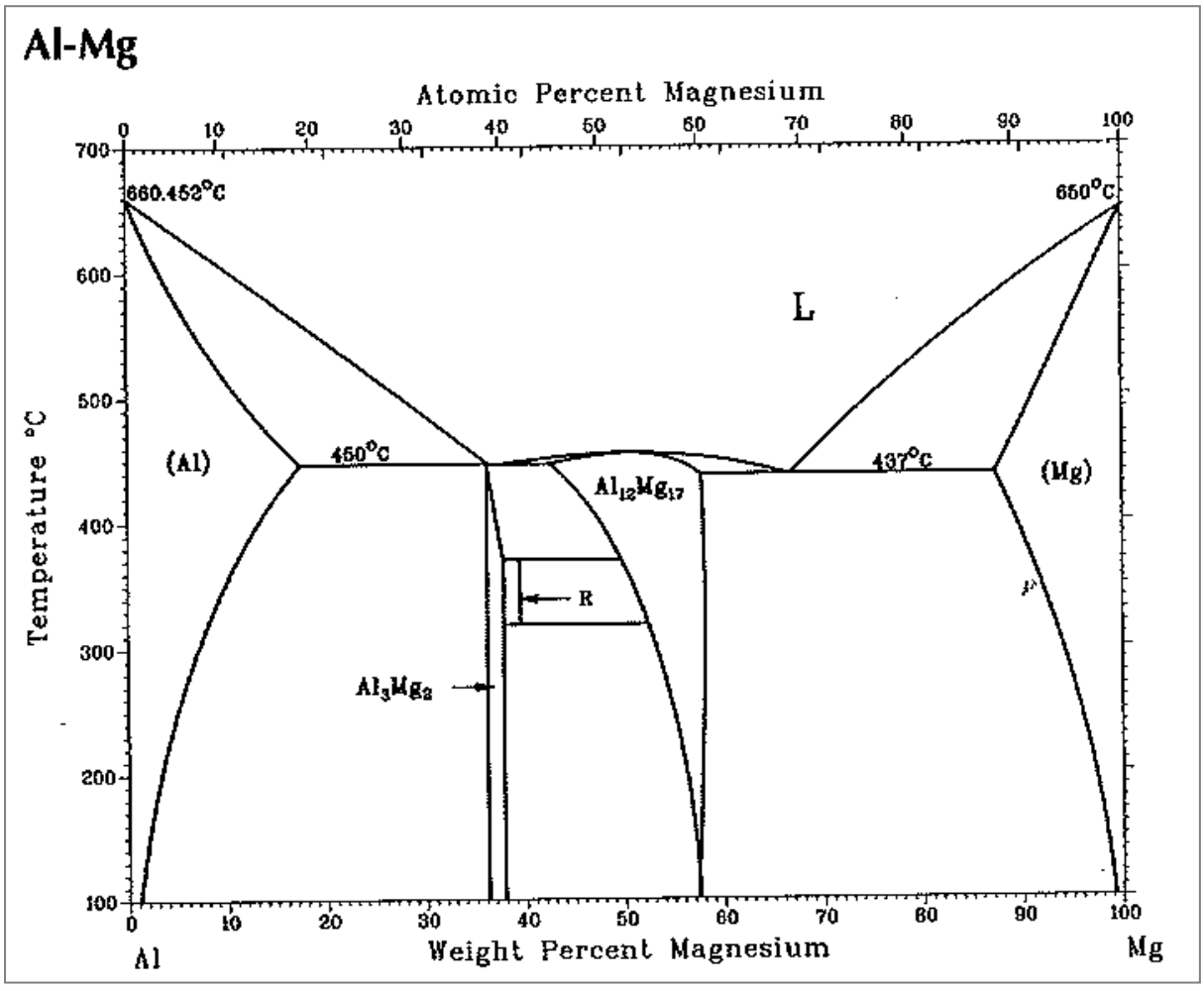


**Figure 13: Al-Mg phase diagram**

These metals are very reactive when molten in an oxidizing environment. Although it is common practice to melt Al in an air atmosphere without significant losses of Al to the slag (dross) as $Al_2O_3$, similar practice of melting Mg results in flaring and oxidation of Mg to MgO. These differences are due to the morphology of the oxide formed upon oxidation of the metal. Al forms a stable $Al_2O_3$ film covering the exposed metal surface and therefore preventing further oxidation of the metal. Mg forms discrete or non-contiguous oxide which

does not inhibit further oxidation of the exposed surface. Therefore, the use of an appropriate Al-Mg alloy for the alumino-magnesiothermic production of NiB would minimize the flaring of Mg in air and thus improve the $B_2O_3$ reduction reaction extent.

### *Oxygen Systems*

It is common practice that D.C. arc furnaces have a controlled atmosphere when processing high value materials which either oxidize in an air atmosphere. In other instances, these atmospheres are designed to improve reaction kinetics and metal recovery. The control of the furnace atmosphere requires careful management. This may require specialized gas analysing equipment which when installed monitor the furnace gases. The impact of oxygen in the atmosphere on the individual components of the system can be derived from the phase diagrams containing oxygen.

#### Al-O, Mg-O and Ni-O systems

A highly oxidizing furnace atmosphere may increase reductant consumption. This may occur through several routes:

1. The reductants Al and Mg may react with the oxygen in the furnace atmosphere (forming their respective oxides, $Al_2O_3$ and MgO) and therefore decreasing the amount of reductant available for the reduction of $B_2O_3$.

The high melting temperature of $Al_2O_3$ (2046℃) and MgO (2822℃) as shown on the binary phase diagrams compiled by Wriedt et al (23), (24) suggest that the oxides formed are highly stable (Figures 6 and 7, respectively).

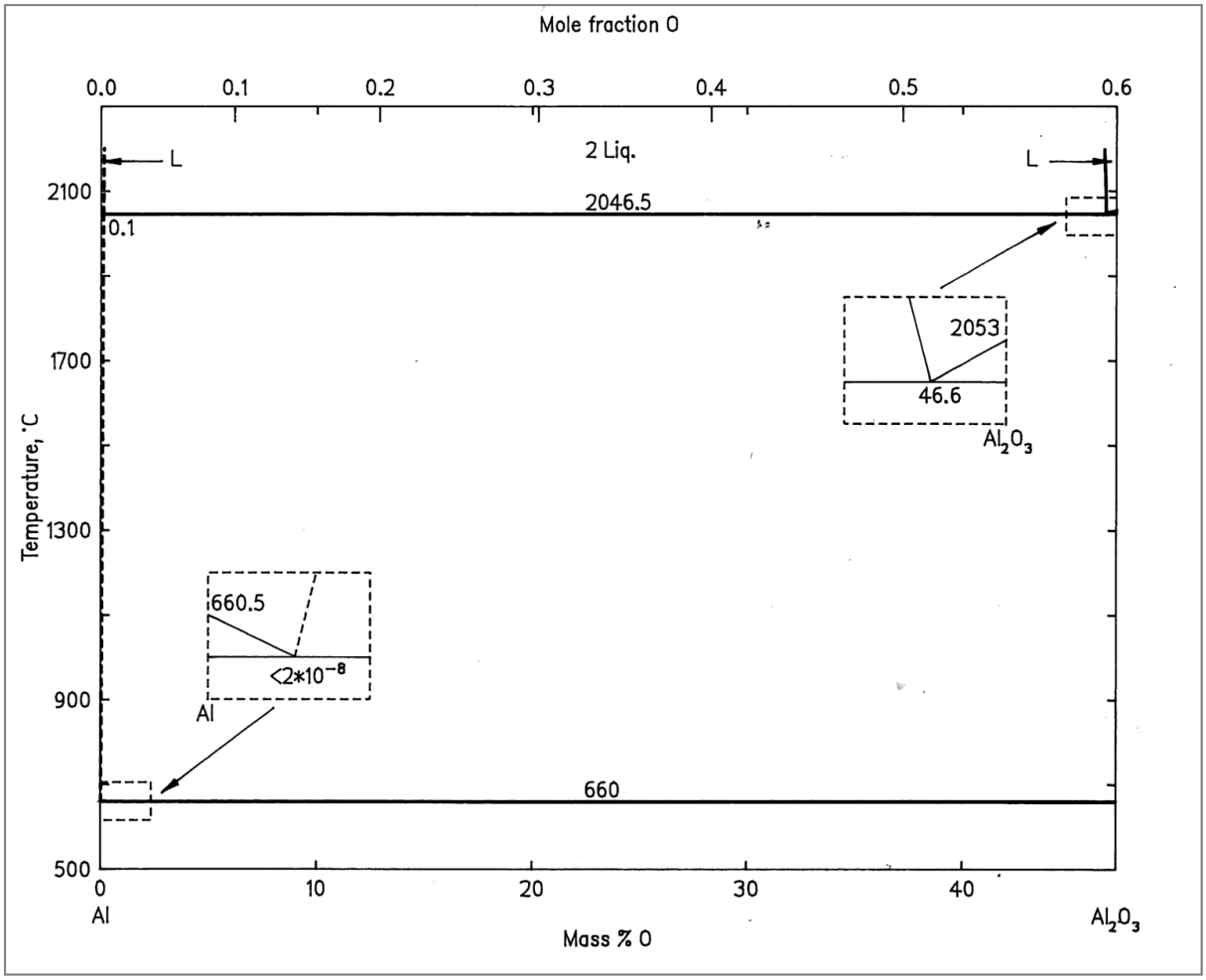


**Figure 14: Al-O phase diagram**

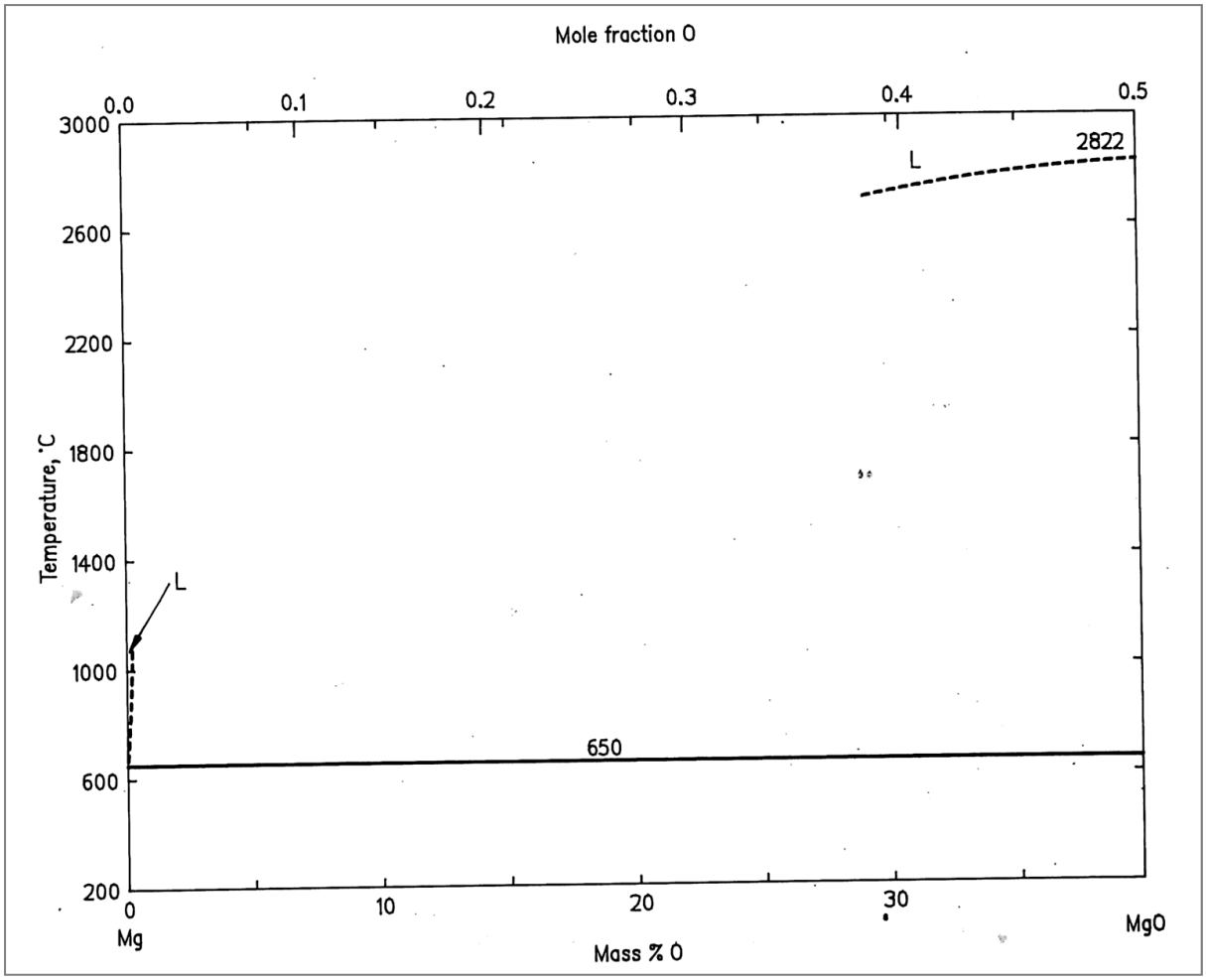


**Figure 15: Mg-O phase diagram**

2. Additionally, the carrier metal Ni may be oxidized to form NiO (β) as depicted in Figure 8 compiled by Neuman, Zhong, and Chang (25) , which itself could be reduced by Al and Mg .

Furthermore, the unreduced NiO (β) can report to the slag phase leading to increased Ni losses.

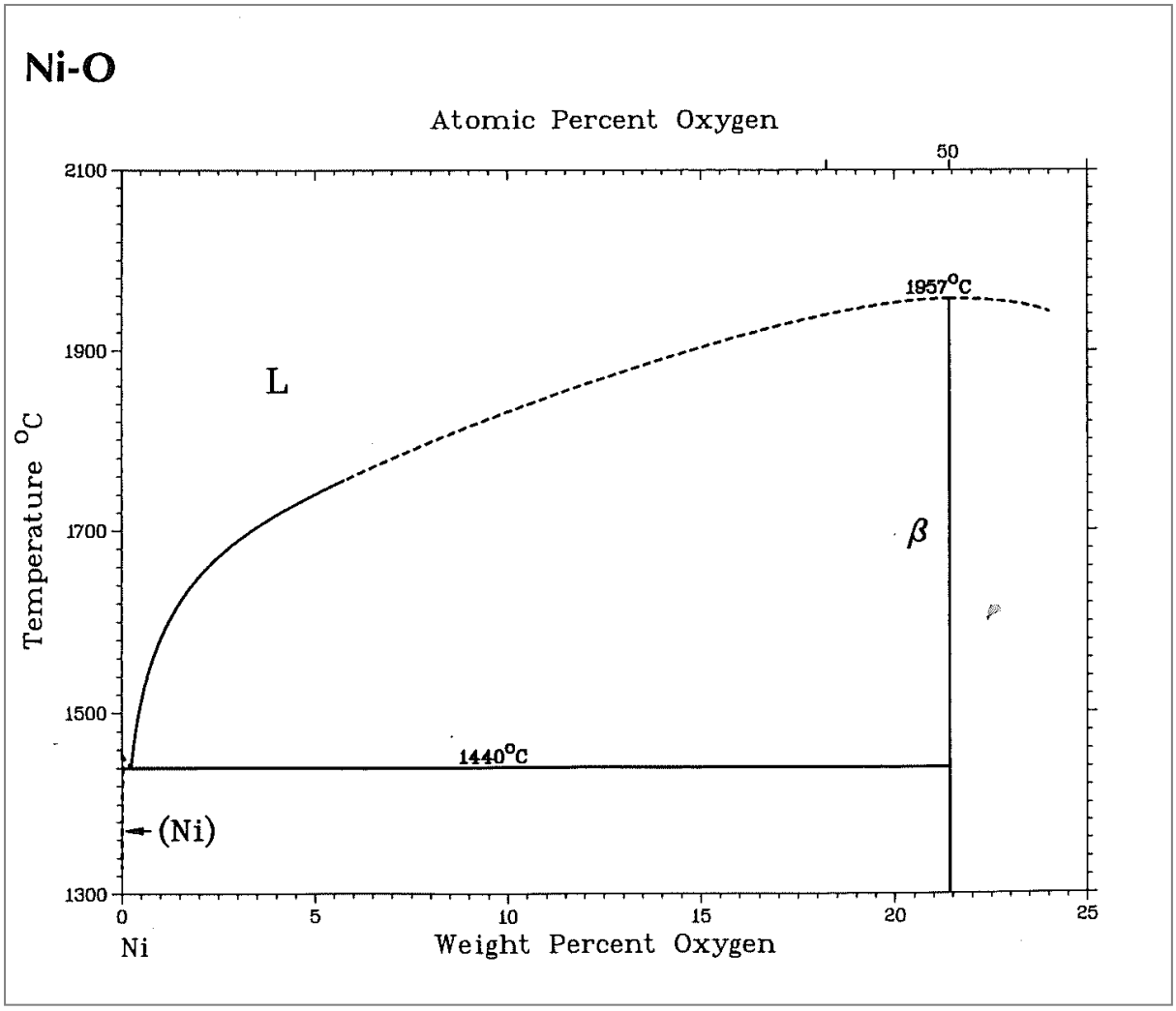


**Figure 16: Ni-O phase diagram**

It is notable that the oxide species that may be formed ($Al_2O_3$, MgO, *and* β-NiO) are high temperature species apart from the $B_2O_3$ which may be formed on oxidation of formed B. If NiO and or $B_2O_3$ are non-fluxing, the resultant slag phase would probably be a high temperature multi-component system.

B-O System

The overall production of B can be limited when the produced B reacts with oxygen in the atmosphere to form oxides of B. ($N_2$ present in the furnace atmosphere is assumed as inert). The most stable oxide of B in the processes discussed is $B_2O_3$. It is possible that $B_2O_3$ sub-oxides may form upon the partial reduction of $B_2O_3$. Therefore the B produced in the sub-reactions can react with the oxygen in the furnace atmosphere to form other $B_2O_3$ sub-oxides (such as $B_2O_2$, $B_2O$ and BO). These unstable oxides would readily react with strong reducers

such as Al and Mg. If Al and or Mg in the system are limited or completely consumed, these sub-oxides may react with the oxygen in the furnace atmosphere and thus reverting to more a stable $B_2O_3$ phase. The complication with partially reduced $B_2O_3$ is that the produced sub-oxides may be in the gas form at furnace temperatures. It was mentioned previously that $B_2O_3$ sub-oxides may be lost to fume resulting in B loss. Unfortunately, the only comprehensive B-O phase diagram as included in the Factsage database (26) does not clearly identify the various oxides of boron (Figure 17).

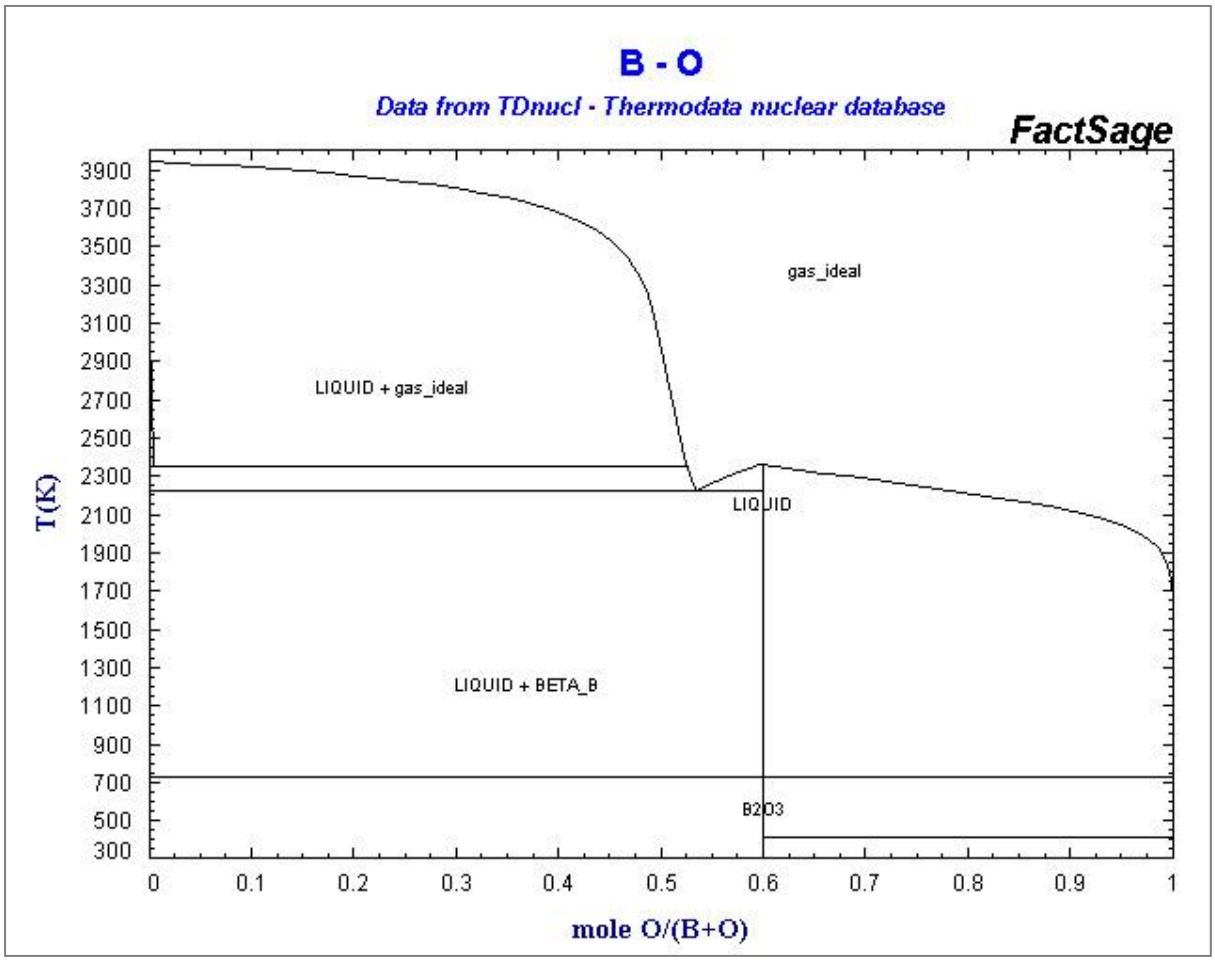


**Figure 17: B-O phase diagram**

In the metallothermic production of NiB the slag formed influences the overall process recovery and practicality. It is therefore necessary that the oxides produced, particularly $Al_2O_3$ and MgO remain fluid in the slag phase to effect good slag metal separation and thus increase alloy yield. As mentioned, this requires operating the D.C. arc furnace at sufficiently high temperatures to keep the slag phase molten or the addition of fluxing agents to reduce the slag melting point.

### 3.4.3 Slag Phase Systems

For the purpose of this study it was assumed that $Al_2O_3$ and MgO are primary components of the slag phase(s) and if any NiO is formed, it is simultaneously reduced to Ni. It was also assumed that the stoichiometric reaction extent was complete and hence no excess $B_2O_3$ in the slag phase. Thus appropriate flux was investigated at zero per cent $B_2O_3$ excess. However, practical metallothermic reactions would contain some excess of the reduced oxide. Therefore, it was necessary to determine the interaction of the flux with excess $B_2O_3$ in the slag phase.

### 3.4.4 Aluminothermic Slag Systems

The slag formed in the aluminothermic process is composed of $Al_2O_3$, unreacted/excess $B_2O_3$ and or flux (CaO or $SiO_2$).

The potential aluminothermic NiB production slag systems

- $Al_2O_3$-CaO
- $Al_2O_3$-$SiO_2$
- $Al_2O_3$-$B_2O_3$
- $Al_2O_3$-$B_2O_3$-CaO
- $Al_2O_3$-$B_2O_3$-$SiO_2$ and;

The high melting temperature of $Al_2O_3$ (2053℃) produced would require a flux. Various compounds may be used as fluxes, but lime (CaO) is known as the most practical flux for alumina. It was observed by Hall (27) that CaO provides superior fluxing capabilities over most metallurgically significant oxides. The effect is particularly superior toward the $Al_2O_3$-rich sections of the binary phase diagram. This can be seen in Figure 18; a binary $Al_2O_3$-X phase diagram, X represents the relevant oxides shown. Evidently, the use of $SiO_2$ as a flux would require significant amounts of $SiO_2$ and would still not reach the $Al_2O_3$-CaO eutectic temperature of 1413℃ and composition of 50% CaO-50% $Al_2O_3$. The $Al_2O_3$-$SiO_2$ eutectic temperature and composition is approximately 1600℃ at 92% $SiO_2$ (Figure 19, compiled by Klug et al (28)).

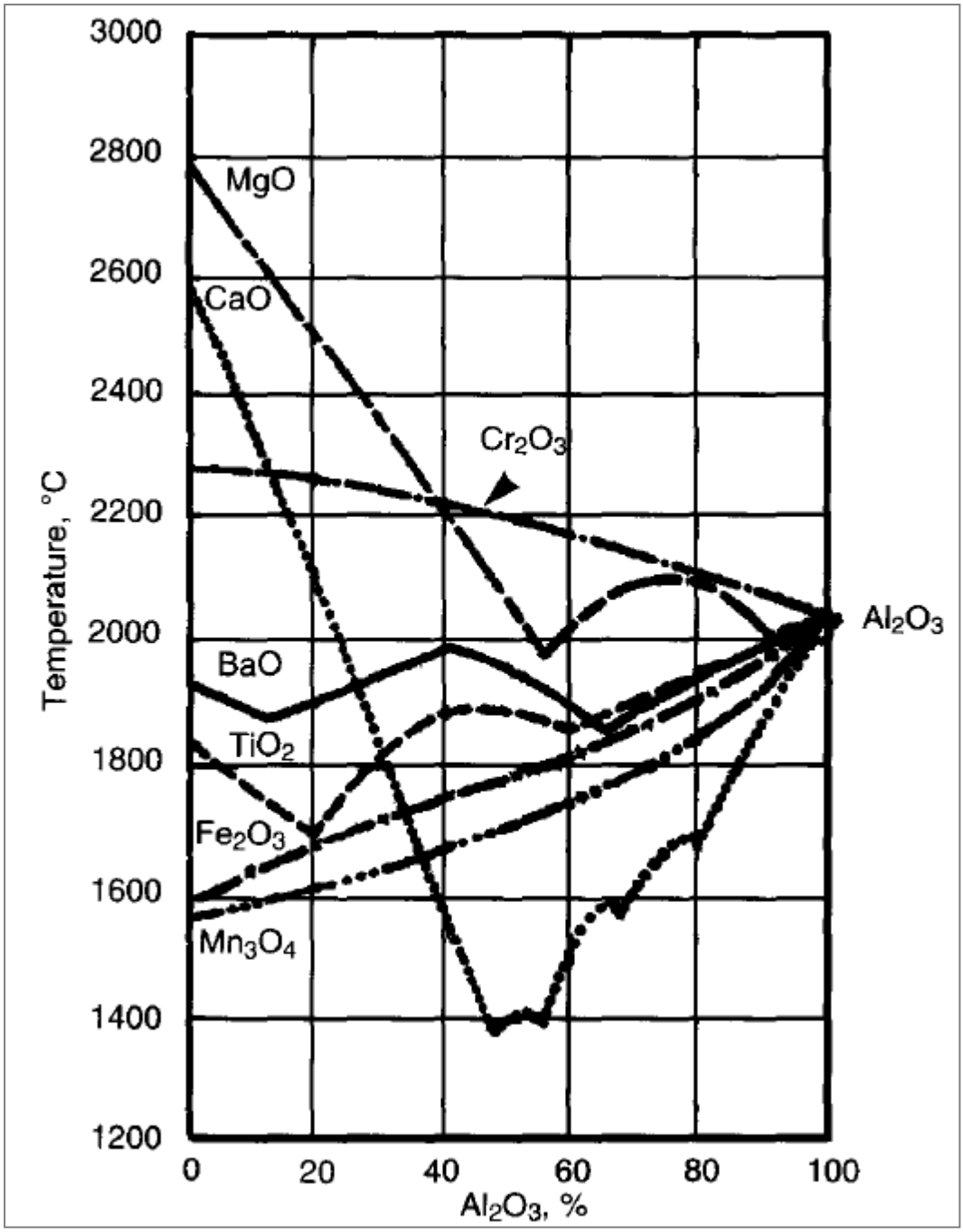


**Figure 18: Melting point curves of binary $Al_2O_3$ slags**

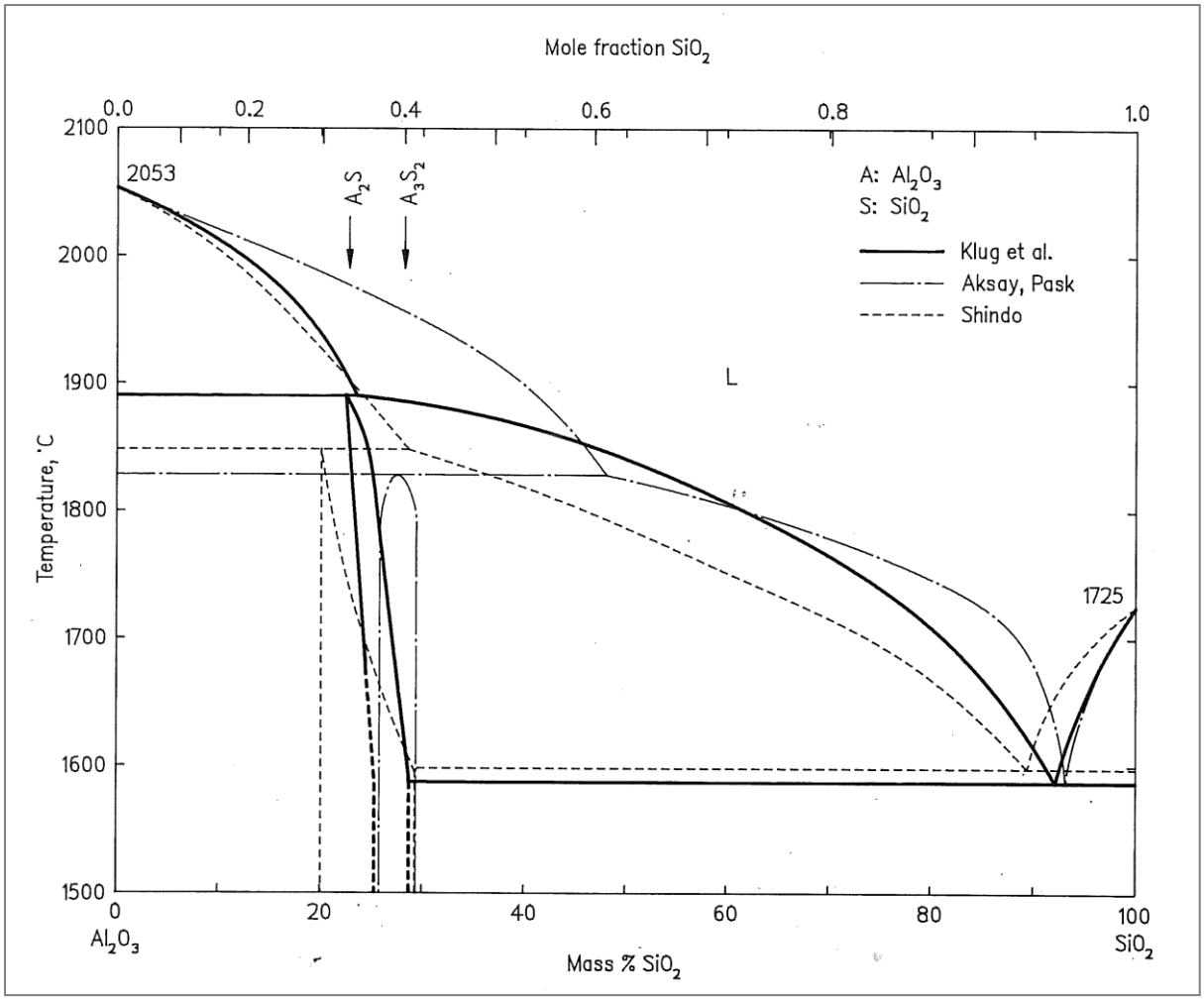


**Figure 19: $Al_2O_3$-$SiO_2$ phase diagram**

<u>$Al_2O_3$-$B_2O_3$ System</u>

The aforementioned slag systems assumed that no $B_2O_3$ reported to the slag phase. But it is common to operate metallothermic reactions with excess target oxide. Hence it is very likely that these systems will contain some $B_2O_3$.

The $Al_2O_3$-$B_2O_3$ binary slag system (obtained from the Factsage database (29)) is a predominantly high temperature system. It would be necessary to increase $B_2O_3$ amounts in this system in order to reduce the slag liquidus temperature (Figure 20). Otherwise, high furnace operating temperature risk lining failure and the associated risk of hot metal burning through the furnace shell. Therefore using an appropriate flux is essential.

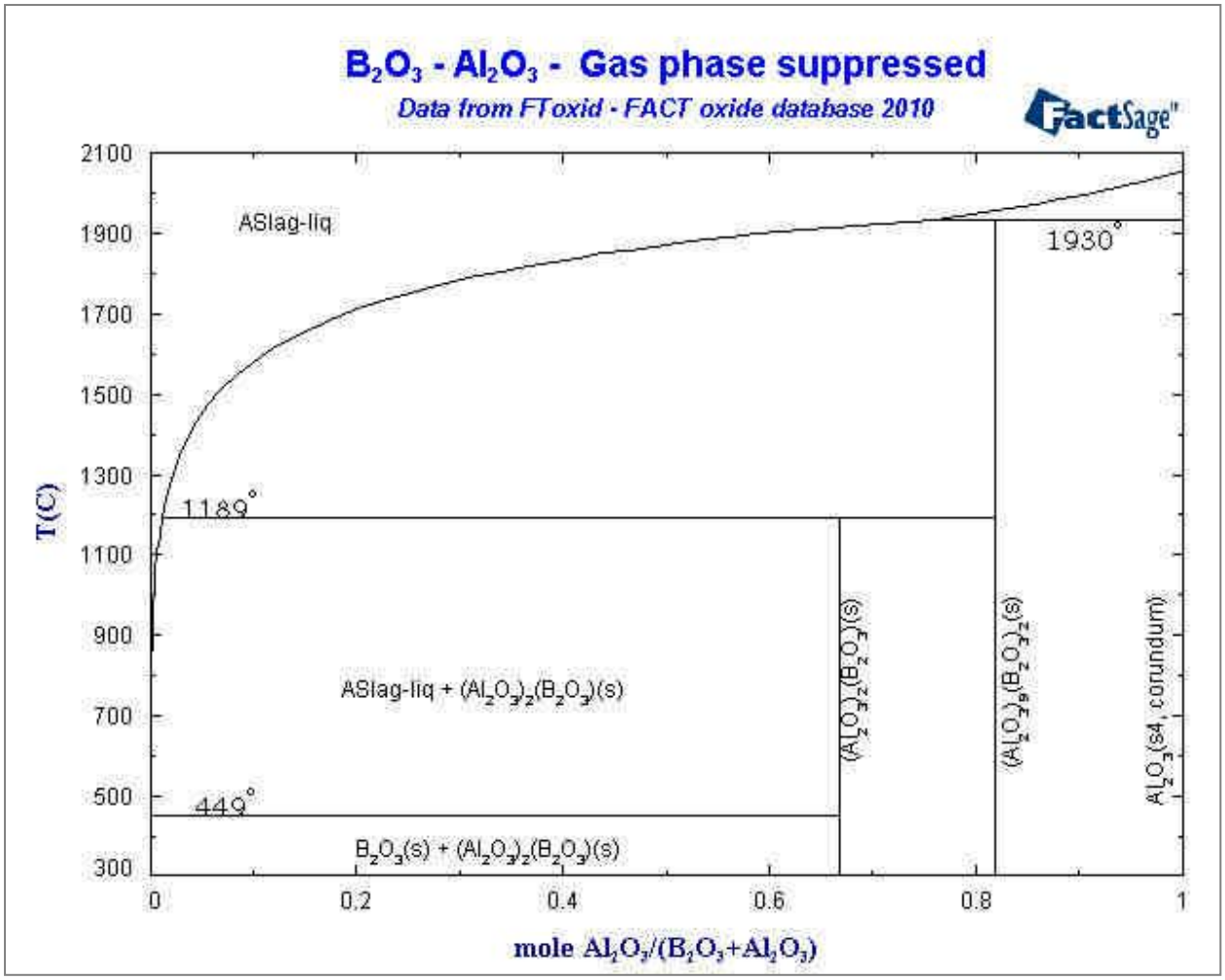


**Figure 20: $Al_2O_3$-$B_2O_3$ binary slag phase diagram in mol. %**

The cost of using large amounts of relatively expensive $B_2O_3$ as an attempt to flux $Al_2O_3$ can be economically prohibitive.

The possible fluxes for this system need to operate at minimum $B_2O_3$ content in the slag and reach a suitably low slag liquidus temperature. Thus using CaO and $SiO_2$ can possibly meet the aforementioned criteria.

<u>$Al_2O_3$-$B_2O_3$-CaO System</u>

As mentioned, CaO lowers the melting temperature of $Al_2O_3$. However, considering the fact that $B_2O_3$ is an acidic oxide, the basic CaO would attract the acidic $B_2O_3$ into the slag phase which could cause boron loss. The $Al_2O_3$-$B_2O_3$-CaO system is not well documented in literature. The system studied by Schafer and Kuzel (30) is an isothermal at 800℃ (Figure 21). Although this presents limitations with regard to species formed above 800℃, the ternary

phase diagram can be used effectively in the poor $B_2O_3$ region. This region (below the $2Al_2O_3$:$B_2O_3$ composition line) is interspersed with various $Al_2O_3$-CaO and CaO-$B_2O_3$ compounds of known melting points and composition. Thus an approximation of the behaviour of the low $B_2O_3$ content slag can be purported.

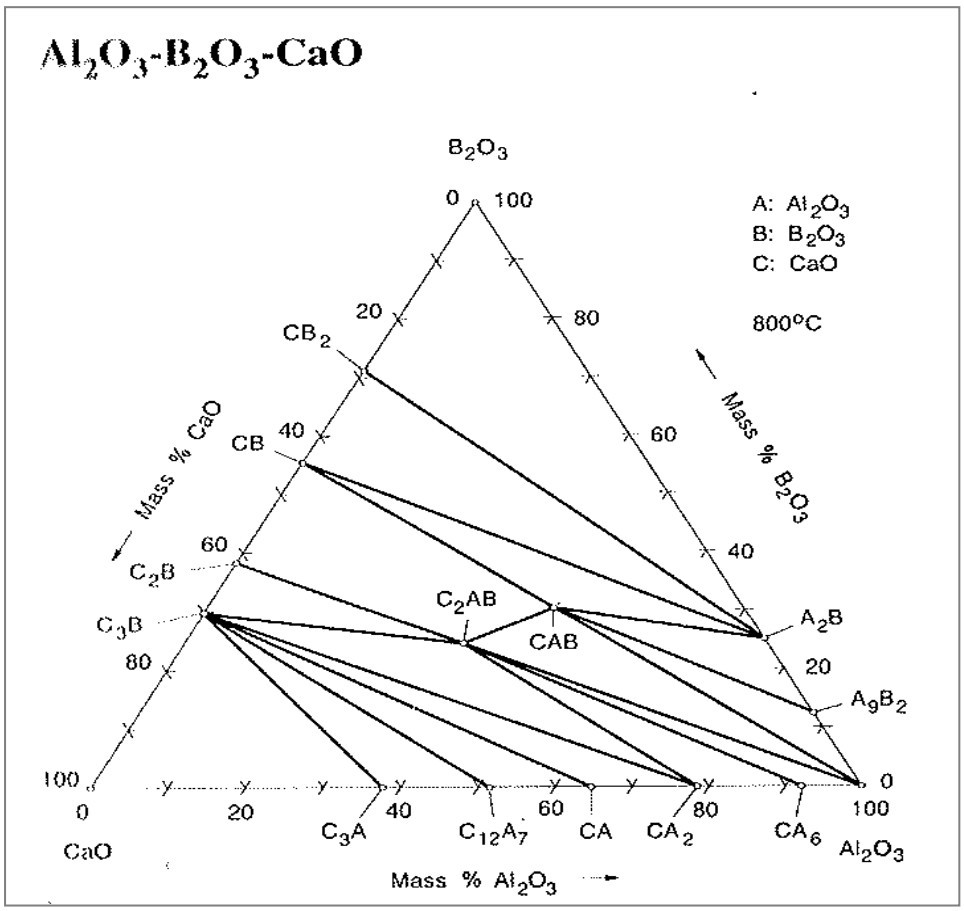


**Figure 21: $Al_2O_3$-$B_2O_3$-CaO isothermal ternary phase diagram at 800℃**

$Al_2O_3$-$B_2O_3$-$SiO_2$ System

Isothermal ternary phase diagrams are useful when determining species and or phases at the relevant temperature. But, more comprehensive phase diagrams are useful in suggesting optimum slag systems.

The $Al_2O_3$-$B_2O_3$-$SiO_2$ system prescribed by Gielisse and Foster (31) is a liquidus system. A slag system below the $2Al_2O_3$:$B_2O_3$ compound line can be optimized to operate between 1500-1650℃ at relatively low $B_2O_3$ mass fraction (Figure 22). However this system may not be suitable at the stoichiometric conditions. It was assumed that complete reduction of $B_2O_3$ occurred at the stoichiometric level. Moreover, even the use of acidic $SiO_2$ may minimize

boron loss to the slag; however care needs to be taken to avoid the preferential reduction of $SiO_2$ in the slag. This may cause Si contamination. Under these assumptions, the $Al_2O_3$-CaO system was suggested as more favourable than the $Al_2O_3$-$SiO_2$system. The detailed discussion of these two systems is presented in the results section of this work

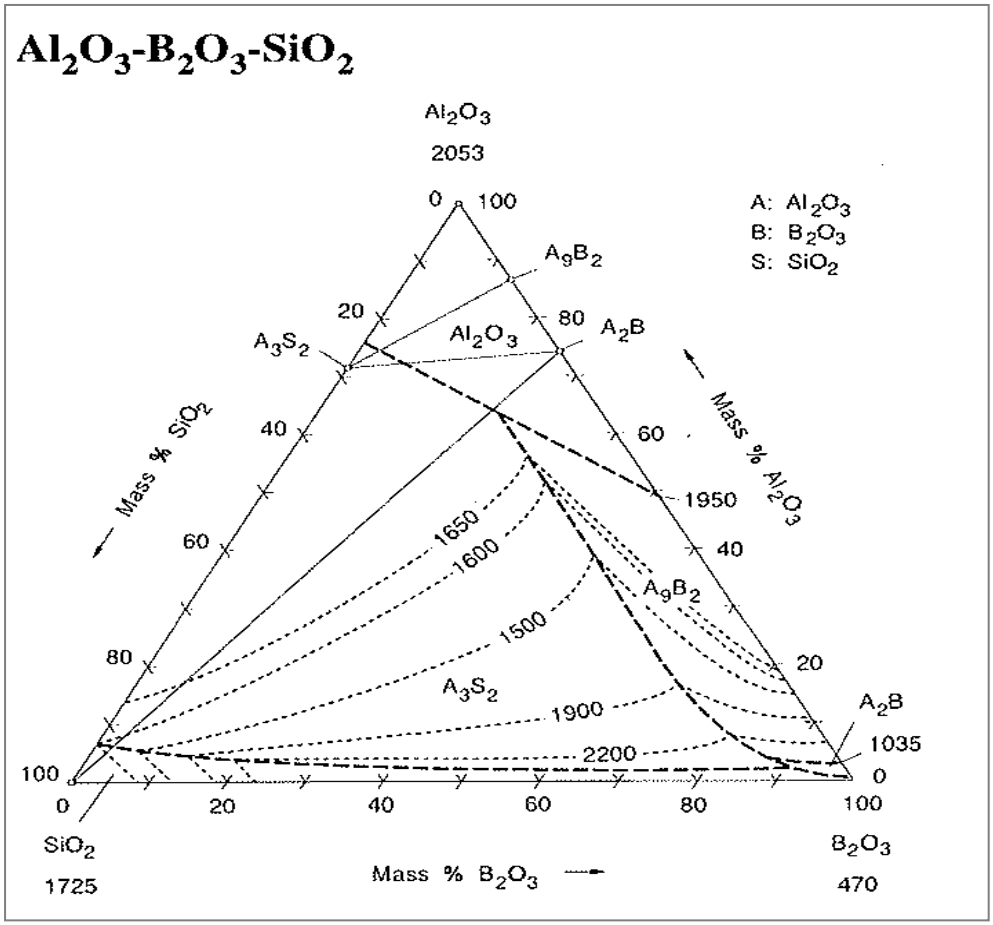


**Figure 22 : The $Al_3O_3$-$B_2O_3$-$SiO_2$ system**

### 3.4.5 Magnesiothermic Slag System

The magnesiothermic reduction yields MgO which may be fluxed by excess $B_2O_3$. The $B_2O_3$-MgO system studied by Miyaga et al (32)as presented in Figure 23 could be used to minimize use of fluxes which may introduce contaminants to the system. The MgO rich eutectic may be used as it can minimize excess $B_2O_3$ requirements.

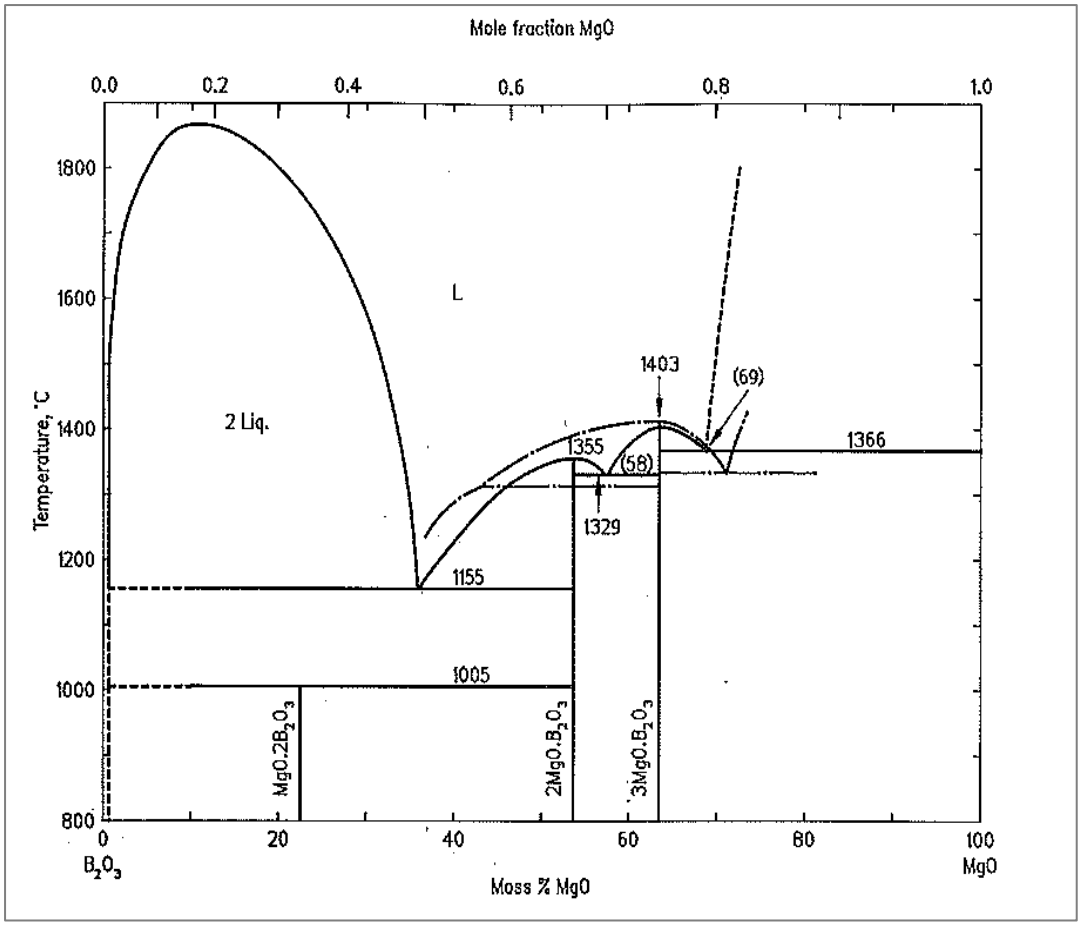


**Figure 23: The $B_2O_3$-MgO system**

### 3.4.6 Alumino-magnesiothermic Slag System

$Al_2O_3$-MgO System

Alumino-magnesiothermic systems form MgO in addition to $Al_2O_3$. MgO is a high melting temperature species which does not flux $Al_2O_3$. Potential alumino-magnesiothermic slag systems may be:

- $Al_2O_3$-MgO
- $Al_2O_3$-MgO-CaO
- $Al_2O_3$-MgO-$SiO_2$
- $Al_2O_3$-MgO-$B_2O_3$
- $Al_2O_3$-MgO-$B_2O_3$-CaO
- $Al_2O_3$-MgO-$B_2O_3$-$SiO_2$

The simplest alumina-magnesiothermic slag system is the $Al_2O_3$-MgO which, may be formed upon complete reduction of $B_2O_3$. Rankin et al. (33)compiled the $Al_2O_3$-MgO binary phase diagram. This system indicates that the eutectic temperature is 1995℃ at 45% MgO content (Figure 24). The high eutectic temperature would thus require the addition of an appropriate flux to reduce the slag liquidus temperature.

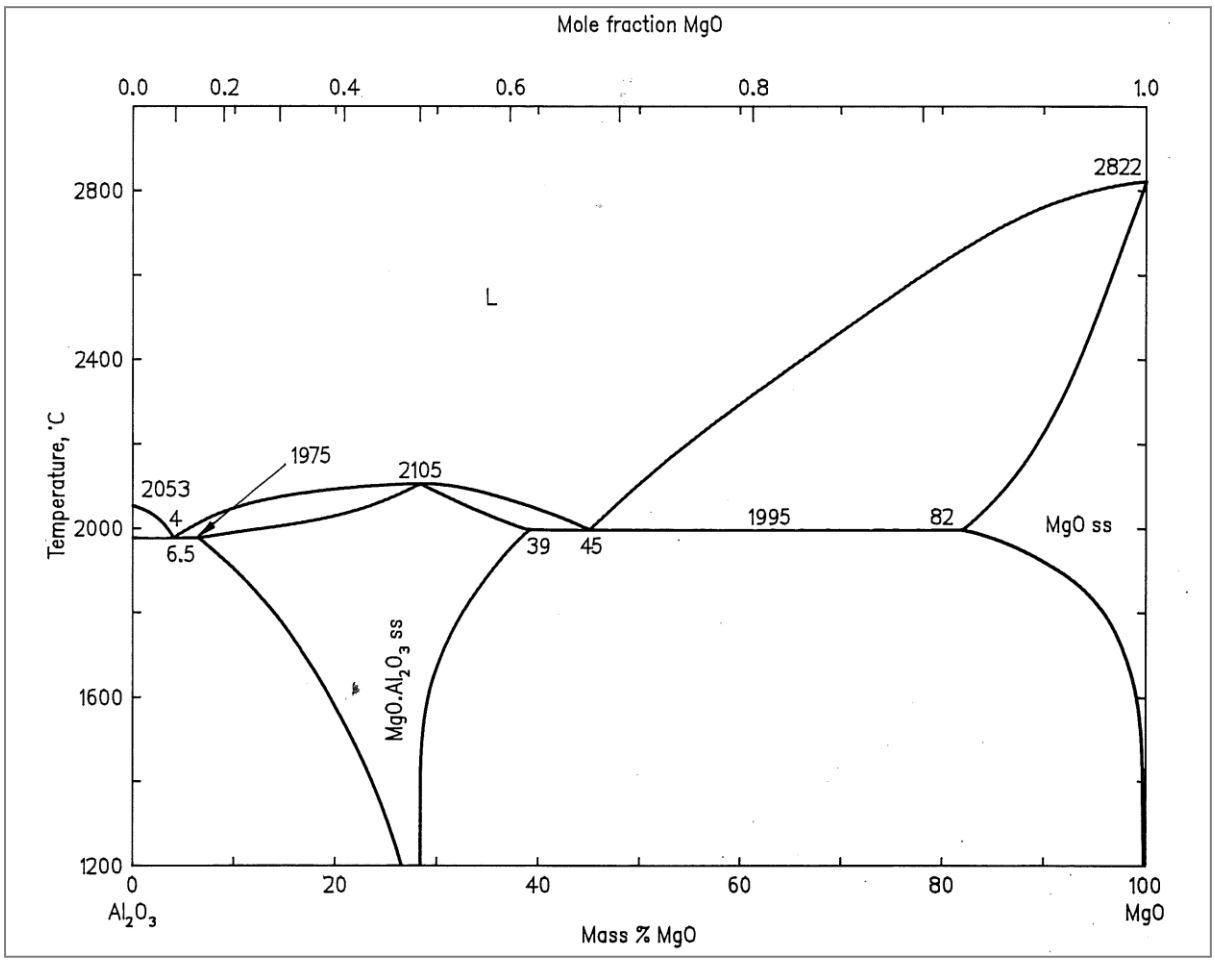


**Figure 24: $Al_2O_3$-MgO binary phase diagram**

<u>$Al_2O_3$-MgO-$B_2O_3$ system</u>

In the alumino-magnesiothermic process, some unreduced $B_2O_3$may report to the slag. Therefore, prior to determining other flux additions, it may be expedient to determine if $B_2O_3$ has a fluxing impact on the slag. If proven, this could simplify the practical operation as $B_2O_3$ is already present in the raw materials thus only necessary adjustments of $B_2O_3$ additions may be reviewed. Furthermore, the addition of other fluxes may introduce contaminants to the system.

$B_2O_3$ is a low melting temperature species compared to $Al_2O_3$ and MgO. Thus, it is possible that excess $B_2O_3$ could flux the formed $Al_2O_3$-MgO. Ternary phase diagrams detailing the thus formed system are limited. Notwithstanding; the $Al_2O_3$-$B_2O_3$-MgO purported by Esmat, Hamzawy and Darwish (34) shows a liquidus/glass region of the system (Figure 25).

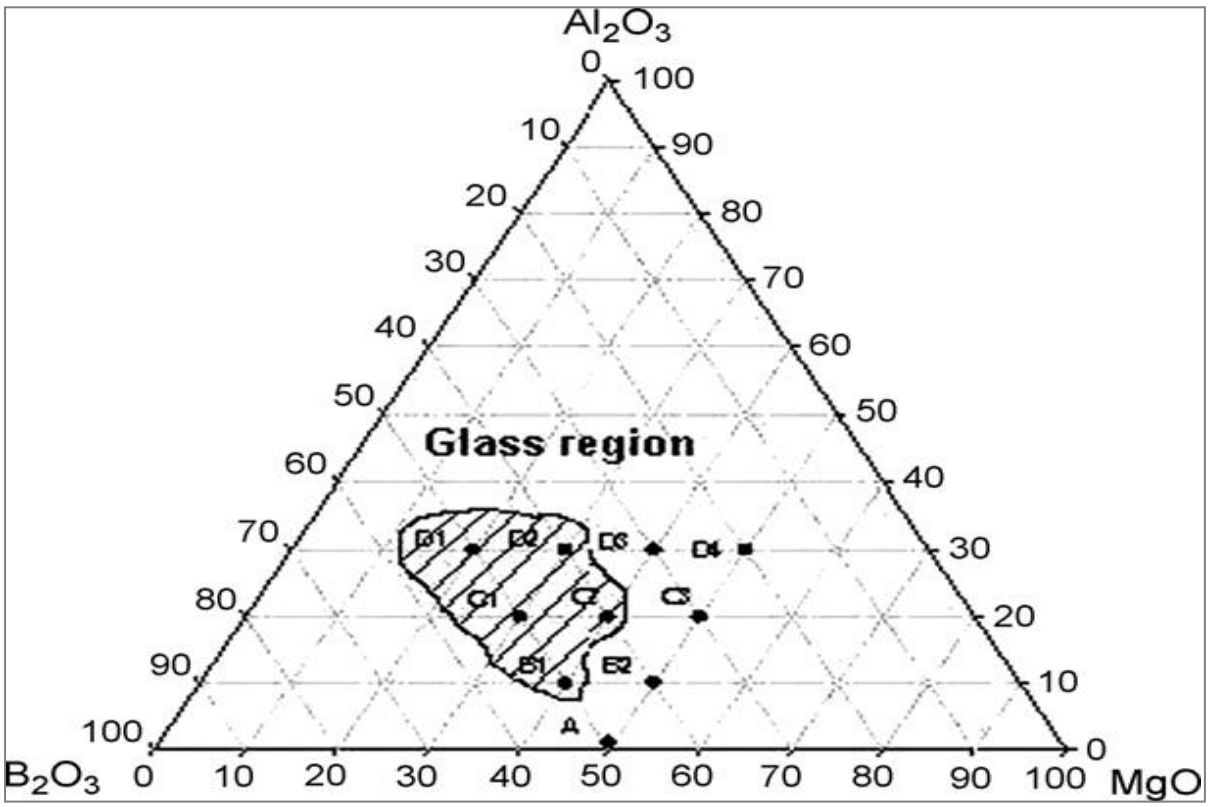


**Figure 25: Ternary phase diagram (mol %) of the $Al_2O_3$-MgO-$B_2O_3$ system with the studied glass system highlighted**

According to Esmat et al. the glass region is a low temperature liquid region. The liquidus temperature ranges from 1300-1400℃. The composition of this glass region which corresponds to the particular points highlighted in the shaded area is tabulated (Table 7).

The ternary system studied by Esmat et al. does not provide sufficient data in accurately determining the alumino-magnesiothermic slag phase.

**Table 7: The investigated liquidus compositions within the $MgO-Al_2O_3-B_2O_3$ system**

| Sample No. | Sample Composition (mol. %) | | | Melting Temperature (℃) |
|---|---|---|---|---|
| | $Al_2O_3$ | $B_2O_3$ | MgO | |
| B1 | 10 | 50 | 40 | 1300 |
| C1 | 20 | 50 | 30 | 1300 |
| C2 | 20 | 40 | 40 | 1400 |
| D1 | 30 | 50 | 20 | 1300 |
| D2 | 30 | 40 | 30 | 1400 |

Kiss et.al (35) investigated the effect of $B_2O_3$ additions on equimolar mixtures of $Al_2O_3$ and MgO with respect to the formation of spinel (spinelization). The experiments were undertaken from 1150 to 1450℃.The degree of spinel formation (spinelization) was reported at 0%, 2.5% and 5% $B_2O_3$ addition. The results are presented in Table8.

**Table 8: The dependence of the degree of spinelization on thermal treatment conditions and system composition**

| Mixture | Degree of Spinelization (%) | | | |
|---|---|---|---|---|
| | 1150℃ | 1250℃ | 1350℃ | 1450℃ |
| 0% $B_2O_3$ | - | 15.2 | - | 57.0 |
| 2.5%$B_2O_3$ | 31.5 | 51.0 | 96.0 | 97.0 |
| 5.0% $B_2O_3$ | 37.0 | 52.5 | 97.0 | 98.0 |

The experimental results show that $B_2O_3$ addition increases spinel formation with increasing treatment temperature.

Further investigations of the $Al_2O_3$-MgO-$B_2O_3$ system in literature, such as the investigations by Sokolov et al. (36) also indicated that $B_2O_3$ is an effective spinel promoter. Therefore; contrary to Chang-ye and Zhang-Guo, and Esmat et al, the effect of $B_2O_3$ on the $Al_2O_3$-MgO system is mainly refractory. This is significant because any unreduced $B_2O_3$ that can report to the slag may increase the likelihood of spinelization. Spinel slags are highly refractory and may cause significant metal losses due to entrainment of metal in the slag.

It is inevitable that due to the unavailability of liquidus $Al_2O_3$-$B_2O_3$-MgO type systems, either $Al_2O_3$-MgO-flux systems or more complex quaternary systems need to be investigated for suitability.

Herein it was discussed that CaO and $SiO_2$ as fluxes of the aluminothermic slags. These components (CaO and $SiO_2$) are known as suitable fluxes for $Al_2O_3$-MgO systems.

$Al_2O_3$-CaO-MgO System

The $Al_2O_3$-CaO-MgO system (compiled by Rankin et al. (37)) shows that the MgO-poor regions are characterized by decreasing liquidus temperature. This trend is particularly discernible at the 50% $Al_2O_3$-50% CaO region as highlighted (Figure 26). It is a possibility that the $Al_2O_3$: MgO ratio of the formed alumino-magnesiothermic slag would shift the system away from the MgO poor area. This shift would result in an MgO rich area with the consequential high temperature liquidus.

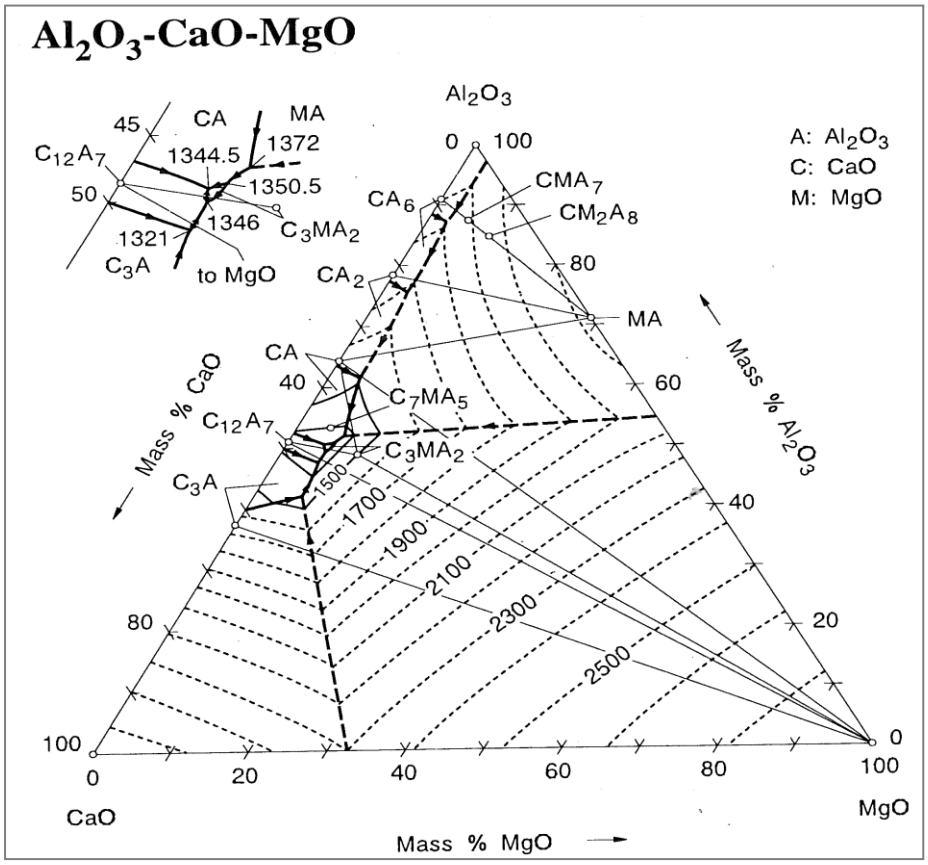


**Figure 26: $Al_2O_3$-CaO-MgO liquidus ternary system**

$Al_2O_3$-MgO-$SiO_2$ System

Silica ($SiO_2$) can be used to lower the melting point of the alumina-magnesia slag. The additional benefit of using $SiO_2$ is that is comparatively low cost and available (i.e. common sand).

The cordierite region of the $Al_2O_3$-MgO-$SiO_2$ system (38)can be suitably used for stoichiometric process (Figure 27). The addition of acidic $SiO_2$ may promote boron recovery. However, there is a risk of preferential reduction of $SiO_2$ at elevated temperature as mentioned previously.

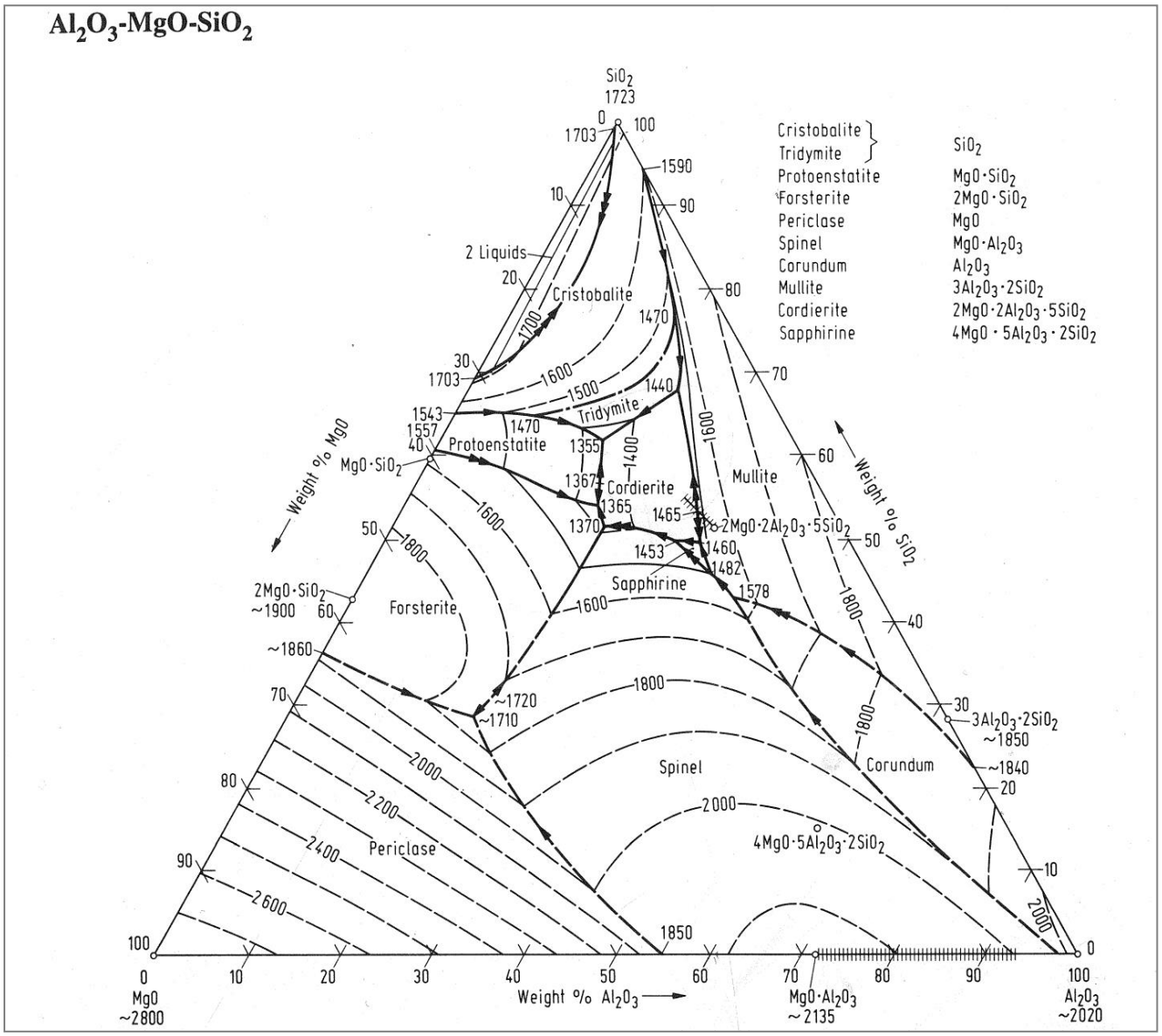


**Figure 27: $Al_2O_3$-MgO-$SiO_2$ liquidus ternary system**

It is notable that irrespective of the flux used in either NiB production process, that additional heat would be required to raise the temperature for adequate mixing. Furthermore, flux addition increase the slag mass as compared to non-fluxed slag. Therefore it is expected that the overall energy requirement would increase. Thus the heat and material balance should account for the influence of fluxes on the overall process.

# 4 EXPERIMENTAL APPARATUS AND PROCEDURE

## 4.1 Experimental Apparatus

Typical metallothermy requires high temperatures and therefore additional energy input, if the process is not self-sustaining. It is common practice to supply additional energy to the system, through electrical energy whether by arc or induction furnace practice. However, in some cases, highly oxidic chemicals can be used to supply the additional heat of reaction. In other cases, pre-heating of reactants may yield a sufficiently autothermic reaction.
However; the use of chemical reaction boosters and or pre-heating of reactants in metallothermy present several practical challenges. These challenges are detailed under the Practical Considerations section of this report. Moreover gas fired furnaces may be used. Gas fired furnaces are generally limited to processes that require lower temperatures than common metallothermic processes.

The additional energy input, whether electrical or chemical energy is typically required to produce liquid products. Liquid slag and metal interact more readily than solid products. These interactions may be manipulated by metallurgist to yield desired products. The furnace design must also cater for the formation and removal of liquid products. It may be necessary to tap the slag and metal if semi-continuous production is required. These practical considerations need to be addressed prior to assembling the furnace.

The production of NiB by the aluminothermic, magnesiothermic and alumino-magnesiothermic processes was investigated in a D.C arc furnace. The reasons for the selection of a D.C. arc furnace are herein discussed.

### 4.1.1 200 kVA D.C. arc furnace

The production of boron alloys is typically undertaken in electric arc furnaces. Tasyurek et al and Yucel et al investigated the production of FeB in electric arc furnaces. Moreover Zhang-Guo and Chang-ye reported that induction furnace production of NiB was possible.
Induction furnaces are generally used for melting massive metallic charges. Reactants used for metallothermy are generally finely divided, granular or powder. In some cases, metal powders may be melted in induction furnaces; however it is uncommon to try melting

electrically non-conductive charges in an induction furnace. Where the metallothermy reactants are a mixture of metal and non-metallic constituents, it requires careful balance to avoid dispersing the metallic phase in the bulk charge to avoid rendering it electrically non-conductive. This may occur when the proportion of electrically insulating non-metallic reactants is significantly greater than the metallic reactants. Contrarily, it may be required that the furnace charge be well mixed to effect good reaction practice.

A D.C. arc furnace overcomes these constraints. A D.C. arc furnace may be designed to melt a completely non-metallic charge as is the case in slag re-melting. Furthermore, D.C. arc furnaces do not necessarily need an electrically conductive charge. Although Zhang-Guo and Chang-ye utilized an induction furnace in their investigations, a D.C. arc furnace may be more suitable in the production of NiB where the bulk charge consists a greater proportion of insulating non-metallic components.
Furnace electrode control practice may be implemented to effect various physical changes to the bulk charge. The electrode may be sub-merged under the slag phase to super heat the metallic phase below (it is common that the slag phase is of lower density than the metallic phase). Open arc processing may be instigated to super heat the slag phase. These and other parameters provide a processing advantage over the induction furnace melting used by Zhang-Guo and Chang-ye.

In semi-continuous production, a D.C. arc furnace may be designed with metal and slag tap-holes at different heights on the furnace body. This allows the separation of the metallic and slag phases during tapping or decanting of liquid products. In some cases, the slag may be selectively decanted/ tapped to increase metal furnace capacity. The design of induction furnaces (i.e. induction coil surrounds the reactor) does not readily allow for this separation. If needed, induction furnace products are commonly separated post decanting. Thus, it may be difficult to maintain a metallic heel in the furnace if the furnace capacity is to be fully exploited for metal holding/production. This was not a significant consideration in this work.

The advantage of using D.C. arc furnace for the production of NiB is that the commercial production of the alloy is undertaken in such furnaces. For this and other reasons previously explained, it was the opinion of this author that a D.C. arc furnace was the most suitable equipment for this investigation.

The experimental runs of this study were conducted in a single electrode 200kVA D.C. arc furnace. The details of the furnace are depicted in Figure 28. The D.C. arc furnace was constructed from a steel shell without water cooling. A graphite crucible was the hot face of the furnace. A self-baking carbon paste was installed at the bottom of the crucible to protect the relatively thin (20mm) crucible bottom from excessive heat and stress. A castable alumina-magnesia refractory was sandwiched between the external steel shell and the graphite crucible to provide thermal insulation and electrical isolation of the furnace.

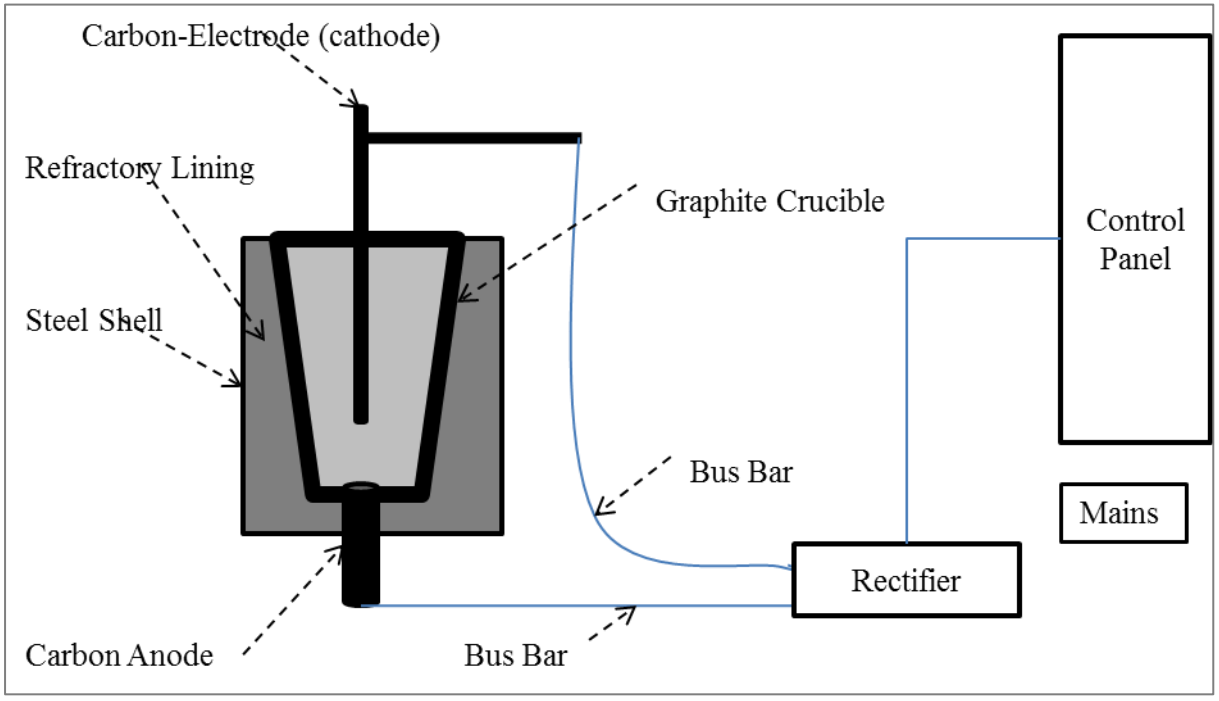


**Figure 28: Schematic of D.C. arc furnace arrangement**

### 4.1.2 Refractories

The choice of refractory is very important in D.C. arc furnace operation. The furnace refractory needs to fulfil multiple roles**.** The refractories need [1] to contain the reaction without failing, [2] provide thermal and electrical insulation of furnace body and [3] be inert to chemical attack of the reactants.

#### *4.1.2.1 Thermal Shock Resistance and Electrical Isolation*

The refractory chosen as the furnace lining material needs to be electrically non-conductive or electrically isolated to avoid making the furnace body live. Thus electrically conductive linings such as graphite crucibles/bricks need to be isolated. An electrically live furnace body

poses high safety hazard, hence the use of proprietary alumina-magnesia refractory between the steel shell and the graphite crucible

The refractory used in the furnace lining should generally be resistant to thermal shock because operating a D.C. arc furnace involves rapid heating from cold. If the refractory lining were to crack due to the stresses imposed by heating from ambient temperature, this can cause lining failure which poses a safety hazard. Due to the design of the furnace lining and shell, the graphite crucible was constantly under compression. The thermal expansion of the alumina-magnesia refractory increased the forces on the graphite crucible, in effect increasing the strength of the crucible. Therefore if the crucible were to crack, there was sufficient force on the crucible to mitigate crack propagation. Moreover, the authors referred to previously conduct their investigations in graphite crucibles/lining without any reported failure.

#### *4.1.2.2 Thermal Insulation*

The furnace lining must withstand high temperatures without melting. Graphite has melting temperature above 3000°C and would not melt under the conditions investigated. Moreover, the technical datasheet of the proprietary castable refractory indicated that the maximum operating temperature is 1850°C. However, graphite has a high thermal conductivity as compared to common refractories as depicted in Figure 29 (Lecture Notes, (39)).

The 200kVA D.C. arc furnace used was not water cooled; therefore the insulating properties of the castable refractory lining are important in order to avoid excessive heat loss. If the refractory is poorly insulating, the steel furnace shell may be raised to its softening temperature resulting in loss of structural strength of the shell. The castable refractory supplier informed the author that the thermal conductivity properties of this castable were between the $Al_2O_3$ and MgO trends as shown in Figure 29.

The roof lining is typically a castable refractory in production scale D.C. arc furnaces. However, in this work since metal and slag were manually tapped from the top, it was necessary to avoid a top-heavy structure. However it was also important to provide sufficient insulation from radiant heat losses. The furnace roof was insulated by using 96 kg/m$^3$ ceramic wool. This assisted in minimizing radiant heat losses and material loss on ignition without negatively affecting the centre of gravity of the furnace.

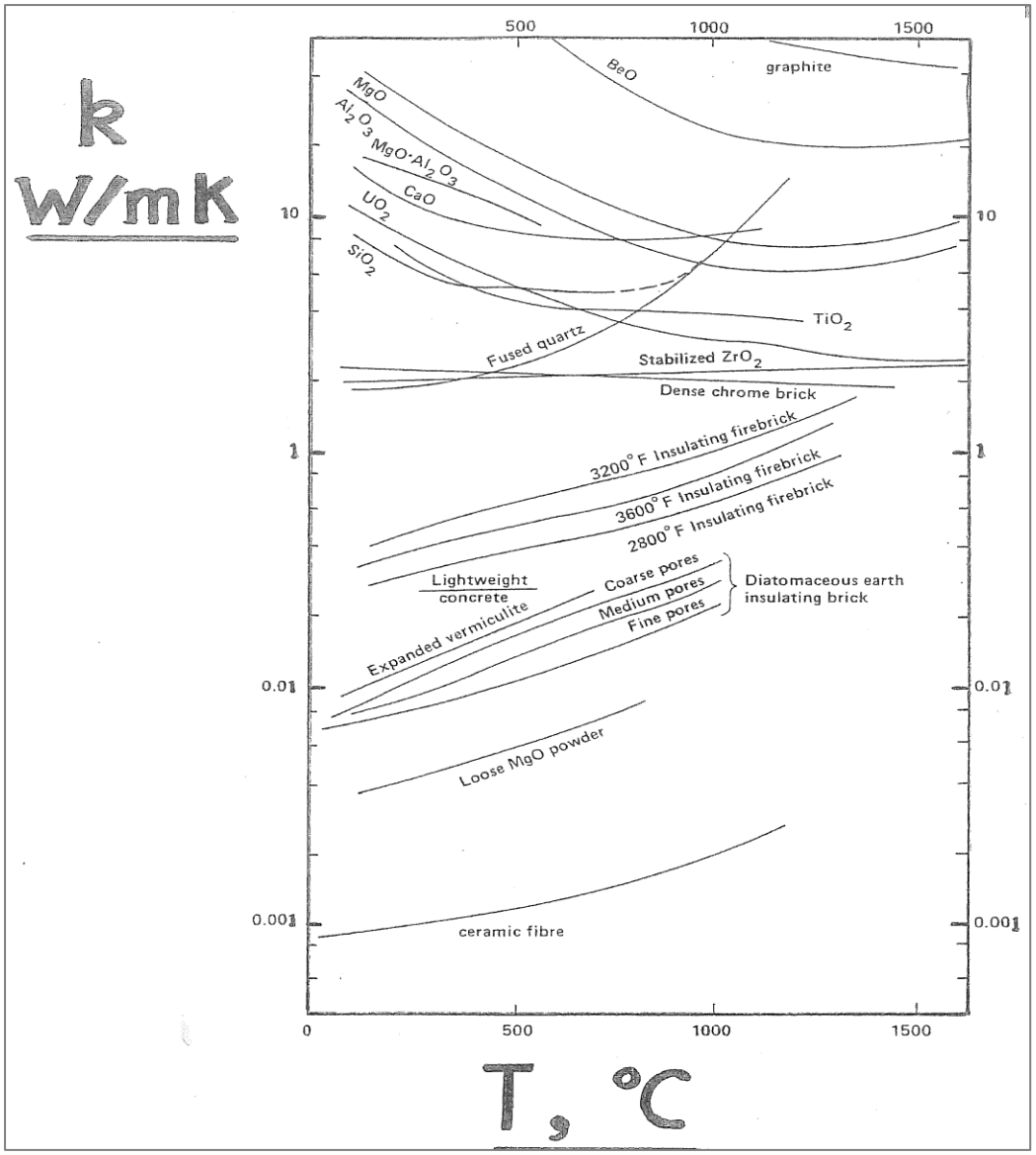


**Figure 29: Thermal conductivity of various refractory materials**

### *4.1.2.3 Resistance to Chemical Attack*

The refractory must be resistant to chemical attack. $B_2O_3$ has significant fluxing properties over several oxides. However, the carbothermic reduction of $B_2O_3$ is endothermic. As mentioned, in the literature review Tasyurek et al reported a carbon content of carbothermic NiB to range between 0.06-0.07% t after 60 minutes of reaction time. Moreover Yucel et al also reported that the C content of NiB sampled from the bottom of the furnace near the hot zone was 0.1%. The conditions underneath the electrode are characterized by high temperatures which could promote carbide formation reactions. These observations indicated that once B was formed, boron-carbides did not readily form. Moreover, a comparison of

Gibbs free energy change (of the Ellingham Diagram) for the carbothermic and aluminothermic/magnesiothermic reduction of $B_2O_3$ favoured the metallothermic processes mentioned. Thus the reduction of $B_2O_3$ would primarily be through the metallothermic rather than the removal of C from the crucible to effect $B_2O_3$ reduction. This may contribute to or prolong crucible life.
The chemical interaction between the graphite crucible and input materials was investigated and is reported in this work.

The self-baking furnace bottom as common to arc furnace alloy production contained maximum 5% ash. However, the proprietary chemical analysis of this ash was not supplied. Ash typically contains oxides of silicon, iron, aluminium and sodium. Hence it would be possible that some ash from the bottom would be reduced, particularly silica and iron oxides. Sodium oxides would typically volatilize at the operating temperatures.

### 4.1.3 Challenges of D.C. Arc Furnace Operation

There are multiple challenges in operating a D.C. arc furnace. These challenges have been discussed with reference to the furnace lining. The other problems that may be encountered in operating a D.C. arc furnace are arc flare, anode meltdown and temperature measurement.

#### *4.1.3.1 Arc Flaring*

Arc flaring occurs when the arc produced by the electrode skews away from the anode and electrical contact is obtained through the furnace wall. This transfers the energy to the furnace lining or wall. Excessive arc flaring may cause erosion of the refractory furnace wall. This was prevented by operating the furnace with minimum open arc. Moreover, the automatic control of the electrode was controlled by voltage. This meant that as the electrode was raised away from the anode, the voltage requirement increased in order to overcome the resistance of the burden. The raising of the electrode height was controlled to result in minimum open arc to mitigate arc flaring.

#### *4.1.3.2 Mitigating Anode Meltdown*

High temperatures are typical at the anode, so it was decided that a graphite anode mitigated the risk of anode meltdown which is generally observed with multi-pin metal anodes. The graphite anode was connected to a copper bus bar underneath the furnace.

#### *4.1.3.3 Temperature Measurement*

The highest operating temperature of this furnace is 1800℃, whereas the maximum safe operating temperature was 1650℃. The temperature was measured by an immersion thermocouple with a reliable operating range from 0 to 1800℃.

#### *4.1.3.4 Furnace Capacity*

The maximum charging capacity of the D.C. arc furnace was 50kg which was considered suitable for sample masses producing 10kg of alloy

## 4.2 Experimental Procedure

A 150kg maximum capacity scale was used to weigh out the samples and the charge products.
Each batch input material was weighed and batches were mixed in the small-scale concrete-type mixer for 10 minutes. The mixer was then carefully emptied into a collection bin prior to loading the furnace.

Prior to loading the furnace, it was important that an electrical contact between the electrode and anode was established. This was achieved by lowering the electrode to form an electrical contact with the anode prior to charging of materials and when furnace power was switched off. This ensured safe and effective electrical ignition of charge. The whole charge was loaded in the furnace whilst the electrode was in contact with the anode thereafter the furnace power was switched on. After ignition of charge, ceramic fibre with a small observation window was used as the furnace lid or roof.

When the furnace power was switched on, maximum current draw occurred due to the proximity of the electrode and anode. The current draw was reduced by raising the electrode until an arc was struck. Once the arc was struck, the electrode was raised slowly through the furnace burden. This ensured that the electrical contact of the electrode and anode through the arc was not broken. The high temperature of the arc ignited the charge. As the reaction continued, a fluid slag layer formed. The electrode was raised just above the slag layer in order to maintain a consistent arc.
The process time was recorded from the time the furnace power was switched on.

After the 30 minutes of experimentation, the contents of the furnace were decanted into a cast iron chill mould.
The 30 minutes reaction time was determined from industrial experience, in which more than 50kg metal producing thermites were completely reacted in the same time. Therefore at 10kg anticipated metal production, the 30 minutes reaction time was considered adequate.

Temperature measurements were taken at the end of the process. If the temperature was higher than the 1650℃ this posed a risk to downstream handling of the decanted material. The cast iron chill of which the furnace contents were decanted into would melt and the metal would burn through. This phenomenon has been observed in related thermite experiments.
Thus, if furnace temperatures exceeded 1650℃ at the end of the reaction, the furnace was allowed to cool. Frequent temperature measurements were done as the furnace was cooling. Once the furnace contents reached 1650℃ (±20℃) contents were decanted into the chill.

### 4.2.1 Sample Preparation

From an industrial point of view, in order to analyse samples and obtain reliable analytical and production data, a 10kg total mass of alloy products was considered as sufficient.

After solidification and cooling of the chill contents, the slag and metal were separated by mechanical means. The metal was weighed in order to assist in metal recovery calculations. Metal and slag samples for chemical analysis were prepared. They were prepared by separately crushing the metal or slag and retrieving a 50g sample. The metal was analyzed for the B content and Al, Fe, Mg, Si, P and C in an attempt to determine the relative purity of the alloy. Ni reported was by balance. ICP-OES wet chemical analysis was used for all the elements except C, where the LECO™ carbon-sulphur combustion technique was used. The slag samples were analysed by similar ICP-OES analysis method. The $B_2O_3$, MgO, $Al_2O_3$, $SiO_2$, and CaO content was deduced from the ICP-OES elemental results of the slag.

The furnace was cleaned of any remnants of the previous reaction before each experimental run. This was done to minimize cross-contamination of runs.

### 4.2.2 Input Materials

The experimental runs were categorized into [1] Aluminothermic, [2] Magnesiothermic and [3] Alumino-magnesiothermic experiments. The calculated thermochemical data was used to determine the quantities of input materials for the respective processes.

#### *4.2.2.1 Aluminothermic Input Materials*

The input materials of the aluminothermic experiments are presented in Table 9.

**Table 9: Purity of aluminothermic input materials**

| **Raw Material** | **% Purity** |
|---|---|
| $B_2O_3$ | 98.8 |
| Ni | 99.9 |
| Al | 96.0 |
| CaO from calcined $CaCO_3$ | 92.0 |

As the input materials were less than 2mm in size, it was important to use calcined $CaCO_3$. The calcination of $CaCO_3$ generates $CO_2$gas which may blow off some of the charge material. The specific physical data sheets of these materials were appended.

A stoichiometric charge was the first run in each of the experiments. Thereafter, excess amounts of Al and $B_2O_3$ were varied for each successive run. When Al was varied, $B_2O_3$ was fixed at the stoichiometric requirement. Thereafter; when $B_2O_3$ excess was changed the Al requirement was fixed at the stoichiometric equivalent. Increasing $B_2O_3$ excess was instituted to promote B yield and refine the alloy of Al.

#### *4.2.2.2 Magnesiothermic Input Materials*

The magnesiothermic reactions were relatively simple because the MgO was fluxed by $B_2O_3$. The input materials of this reaction were NiMg fines, supplementary Mg chips (between 2-20mm) and $B_2O_3$. Table 10 presents the relative purity of the raw materials used in the magnesiothermic experiments.

**Table 10: Purity of magnesiothermic input materials**

| Raw Material | % Purity |
|---|---|
| $B_2O_3$ | 98.8 |
| NiMg | 2.17:1 mol ratio |
| Mg | 99.98 |

Similar experimentation logic as in the aluminothermic reactions was applied to the magnesiothermic reactions. The influence of the reactants, Mg chips and $B_2O_3$, were investigated. The chemical specification of the Mg chips used is appended. The Mg content of NiMg was fixed at 2.17mol Ni to 1mol Mg.

#### *4.2.2.3 Alumino-magnesiothermic Input Materials*

The input materials of the alumino-magnesiothermic process were Al, $B_2O_3$, NiMg fines and $SiO_2$ which was used as flux. The +2mm NiMg fines were screened off and -2mm fines were used. Silica ($SiO_2$) was similarly screened with a 2mm screen and the -2mm fraction was used as flux. The relative purity of these input materials is presented in Table 11. The chemical and size distribution data of the input materials is appended.

**Table 11: Purity of alumino-magnesiothermic input materials**

| Raw Material | % Purity |
|---|---|
| $B_2O_3$ | 98.8 |
| NiMg | 2.17:1 mol ratio |
| Al | 96.0 |
| $SiO_2$ | 99.4 |

The excess amount over the stoichiometry requirement was successively increased for Al and $B_2O_3$.The investigation of Mg (dissolved Mg) impact on the NiB production process requires special consideration; because the Mg content in NiMg alloys as discussed earlier is a limiting factor for NiB production.

# 5 RESULTS

## 5.1 Thermodynamic Studies and Calculation of Metal and Relevant Slag Systems

The HSC 6.1 ™ thermodynamic software package uses an extensive in-built thermochemical dataset of over 20000 species for various thermodynamic calculations. The software package was used to determine the enthalpy and entropy changes and heat capacity to determine thermodynamics involved in the production of NiB. The relative energy requirement for the process was determined by the overall heat balance of the NiB system. The thermo-chemistry computer simulations were based on the metallothermic reduction principles.

### 5.1.1 Metallothermic Reduction of $B_2O_3$

As mentioned earlier, the Gibbs free energy rule assisted in determining the most suitable reductant for the reaction. The HSC 6.1™ program computes data on Gibbs free energies of formation. The results of these calculations were projected as an Ellingham Diagram.

The reduction of $B_2O_3$ produces elemental B, which was dissolved in Ni to form NiB. The reaction may be represented by the equation:

$$zM + B_2O_3 = zMO_{3/z} + 2B(in\ Ni) \quad \text{(eq.3)}$$

There are various metals used for metallothermic reduction, such as Si, Al, Mg and Ca. The reduction of $B_2O_3$ by these metals can be described by the following chemical reactions:

$$^3/_2\, Si + B_2O_3 = {}^3/_2\, SiO_2 + 2B \quad \text{(eq.4)}$$

$$2Al + B_2O_3 = Al_2O_3 + 2B \quad \text{(eq.5)}$$

$$3Mg + B_2O_3 = 3MgO + 2B \quad \text{(eq.6)}$$

$$3Ca + B_2O_3 = 3CaO + 2B \quad \text{(eq.7)}$$

The standard free energies of formation of the reactants were obtained from the thermochemical tables compiled by E.T. Turkdogan (40) and are presented in Table 12.

**Table 12: Standard free energy of substances relevant to NiB production**

| Substance | Standard free energy of formation, ΔG° (J/mol) |
|---|---|
| $B_2O_3$ | -1228841+210.0T |
| $SiO_2$ | -896255+170.7T |
| $Al_2O_3$ | -1687240+326.8T |
| MgO | -729606+204.1T |
| CaO | -560656+83.9T |
| NiB | -175728+8.4T |

The Ellingham Diagram depicts the standard free energy changes of the above reactions (eq.4 to eq.7) (Figure 30).

The plots of Si, Al, Mg and Ca showed that these reductants could reduce $B_2O_3$ at the temperature range depicted in the diagram. The feasibility of such reactions could be identified since all the reductant lines plotted were below the $B_2O_3$ line, across this temperature range depicted. The only exception was the Si line, which intersected the $B_2O_3$ line at 1750℃. As stated earlier, the feasibility of a reaction does not provide reaction kinetics data.

Calciothermic reduction was found to be the most thermodynamically favourable process as shown on the Ellingham Diagram and silicothermic reduction the least favourable process (Figure 30).
The Gibbs free energy of formation was not the only criterion used to choose the most appropriate reductant. In addition to the thermodynamics, chemical stability, reductant consumption rate per unit of B produced and the cost of the reductant were criteria used to determine the most suitable reductant.

### 5.1.2 Reductant Consumption Rate and Cost per unit B Produced

The stoichiometric relationship between the reductants and boron shown in reactions eq.4 to eq.7 has a direct impact on the reductant requirement rate. Table 13 shows the cost of the stoichiometric reductant requirement to produce 1.0kg of B. The cost of reductant has been sourced from various suppliers.

**Table 13: Cost and consumption rate of reductant per kg B produced**

| Reductant | US$/kg Reductant | kg reductant /kg B produced | US$/kg B produced |
|---|---|---|---|
| Si | 1.825 | 1.949 | 3.556 |
| Al | 2.000 | 2.496 | 4.992 |
| Mg | 2.825 | 3.373 | 9.528 |
| Ca | 4.723 | 5.562 | 26.264 |

It is evident that calciothermic reduction would be the most reductant and cost intensive process.

The NiB alloy specification has a 0.50% maximum Si content. Hence, the least thermodynamically favourable reaction (the silicothermic process) may require high reductant excess to drive the reaction to completion. High Si reductant excess might cause Si contamination of the alloy. The combination of the above factors precludes Si and Ca as potential reductants.

The Al and Mg based processes were chosen for the relatively low reductant cost and also the ability to use the passivated Mg in NiMg alloy fines and other reasons mentioned in the introductory chapter of this report.

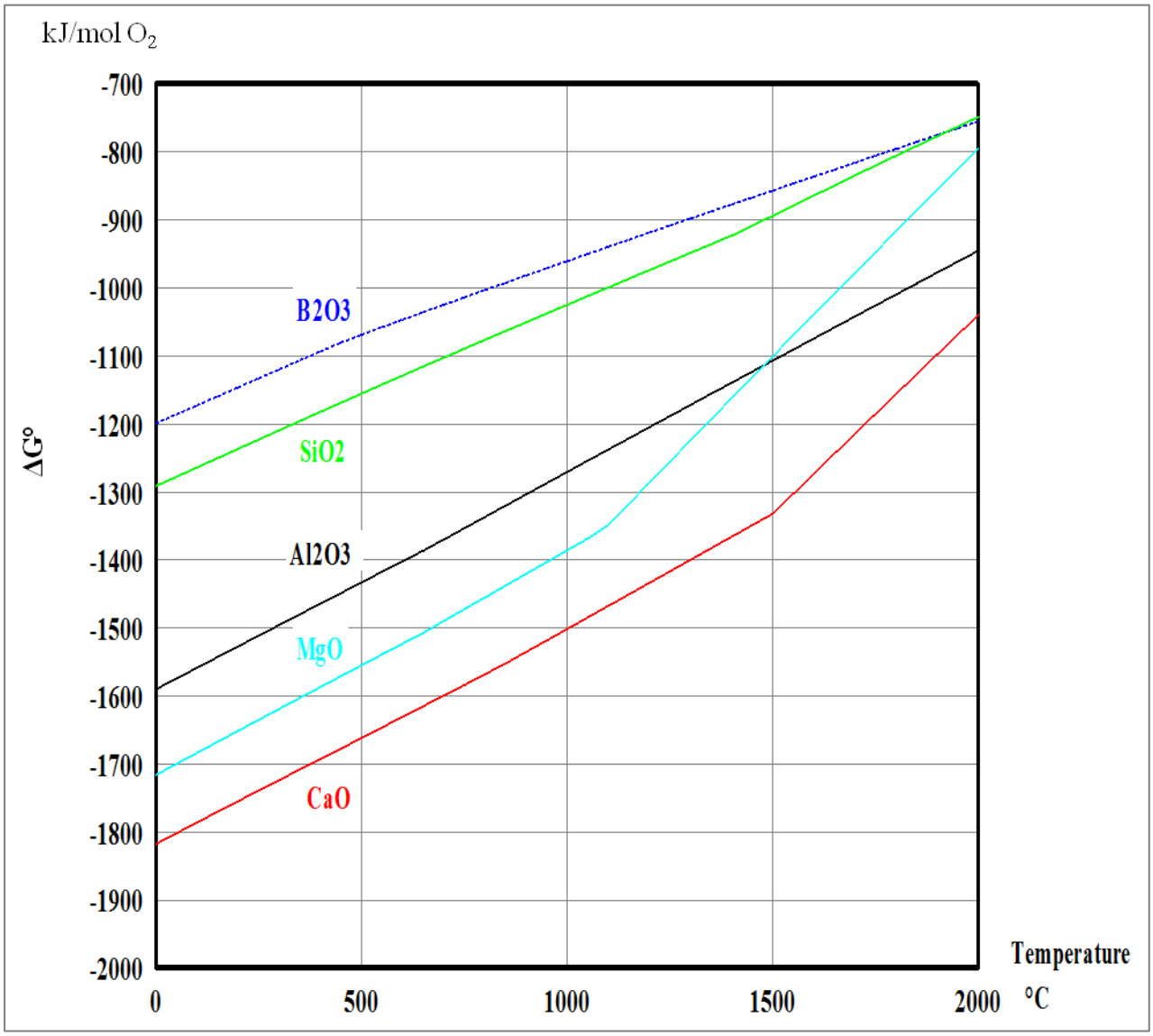


**Figure 30: Ellingham diagram showing the $B_2O_3$, $SiO_2$, $Al_2O_3$, MgO and CaO Gibbs free energy**

### 5.1.3 Aluminothermic and Magnesiothermic Reactions

All the aforementioned reactions (of which Si, Al, Mg and Ca, are reducing agents) are exothermic. However, it is the aim of this work to investigate the aluminothermic, magnesiothermic and the alumino-magnesiothermic production of NiB.

The heat output of the aluminothermic and magnesiothermic reduction of $B_2O_3$, reactions (eq.8) and (eq.9) respectively, are shown.

$$Al + \frac{1}{2}B_2O_3 + Ni = \frac{1}{2}Al_2O_3 + NiB \qquad \text{(eq.8)}$$

$$\Delta H^\circ_{298} = -248.34\ kJ/mol\ Al$$

$$\Delta G^\circ_T = -404928 + 66.8T\ J/mol$$

$$Mg + \frac{1}{3}B_2O_3 + \frac{2}{3}Ni = MgO + \frac{2}{3}NiB \qquad \text{(eq.9)}$$

$$\Delta H^\circ_{298} = -208.59\ kJ/mol\ Mg$$

$$\Delta G^\circ_T = -437144 + 139.7T\ J/mol$$

These reactions, although exothermic, are not autothermic. Thus the metal and slag phase will not separate adequately without additional heat. The guideline for autothermic aluminothermic reactions is that $\Delta H^\circ_{298}$ of the reaction should be less than $-300$kJ/mol Al. This guideline proposed by W. Dautzenberg in *Metallurgie der Ferrolegierungen* (12). Later and more comprehensive guideline suggested by Gupta (41) ,states that the heat of reaction per gram of charge (either reactants or products) should be between 540 cal. (2259J) and 950 cal. (3975J) for a controlled autothermic reaction. If the heat of reaction is below 2260J the reaction would not be autothermic. However, if the heat of reaction is more than 3980J per gram of charge, the reaction may be violent or even explosive. The heat of reaction (eq.8) was found to be 492.6 cal. or 2061J per gram of charge. Thus the two guidelines were in agreement showing that the reaction (eq.8) would not be autothermic.

The heat of reaction per gram of charge for the magnesiothermic reaction (eq.9) was found to be 2407J. However, it is noteworthy that, the MgO formed in the magnesiothermic reaction has a higher melting point (2822°C) than $Al_2O_3$ (2053°C). Therefore, it is logical that the magnesiothermic reaction could require more additional heat as compared to the aluminothermic reaction. The guidelines purported by Gupta and Dautzenberg are illustrative and not prescriptive.

Heat of reaction was one of the criteria used to determine reaction thermodynamics. However, the free energy change of reaction was the main criterion used to determine the feasibility of reaction. Thus, by substituting the operating temperature of 1650°C or 1923K

into the relevant standard free energy change equation, the feasibility of the reaction may be deduced.

Therefore, in the case of the aluminothermic production of NiB as presented by reaction (eq.8), the standard free energy change may be computed:

$$\Delta G^{\circ}{}_{1923} = -404928 + 66.8 \times 1923$$

$$\Delta G^{\circ}{}_{1923} = -276471.6 \ \ J/mol$$

The negative value showed that under standard conditions, it would be possible to produce NiB through reaction (eq.8).

The same computation may be applied for the magnesiothermic reaction (eq.9):

$$\Delta G^{\circ}{}_{T} = -437144 + 139.7 \times 1923$$

$$\Delta G^{\circ}{}_{1923} = -168500.9 \ \ J/mol$$

Similarly, the magnesiothermic production of NiB as represented by reaction (eq.9) was determined to be feasible under standard conditions.

### 5.1.4 Dual Reduction Thermochemistry

The net reaction of aluminothermic and magnesiothermic reductions reactions (eq.8) and (eq.9) as expressed per mol Al may be written as:

$$Mg + Al + \frac{5}{6}B_2O_3 + \frac{5}{3}Ni = \frac{1}{2}Al_2O_3 + MgO + \frac{5}{3}NiB \qquad \text{(eq.10)}$$

The heat of reaction, $\Delta H^{\circ}{}_{298}$ (eq.10) was determined to be $-456.93$kJ/mol Al or 2206J/g of charge

The high energy output of this reaction can promote good slag and metal separation. Although in this case, the two autothermic reaction heat guidelines were not in agreement. The later guideline, as purported by Gupta (41), suggested that reaction (eq.10) would not be autothermic. Whereas the heat of reaction per mol of Al guideline (suggested by

Dautzenberg) indicated that reaction would be autothermic. It was previously mentioned that the autothermicity guideline as proposed by Dautzenberg was limited to wholly aluminothermic reactions (12). It was such that the later guideline was more useful as it covered a wide range of metallothermic reactions, inclusive of reactions where more than one metal was used as a reductant.

The standard free energy change of the combined reactions as represented by reaction (eq.10) was equivalent to the sum of the standard free energy change of reactions (eq.8 and eq.9). The standard free energy change of reaction (eq.10) with respect to temperature can be written as:

$$\Delta G^{\circ}{}_{T}(eq.10) = \Delta G^{\circ}{}_{T}(eq.8) + \Delta G^{\circ}{}_{T}(eq.9)$$
$$= -404928 + 66.8T - 437144 + 139.7T$$
$$\Delta G^{\circ}{}_{T}(eq.10) = -842072 + 205.5T\ J$$

. Thus as 1923K the standard free energy of reaction (eq.10) may be found. The operating temperature may be substituted into the T term of the above reaction to determine the feasibility of the reaction as follows:

$$\Delta G^{\circ}{}_{T}(eq.10) = -842072 + 205.5 \times 1923$$
$$\Delta G^{\circ}{}_{1923}(eq.10) = -446895.5\ J$$

The dual reduction of $B_2O_3$ with Al and Mg to form NiB according to reaction (eq.10) at 1650°C is comparatively more negative than the individual reactions (eq.8) and (eq.9). It therefore can be concluded that under standard conditions, reaction (eq.10) would be more feasible than either reaction (eq.8) or (eq.9).

#### *5.1.4.1 The use of Mg in NiMg fines*

The molar ratio of NiMg in reaction (eq.9) was 2:3. However, the molar ratio of Ni: Mg in NiMg fines under consideration ranges from 1.95:1 up to 2.35:1. The common Ni: Mg ratio of the NiMg fines used was 2.17:1. The magnesiothermic reaction using common NiMg alloy with the omission of the inherent 2.17 mols of carrier Ni, is represented in (eq.11):

$$Mg(in\ 2.17Ni) + \frac{1}{3}B_2O_3 = MgO + \frac{2}{3}B(\ in\ 2.17Ni) \qquad \text{(eq.11)}$$

Unlike reaction equation (eq.9), reaction (eq.11) does not produce metallic NiB compound or Ni-B alloy with B content (by atomic mass) greater or equal to 15%. The alloy produced by

the reaction (eq.11) contains 2.17mols of Ni and 0.666mols of B. The composition of such produced alloy can be calculated from the molar weights.

The masses of B and Ni in the alloy can be obtained as follows:

$$Mass\ of\ Ni = mols\ of\ Ni \times Mw_{Ni}$$

$$Mass\ of\ Ni = 2.17 \times 58.69 = 127.36g$$

$$Mass\ of\ B = mols\ of\ B \times Mw_{B}$$

$$Mass\ of\ B = \frac{2}{3} \times 10.81 = 7.21g$$

The mass percentage of B in the alloy can then be calculated by using the following equation:

$$Mass\ \%\ of\ i = \frac{mass\ of\ i}{Total\ mass\ of\ Alloy} \times 100\%$$

$$Mass\ \%\ of\ B = \frac{7.21}{127.36 + 7.21} \times 100\%$$

The B content of the alloy was calculated to be 5.36%, and the balance Ni. The computation showed that utilizing Mg in NiMg fines would not yield the required B content of the alloy. Thus additional reductant would be required to boost the B content of the alloy formed according to reaction (eq.11). Al and or additional Mg may be used as reductants.

#### *5.1.4.2 Supplementary Mg*

The use of additional Mg to boost the B content of reaction (eq.11) posed two challenges. First, the NiMg fines under consideration were generated as a by-product of the NiMg master alloy production process. It was as previously stipulated that the Mg content of these alloys and their subsequent fines were fixed. Moreover, the Mg content of the NiMg master alloys mentioned would not result in the minimum B specification of the final alloy. Therefore, investigating the effect of Mg in the NiB formation process invariably resulted in the use of unalloyed Mg. The Mg used was in the form of 2-20mm chips.

The use of Mg chips led to the second challenge. At high temperatures, dissolved or alloyed Mg behaves far differently to pure unalloyed Mg. The boiling point of pure Mg is at a relatively low temperature of 1088°C when compared to the desired operating temperature of 1650°C. The reaction and rate kinetics of the possible Mg reduction and of the evaporation of Mg below 1088°C were unknown. Therefore, if unalloyed Mg completely reacts with $B_2O_3$ before the boiling point, it could be possible to use Mg chips to supplement the B yield of the reduction reaction (eq.11).

Such a reduction reaction was assumed to follow reaction (eq.12), which may be written as:

$$\frac{4.51}{2}Mg(unalloyed) + Mg(in\ 2.17mol\ Ni) + \frac{2.17}{2}B_2O_3 = \frac{6.51}{2}MgO + 2.17NiB \quad \text{(eq.12)}$$

The Mg chips used for this work ranged between 2-20mm.Unlike Al, Mg does not form a contiguous passivating oxide layer around the Mg particle. Spontaneous oxidation of Mg may occur upon contact with oxygen in the atmosphere or water vapour. In bulk Mg particles, the Mg oxidation reaction is relatively slow because Mg ingots (100-600mm) need not be stored under special atmospheres to prevent excessive oxidation. However; Mg powder (-2mm) readily reacts with moisture and oxygen from the atmosphere. This can cause significant handling hazards particularly when the Mg is agitated. Such conditions could be found during mixing of reactants in the small-scale mixer. It was therefore decided that the use of Mg powder (-2mm) posed significant handling hazards due to the inherent reactivity of Mg.

#### *5.1.4.3 Supplementary Al*

The other reductant that was investigated, along with alloyed Mg, was Al. Al has several practical advantages over Mg.

Although the standard free energy change of the aluminothermic reduction reaction (eq.8) was determined to be less negative than the magnesiothermic reaction (eq.9), Al has a higher boiling point than Mg. The boiling point of Al was found to be 2519°C. The benefit of the higher boiling point was that Al could be reacted with $B_2O_3$ with minimal evaporation at the desired operating temperature. Moreover, the low vapour pressure ensured safe operating conditions without excessive pressure build-up in the furnace. Although the vapour pressure of Al and unalloyed Mg were not recorded, it was observed during the experiments that Mg volatilized more readily. Conversely the wholly aluminothermic process indicated no flaring of Al.

The dual utilization of Al and NiMg fines followed a similar approach to reaction (eq.12). The Mg in the equation represents the alloyed Mg. The reduction of $B_2O_3$ with supplementary Al and dissolved Mg was assumed to be represented by reaction (eq.13):

$$2.17(Ni) + (Mg) + \frac{4.51}{3.00}Al + \frac{3.26}{3.00}B_2O_3 = MgO + \frac{4.51}{6.00}Al_2O_3 + 2.17NiB \quad \text{(eq.13)}$$

Reactions (eq.11) to (eq.13) included alloyed reductants and thus deviated from standard conditions. Therefore, the standard free energy and heat of reaction could not be strictly applied.

Due to the lack of thermochemical data for the non-standard reactions, in an attempt to prove or disprove that the autothermicity of reaction (eq.13) a charge designed to yield 1.0kg NiB alloy was prepared. A1.0kg Fe producing hematite thermite charge was designed for comparison purposes. The hematite thermite is known to be autothermic. The charges were reacted in separate crucibles and compared with respect to slag metal separation.
Upon examination of reaction products, it was observed that the hematite thermite (Specimen A) reaction produced a well separated metal and slag as shown in the photograph (Figure 31). Comparatively, the alumino-magnesiothermic NiB producing bench scale experiment produced small metal spheroids (<5mm diameter) that were distributed throughout the slag matrix .No characteristic metal button at the bottom of the crucible was observed as can be seen in Specimen B (Figure 31).

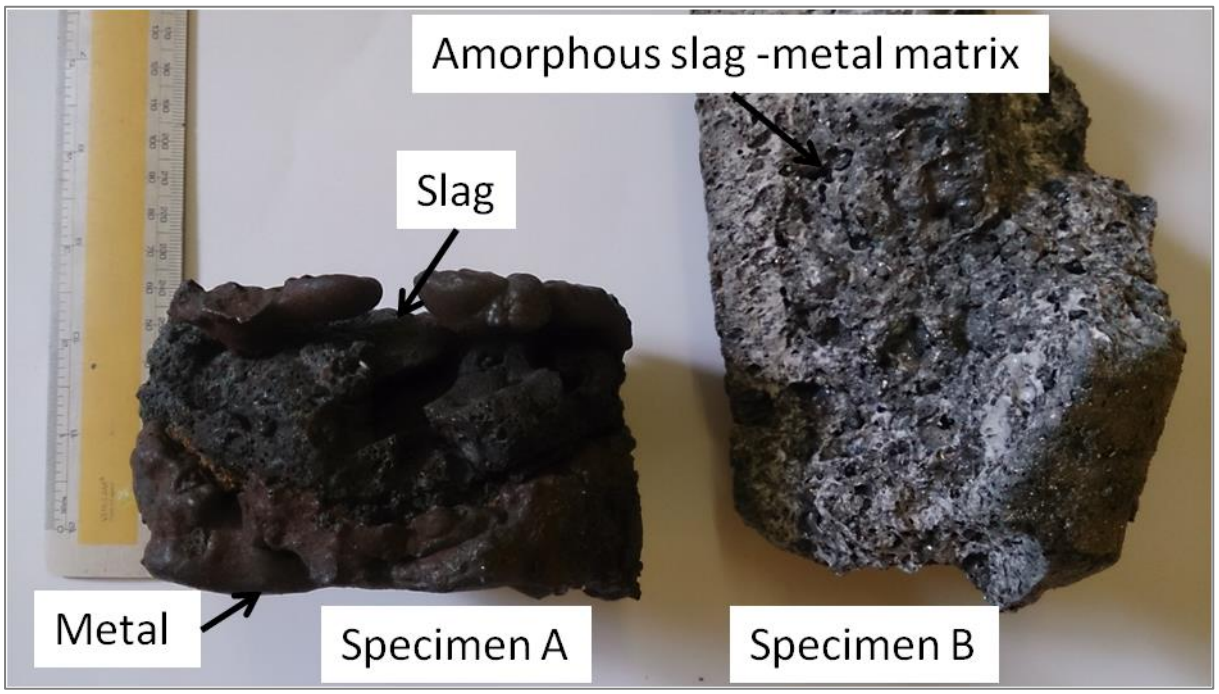


**Figure 31: Photograph of products of the hematite and alumino-magnesiothermic crucible experiments**

### 5.1.5 Appropriate Slag Systems and Fluxes

It was apparent that the alumino-magnesiothermic reduction (eq.13) reaction required additional heat energy and or fluxing agents to promote good metal slag separation.

It was also calculated that the aluminothermic reaction (eq.8) would require additional heat and or flux to yield well separated metal and slag.

The additional heat, provided by the D.C. arc furnace, not only assisted in providing required heat for good slag metal separation; but provided additional scope for fluxing the formed slags without negatively affecting the heat balance.

The main assumption regarding the aluminothermic, magnesiothermic and alumino-magnesiothermic experiments was that all stoichiometric $B_2O_3$ was reduced. Additionally, other experiments were benchmarked against the stoichiometric experiments' flux amounts in an effort to minimize the number of variables per experimental run.

#### *5.1.5.1 Aluminothermic Reaction Fluxes*

As per previously discussed reasons, CaO was found to be the most appropriate flux in the aluminothermic process. The flux addition for the process was aimed at the 50% $Al_2O_3$-50%CaO eutectic region.

#### *5.1.5.2 Magnesiothermic Reaction Fluxes*

The magnesiothermic reduction of $B_2O_3$ according to reaction (eq.12) generates MgO as the only slag component. MgO can be fluxed with excess $B_2O_3$ to obtain the eutectic at 69%MgO as depicted in Figure 23.

#### *5.1.5.3 Alumino-magnesiothermic Reaction Fluxes*

The slag generated from the complete reduction of $B_2O_3$ with Mg and Al would be constituted of the oxides of the reductant metals. That is MgO and $Al_2O_3$. Assuming complete reduction of $B_2O_3$ in reaction (eq.15), the slag would thus be a mixture of 34.5% MgO and the balance $Al_2O_3$. Such a system melts at 2053℃ (Figure 24). Additionally, the $Al_2O_3$-MgO phase diagram shows that the slag would form spinel upon solidification (Figure 24).
Due to the propensity of $B_2O_3$ to promote spinelization as reported by Kiss et al. and Sokolov et al., and limited data on the $Al_2O_3$-MgO-$B_2O_3$ systems, $B_2O_3$ self-fluxing could be inappropriate. Furthermore, the stoichiometric alumino-magnesiothermic reaction would contain 34.5% MgO and balance $Al_2O_3$. Using CaO to flux such produced system would require significant amounts of CaO to reduce the liquidus temperature. Conversely, $SiO_2$ flux

additions to yield the cordierite region (Figure 27) would be minimal and hence it was selected as an appropriate flux.

### 5.1.6 Input materials and Refractory interaction

At high temperatures, the reactants may interact with the furnace lining. Therefore it was necessary to determine interaction between the input materials and refractory.
The reactions were undertaken in a graphite crucible with a carbon-paste bottom. Thus, it would be possible for carbon (from the crucible and paste) to react with the input materials.

Literature information showed that the carbothermic production of NiB is a common production process. Tasyurek et al showed that the carbothermic reduction of NiB on similarly configured furnace D.C. arc furnace was feasible. Moreover, the authors did not report any excessive wear of graphite lining and subsequent C pick up to the alloy.
The carbothermic reduction of $B_2O_3$ may be represented by reaction (eq.14):

$$3C(\ lining) + B_2O_3 = 2B(in\ Ni) + 3CO(gas) \qquad \text{(eq.14)}$$

$$\Delta G^\circ{}_T\ (eq.14) = 885669 - 467.4T\ \ J$$

$$\Delta G^\circ{}_{1923}\ (eq.14) = 885669 - 467.4 \times 1923$$

$$\Delta G^\circ{}_{1923}\ (eq.14) = -13141\ J$$

The reaction (eq.14) is therefore feasible at the intended operating temperature of 1923K. However the standard free energy of the metallothermic reduction reactions at the operating temperature was found to be more negative than the carbothermic process reaction (eq.14). The removal of carbon from the lining could occur at the interface between the lining and $B_2O_3$. Lining wear may occur when excess $B_2O_3$ is present in the system, after when all the metallothermic reactions have gone to completion.

In addition, carbides may form when the produced B reacts with the graphite lining. This reaction may be represented by the follow reaction (eq.15):

$$C(\ lining) + 4B\ (in\ Alloy) = B_4C \qquad \text{(eq.15)}$$

$$\Delta G^\circ{}_T\ (eq.15) = -41505 + 1.33T\ \ J$$

$$\Delta G^\circ{}_{1923}\ (eq.15) = -41505 + 1.33 \times 1923$$

$$\Delta G^\circ{}_{1923}\ (eq.15) = -38947\ \ J$$

The $B_4C$ formation was determined to be feasible at the operating temperature of 1932K. The standard free energy of this reaction indicated that $B_4C$ may be formed. Since $B_4C$ has a high melting point of 2350°C, any $B_4C$ that could be formed might not be dissolved during the

experiments. This could result in the deposition of $B_4C$ in the furnace. However, it was mentioned previously that the free energy of a reaction does not indicate the reaction rate or kinetics. Therefore even though it would be feasible to produce $B_4C$ according to reaction (eq.15), the rate of $B_4C$ formation could be minimal. The standard free energy change of reaction (eq.15) is similar to the standard free energy of formation of NiB compound from Ni and B. However, the conditions during the reactions deviate from standard conditions hence the preferential formation NiB and low C in the alloys produced by the carbothermic process as reported by Tasyurek et al (8).

The supplier of the carbon paste did not disclose the chemical composition of the self-baking bottom. However, it was mentioned that the paste contained ash up to 5%. Therefore, the metallothermic reduction of the ash components could occur. As mentioned previously, it was assumed that the ash contained oxides of silicon, iron, aluminium and sodium. Sodium oxide ($Na_2O$) may be reduced to Na; however Na boils at 883°C. Hence at the operating temperature considered, any formed Na would volatilize when reduced by input Al or Mg according to the reactions:

$$3Na_2O(in\ ash) + 2Al = 6Na(g) + Al_2O_3 \qquad \text{(eq.16)}$$
$$\Delta G^{\circ}{}_{1923}(eq.16) = -864011\ J$$

$$Na_2O\ (in\ ash) + Mg = 2Na(g) + MgO \qquad \text{(eq.17)}$$
$$\Delta G^{\circ}{}_{1923}\ (eq.17) = -322317\ J$$

As depicted in the Ellingham Diagram (Figure 2), $Fe_2O_3$ can be reduced by both Al and Mg. The calculated standard free energy change of $Fe_2O_3$ reduction indicated that Fe contamination of alloy could occur. The respective aluminothermic and magnesiothermic reduction of $Fe_2O_3$ at the operating temperature in the ash may be represented by the following reactions:

$$Fe_2O_3\ (in\ ash) + 2Al = 2Fe + Al_2O_3 \qquad \text{(eq.18)}$$
$$\Delta G^{\circ}{}_{1923}(eq.18) = -728135\ J$$

$$Fe_2O_3(in\ ash) + 3Mg = 2Fe + 3MgO \qquad \text{(eq.19)}$$

$$\Delta G^{\circ}_{1923}\,(eq.19) = -831074\ J$$

Moreover, Figure 30 showed that aluminothermic and magnesiothermic reduction of $SiO_2$ can occur according to reactions:

$$\frac{3}{2}SiO_2(in\ ash) + 2Al = \frac{3}{2}Si + Al_2O_3 \qquad \text{(eq.20)}$$

$$\Delta G^{\circ}_{1923}(eq.20) = -208681\ J$$

$$SiO_2(in\ ash) + Mg = Si + 2MgO \qquad \text{(eq.21)}$$

$$\Delta G^{\circ}_{1923}(eq.21) = -207747\ J$$

Bitumen and bitumen products such as the binder used in the self-baking carbon paste typically contain sulphur and phosphorus. Thus it would be possible that sulphur and phosphorus from the binder could report to the alloy.

## 5.2 Process Data

The charge composition and process data for the aluminothermic, magnesiothermic and alumino-magnesiothermic experimental runs are presented in Tables 14, 15 and 16, respectively. Along with the reaction time and maximum recorded temperatures. The charge compositions were calculated and prepared from the thermochemical data discussed.

**Table 14: Aluminothermic charge compositions and maximum recorded reaction temperature**

| Run No. | % Excess | $B_2O_3$ (kg) | Ni (kg) | Al (kg) | CaO flux (kg) | Reaction T (℃) | Reaction time (min) |
|---|---|---|---|---|---|---|---|
| 1 | 0% | 5.04 | 8.50 | 3.91 | 7.38 | 1680(1675) | 30 |
| 2 | 5% Al | 5.04 | 8.50 | 4.10 | 7.38 | 1698 | 30 |
| 3 | 10%Al | 5.04 | 8.50 | 4.30 | 7.38 | 1663 | 30 |
| 4 | 15% Al | 5.04 | 8.50 | 4.49 | 7.38 | 1658 | 30 |
| 5 | 5% $B_2O_3$ | 5.29 | 8.50 | 3.91 | 7.38 | 1671 | 30 |
| 6 | 10%$B_2O_3$ | 5.55 | 8.50 | 3.91 | 7.38 | 1656 | 30 |
| 7 | 15%$B_2O_3$ | 5.80 | 8.50 | 3.91 | 7.38 | 1666 | 30 |

Run No. 1 corresponds to the stoichiometric aluminothermic experiment. The first run was difficult to anticipate the process behaviour. Excessive fluctuations of furnace voltage and

current input resulted in inconsistent furnace operation and it was decided to exclude the results of the initial attempt. Thus it was considered to repeat this run. Better control of the process was achieved by setting finer control limits of the furnace voltage and current input at the furnace control panel. The maximum reaction temperature of the repeat run was 1675°C.

In the aluminothermic experiments, Run No. 2-4 represented the Al variation with respect to the percentage excess over the stoichiometry. Run No.5-7 were the $B_2O_3$ variable experiments (Table 14).

In the magnesiothermic experiments the variable investigated was Mg, in the form of Mg chips. The $B_2O_3$ excess was assumed adequate due to the use of $B_2O_3$ flux in addition to the reactant $B_2O_3$. Table 15 details information regarding the charge recipes and the maximum reaction temperature recorded.

**Table 15: Magnesiothermic charge compositions and maximum recorded reaction temperature**

| Run No. | % Excess | $B_2O_3$ (kg) | Mg chips(kg) | NiMg (kg) | $B_2O_3$ self (kg) | Reaction T (°C) | Reaction time (min) |
|---|---|---|---|---|---|---|---|
| 8 | 0% | 5.04 | 3.64 | 10.14 | 7.16 | 1754 | 30 |
| 9 | 5% Mg | 5.04 | 3.82 | 10.14 | 7.16 | 1756 | 30 |
| 10 | 10%Mg | 5.04 | 4.00 | 10.14 | 7.16 | 1707 | 30 |
| 11 | 15% Mg | 5.04 | 4.19 | 10.14 | 7.16 | 1779 | 30 |

Run No. 8 corresponded to the stoichiometric magnesiothermic charge recipe. Thereafter excess Mg was investigated in the subsequent experimental runs (Run No. 9-11).

Run No.12 was the stoichiometric alumino-magnesiothermic experiment. In the alumino-magnesiothermic experiments, Runs No. 13-18 were the experiments which Al was varied with respect to percentage excess over the stoichiometric requirement. In Run No.16-18, $B_2O_3$ percentage excess was varied (Table 16).

The reaction temperature recorded was the temperature measured at the end of the experimental run.

**Table 16: Alumino-magnesiothermic charge composition and maximum recorded reaction temperature**

| Run No. | % Excess | $B_2O_3$ (kg) | NiMg (kg) | Al (kg) | $SiO_2$ flux (kg) | Reaction T (℃) | Reaction time (min) |
|---|---|---|---|---|---|---|---|
| 12 | 0% | 5.04 | 10.14 | 2.70 | 7.81 | 1779 | 30 |
| 13 | 5% Al | 5.04 | 10.14 | 2.83 | 7.81 | 1798 | 30 |
| 14 | 10%Al | 5.04 | 10.14 | 2.97 | 7.81 | 1756 | 30 |
| 15 | 15% Al | 5.04 | 10.14 | 3.11 | 7.81 | 1800 | 30 |
| 16 | 5% $B_2O_3$ | 5.29 | 10.14 | 2.70 | 7.81 | 1754 | 30 |
| 17 | 10%$B_2O_3$ | 5.55 | 10.14 | 2.70 | 7.81 | 1769 | 30 |
| 18 | 15%$B_2O_3$ | 5.80 | 10.14 | 2.70 | 7.81 | 1796 | 30 |

# 6 DISCUSSION

The computer simulations of the thermochemistry were an important step in determining the theoretical feasibility of the production processes investigated. The next step was to prove the thermochemistry by practical experimentation. Deviations from ideal conditions were expected in these experiments. These deviations arose from various influences.

It is well known that the particle size of reactants or granulometry of bulk charge have a significant impact on reaction kinetics. This and other factors were not simulated or investigated.

The experiments were undertaken in pilot-plant scale conditions. This assisted in obtaining operation parameters such as voltage and current settings for good reaction practice.

The results of the aluminothermic, magnesiothermic and alumino-magnesiothermic production experiments are presented in their respective sub-sections.

The results are discussed mainly using the Van't Hoff's Isotherm, that is:

$$\Delta G = \Delta G^\circ + RTlnK$$

This equation applies to non-equilibrium conditions. At equilibrium, the ΔG=0.

Although ΔG° varies with temperature; the effect of temperature is also common to the *RTlnK* term. Therefore it was assumed that ΔG° was fixed for the relevant reaction. Therefore in the Van't Hoff's Isotherm, the ΔG at a given temperature is made up of a fixed term, ΔG° and the variable term *RTlnK*. Moore (42) explained that the equilibrium constant (K) is a factor of the activities of the species in the reaction considered. The ΔG° values were assumed to be equivalent to the ΔG° values of the relevant reactions considered previously. As an example, in the aluminothermic reactions, it was assumed that the ΔG°-T relationship of reaction (eq.8) applies. This assumption although unproven, assisted in the examination of the metallothermic reactions investigated.

## 6.1 Aluminothermic Production Process

The results of the alloys produced by the aluminothermic process showed that the overall recovery of B in the alloy was low (Table 17). The minimum B content was 5.26% which was achieved in Run No.5 which corresponded to 5% excess $B_2O_3$. The maximum B content of the alloy was reported to be 7.59%. This B content was achieved in Run No.7

corresponding to 15% $B_2O_3$ excess. However the maximum B content was found to be less than 50% of the targeted B content of 15.55%. Moreover, the reported Al content was higher than the maximum Al target specification of 0.20%.

**Table 17: Alloy composition of aluminothermic runs**

| Run No. | % Excess | % Ni | % B | % Al | % Fe | % Si | % C | % P | % Mg |
|---|---|---|---|---|---|---|---|---|---|
| 1 | 0% | 77.60 | 5.81 | 12.66 | 1.67 | 1.77 | 0.388 | 0.024 | 0.081 |
| 2 | 5% Al | 77.95 | 5.93 | 12.17 | 1.90 | 1.59 | 0.385 | 0.026 | 0.053 |
| 3 | 10% Al | 78.23 | 6.70 | 11.11 | 1.82 | 1.64 | 0.382 | 0.019 | 0.101 |
| 4 | 15% Al | 78.74 | 6.85 | 10.55 | 1.78 | 1.61 | 0.381 | 0.032 | 0.054 |
| 5 | 5% $B_2O_3$ | 77.30 | 5.26 | 13.87 | 1.67 | 1.43 | 0.384 | 0.030 | 0.052 |
| 6 | 10% $B_2O_3$ | 77.84 | 6.68 | 11.76 | 1.82 | 1.43 | 0.382 | 0.025 | 0.067 |
| 7 | 15% $B_2O_3$ | 78.06 | 7.59 | 10.35 | 2.00 | 1.53 | 0.388 | 0.033 | 0.051 |

The analysis results of the aluminothermic slags produced were presented in Table 18. The main oxides considered were reported.

**Table 18: The aluminothermic slag analysis results in (wt. %)**

| Run No. | % CaO | % $B_2O_3$ | % $Al_2O_3$ | % MgO | % $SiO_2$ |
|---|---|---|---|---|---|
| 1 | 38.31 | 16.42 | 23.20 | 5.12 | 3.40 |
| 2 | 51.00 | 14.52 | 19.41 | 5.06 | 3.23 |
| 3 | 34.57 | 17.39 | 29.68 | 5.32 | 3.85 |
| 4 | 37.08 | 16.26 | 26.93 | 5.34 | 3.64 |
| 5 | 40.84 | 18.90 | 22.86 | 5.39 | 3.23 |
| 6 | 33.29 | 15.55 | 25.21 | 5.21 | 3.59 |
| 7 | 36.35 | 18.16 | 24.85 | 5.06 | 3.55 |

It was evident from the metal and slag analyses results that Al reductant was not completely consumed. Moreover, due to the $B_2O_3$ content of the slags, the results suggested that equilibrium conditions were not reached.

The adjusted mol % of the slag analysis results were presented in Table 19. The wt. % results do not equal 100% because not all elements were analyzed due of cost considerations. The main elements partaking in the reaction were analyzed and a weighted average was computed for the mol% results shown in Table 19.

**Table 19: The aluminothermic slag analysis results in (mol %)**

| Run No. | % CaO | % $B_2O_3$ | % $Al_2O_3$ | % MgO | % $SiO_2$ |
|---|---|---|---|---|---|
| 1 | 51.36 | 17.73 | 17.11 | 9.55 | 4.25 |
| 2 | 61.13 | 14.02 | 12.80 | 8.44 | 3.61 |
| 3 | 45.55 | 18.46 | 21.51 | 9.75 | 4.73 |
| 4 | 48.91 | 17.28 | 19.54 | 9.80 | 4.48 |
| 5 | 51.60 | 19.23 | 15.88 | 9.48 | 3.81 |
| 6 | 47.37 | 17.82 | 19.73 | 10.32 | 4.77 |
| 7 | 48.47 | 19.50 | 18.22 | 9.39 | 4.42 |

As mentioned earlier, the reported B content of the alloy was lower than the target specification. The impact excess Al on the % B and % Al in the alloy was depicted in Figures 32 and 33 respectively. The slag metal reactions for the aluminothermic reactions may be represented by adjusting reaction (eq.8) to depict the species undergoing chemical reaction. The equation may be represented as:

$$Al_{(in\ Ni)} + \frac{1}{2}B_2O_{3(in\ slag)} = \frac{1}{2}Al_2O_{3(in\ slag)} + B_{(in\ Ni)} \qquad \text{(eq.8A)}$$

The application of Van't Hoff's isotherm to reaction (eq.8.A) is:

$$\Delta G(eq.8A) = \Delta G°(eq.8A) + RTln\left(\frac{(a_{B(in\ Ni)}) \cdot (a_{Al2O3\ (in\ slag)})^{1/2}}{(a_{Al(in\ Ni)}) \cdot (a_{B2O3\ (in\ slag)})^{1/2}}\right)$$

As mentioned, the $\Delta G°_T$ or $\Delta G°_T$ *(eq.8A)* was fixed for a specific temperature. The standard free energy change of reaction (eq.8A) would thus be equivalent to the standard free energy change of reaction (eq.5). The standard free energy change is generally expressed as a linear

equation with temperature as the variable term. However, in these experiments, the tap temperature was assumed to be fixed at 1650°C, moreover some minor tap temperature variations occurred. Thus the temperature influence on the experiments was not a real variable. However, given the reactants Al and $B_2O_3$ were varied extensively the *RT-term* was considered.

There are four variables in the *RT-term* which when adjusted influence the overall feasibility or *ΔG (eq8.A)* of the forward reaction (eq.8A).

### 6.1.1 Impact of Al excess on %Al and % B in the Final Alloy

The forward reaction (eq.8A) may be promoted by increasing the activity of Al in Ni. At the recorded reaction temperatures, such an Al-Ni alloy would be in the liquid phase as shown in Al-Ni phase diagram (Figure 10). The thermodynamic activity data for this reaction at the temperatures considered were not obtained. The results showed that the Al content of the alloy was greater than 1wt.%. Therefore it was assumed that the activity of Al in liquid Ni was proportional to the composition of Al in the liquid Ni .Therefore an approximation of Rauolt's law was assumed for the liquid metal phase. That is, when the Al content of the metal phase was increased, then the activity of Al increased.

The forward reaction (eq.8A) could have been promoted under the condition where *ΔG (eq8.A) <0*, or when *ΔG (eq8.A)* was as negative as possible.

This condition could be achieved by increasing the activity of Al in Nickel ($a_{Al(in\ Ni)}$). Increasing ($a_{Al(in\ Ni)}$) reduces and makes the *RT-term* more negative. It can be seen from the results that increasing Al excess increased the B content of the alloy. The increase of the alloy B content with respect to Al excess can be seen in Figure 32. The trend prescribed by the increase in Al excess was positive; however the impact of Al excess on the B pick-up was minimal. The difference in %B content of the alloy from stoichiometric Al and 15% Al excess was found to be only 1.04%. Implementing 15% Al excess yielded a 6.85% B content alloy.

The alloys produced were significantly contaminated with Al. According to reaction (eq.8A), when input Al in the reaction was increased, the methodology required that $B_2O_3$ be fixed. This methodology assisted in determining the influence of the adjusted variable. Therefore, increasing the Al excess risked contaminating the alloy because once all the available $B_2O_3$

was consumed according to reaction (eq.8A), then the unreacted Al could report to the metal. It was earlier reported that Al dissolves in Ni. The Al-Ni phase diagram (Figure 10) showed that at the maximum process temperatures achieved (between1656-1698°C) and at furnace tapping temperature of 1650°C, the binary Al-Ni system would be in the liquid phase. This suggested that no high temperature Al-Ni species could be deposited. The deposition of high temperature species can affect the chemical composition of the tapped alloy. This could occur when the tapping temperature is less than the melting point of the high temperature species. However in these experiments it was evident that the tapped alloy was homogenous.

The relatively high values of %Al in the alloy indicated that the 30 minutes reaction time was inadequate. The %Al in the alloy increased from the stoichiometric level and peaked at 5%Al excess (Figure 33). A decrease of 1.62%Al content of the alloy was obtained from the 5% Al excess to 15%Al excess.

It was shown in the Van't Hoff Isotherm that the forward reaction (eq.8A) was promoted by increasing %Al excess. Therefore, the increasing of %Al excess resulted in an increase in %B content of the alloy. An increase in %B content of the alloy would in effect dilute the available Al in the alloy and thus minimize Al contamination. Such a trend described was observed and was plotted in Figure 32.The percentage increase in B content of the alloys as an effect of % Al excess was marginal. Furthermore the %Al excesses investigated resulted in significant Al contamination that was orders of magnitudes higher than the Al specification.

It was evident that not all $B_2O_3$ was consumed as the %B in alloy did not correspond to the available B in the system. This was possibly due to some losses of $B_2O_3$ to the fume generated during the operation of the D.C. arc furnace. However loss of available B units was primarily through the recovery of $B_2O_3$ to the slag. Therefore it was deemed important to discuss the interaction of the metal and slag.

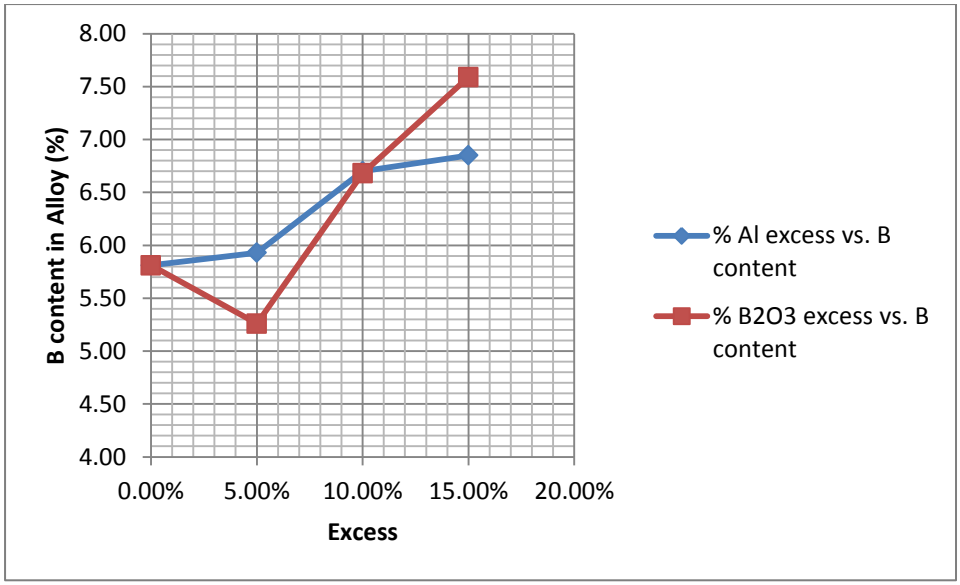


**Figure 32: Impact of al and $b_2o_3$ excess on the %b in the alloy (aluminothermic runs)**

### 6.1.2 Impact of $B_2O_3$ Excess on %B and %Al in the Final Alloy

According to the Van't Hoff Isotherm of reaction (eq.8A), adjusting the activity of $B_2O_3$ in the slag ($a_{B2O3\,(in\,slag)}$) can have an influence on the overall *ΔG (eq8.A)* of the reaction (eq.8A). Increasing in $a_{B2O3\,(in\,slag)}$ has the effect of minimizing the *RT-term* and thus making *ΔG (eq8.A)* more negative. This would promote the forward reaction and hence increase B content of the alloy.

There are various theories that are applied to slag chemistry. However most of these theories are not in agreement and require practical experimentation in order to determine useful thermodynamic data.

In the aluminothermic process considered, data pertaining to the slag considered was inconclusive. Furthermore, information about such slags was limited. The patent regarding acid soluble borate slags only contained chemical information of post reaction or solidified slags (18).

The slag behaviour in this investigation was assumed to follow Temkin's theory of liquid slags. In brief, Temkin's theory assumes slag solution is completely disassociated into ions, no interaction between ions of the same charge and complete randomness. That is two ideal solutions of cations and anions (42).

The relationship was simplified for aluminothermic reactions by Alcock (16), that in the slag phase, the activity of the molecular components must equal the square of the respective mol

fraction. Thus it followed that the activity of the slag components in reaction (eq.8A) were: for $B_2O_3$

$$a_{B2O3\ (in\ slag)} = (X_{B2O3})^2$$

And the activity of $Al_2O_3$:

$$a_{Al2O3\ (in\ slag)} = (X_{Al2O3})^2$$

Where *X* was the mol fraction of the component in the slag.

Substituting the mol fraction into the *ΔG (eq8.A)* yielded the equation:

$$\Delta G(eq.8A) = \Delta G°(eq.8) + RTln\left(\frac{(a_{B(in\ Ni)}) \cdot (X_{Al2O3\ (in\ slag)})^{2/2}}{(a_{Al(in\ Ni)}) \cdot (X_{B2O3\ (in\ slag)})^{2/2}}\right)$$

It was evident that Temkin's law simplified the expression. The mol fraction of the individual components in the slag can be readily deduced from the slag analysis results. Thus, in process plants were slag chemistry is analysed online, adjustments of the slag components may be made by adding other component(s) that have a beneficial influence on the process.

It was suggested that increasing $B_2O_3$ excess increased the available $B_2O_3$ in the system In these experiments. The available $B_2O_3$ would report to the slag phase and consequently increase the $X_{B2O3}$. This would result in decreasing the *RT-term* and making *ΔG (eq8.A)* more negative and subsequently promoting the forward reaction (eq.8A).

Increasing the $B_2O_3$ from 0% to 15% excess (Run No. 1 and 5-7) had a resultant increase in $X_{B2O3}$ during the reaction. This resulted in a proportional increase in B pick-up (Figure 32 and Table 19). This observation followed Temkin's theory with the exception of the 5% $B_2O_3$ excess run (No. 5), which may have been attributable to experimental error. It was also observed that increasing $B_2O_3$ excess decreased the Al content of the alloy, except for the aforementioned 5% $B_2O_3$ run.

Furthermore, the comparison of B content of the alloy and Al in the $B_2O_3$ variable runs (No.5-7) showed that there was a resultant increase in alloy B content. An increase in alloy B content effectively diluted the Al content of the alloy. Therefore increasing the Al and $B_2O_3$ excess was found to have had the same effect on the B and Al content of the alloy.

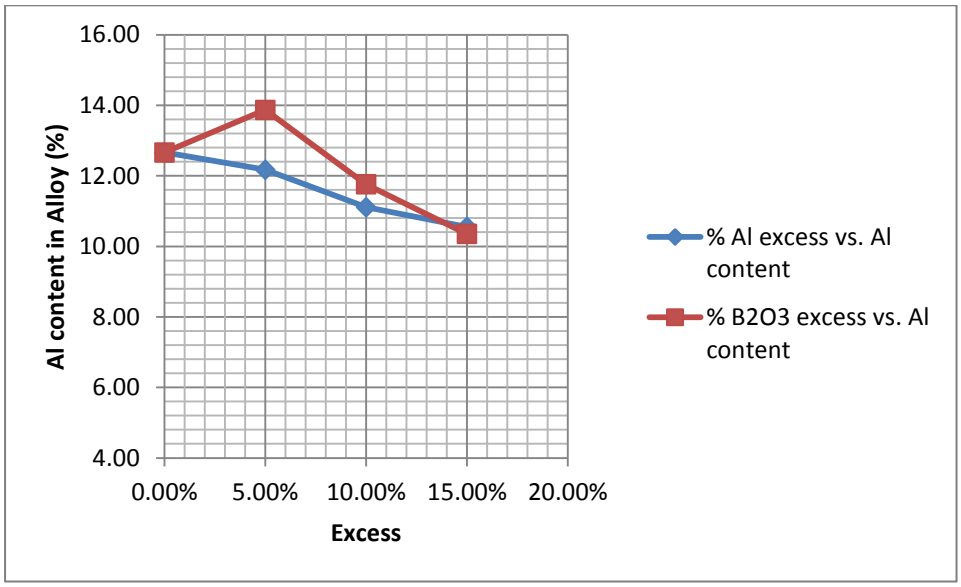


**Figure 33: Impact of Al and $B_2O_3$ excess on the %al in the alloy (aluminothermic runs)**

However, it was seen that the percentage increase in $B_2O_3$ excess was not equivalent to the $X_{B2O3}$ increase. That meant an increase in 5% $B_2O_3$ excess did not result in the equivalent 5% increase in $X_{B2O3}$. This non-linearity was attributable to a number of factors, such as the reaction extent or the degree of completion of reaction (eq.8A). The reaction extent was a factor of the equilibrium constant *K* or *RT*-the term in brackets. It was evident that the slag-metal interactions were complex due to the number of variables. Furthermore, the comparison of the slag composition with respect to $X_{B2O3}$ and the B content of the alloy (of Run No.1-7) showed that there was direct correlation for Run No. 2,3,4,6 and 7. However, negative deviations from Temkin's theory were observed in particular to Run No. 1 and 5. The relatively high $X_{B2O3}$ in these runs did not equate to similarly increased B content of the alloy (Figure 34).

Notwithstanding the aforementioned, two main observations that factored in the experiments were [1] the influence of impure CaO on the process and [2] the loss of $B_2O_3$ due to fume generation.

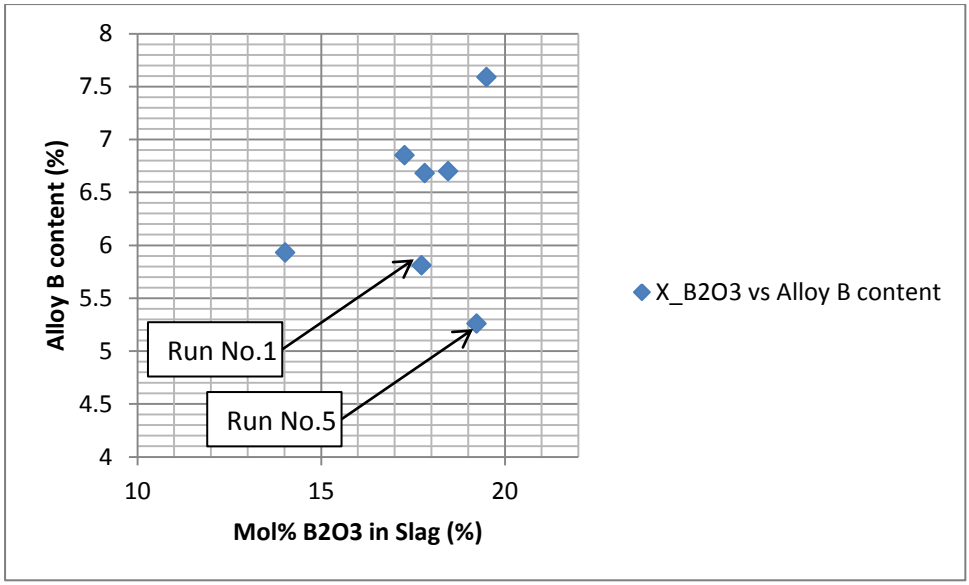


**Figure 34: Impact of $X_{B2O3}$ on alloy B content**

### 6.1.3 The influence of impure CaO on the process

In the experiments were Al was varied, Run No.1-4, $X_{B2O3}$ varied even though the input oxides $B_2O_3$ and CaO were fixed. Additionally, the lime flux used introduced MgO, $SiO_2$ and other unwanted slag formers. It is important to avoid contaminants which may have an unplanned influence on the process. Unfortunately, high purity industrial CaO was not obtained prior to experimentation.

CaO was selected as the most appropriate flux for $Al_2O_3$. The reasons for this choice were discussed earlier. The poor B recovery and the high $B_2O_3$ content of the slags indicated that input $B_2O_3$ was not completely consumed. Evidently, CaO had a beneficial fluxing effect on the process yielding fluid slag which allowed for good metal separation. It was very important to recover the expensive Ni alloy despite of its specification. Recycling and returning Ni in other processes was relatively simple. However the results indicated that CaO had another detrimental impact on the B yield to the alloy. The impact of CaO on the process was believed to be the fact that CaO, a basic oxide, reacted with the acidic $B_2O_3$. The reaction of CaO and $B_2O_3$ in the slag may have produced liquid Calcium Borate(s) as can be expressed by the reaction (which is non-stoichiometric):

$$CaO + B_2O_3 = CaB_2O_4 + excess\ CaO \qquad \text{(eq.16)}$$

It can be observed from this reaction that the reaction effectively reduces the "free" $B_2O_3$ in the slag. However, Temkin's theory disregards such interaction; because the theory assumes complete disassociation of slag components. Regardless of this assumption, the addition of CaO to the reaction dilutes the $X_{B2O3}$. The resultant effect is an increase in the value of the *RT-term,* therefore making the *ΔG (eq.8A)* more positive. A more positive *ΔG (eq.8A)* promotes the reverse reaction (eq.8A). However, it is common metallurgical practice to control the slag properties by modifying its basicity or acidity.

There are various indices that express slag basicity however, there is universal agreement that CaO is a basic oxide and $B_2O_3$ is acidic. Hence, when CaO is added to an acidic slag, slag that may contain $B_2O_3$ or other acidic oxide, the effect would generally be an increase in slag basicity. The modification of slag basicity is normally used in refining reactions. The results of these experimental runs indicated that perhaps Temkin's theory was not completely obeyed.

The fact that the input CaO quantity was fixed should not have negatively affected the $X_{B2O3}$ with particular reference to Run No.5-7, where input $B_2O_3$ was varied. The fact that the metal analyses results of these experiments indicated high Al content suggested that $B_2O_3$ reduction was limited. The low $B_2O_3$ consumption as evidenced and the unexpectedly high $X_{B2O3}$ indicated that a proportion of input $B_2O_3$ was locked in the slag.

A HSC$^{TM}$ reference of the free energy of formation of common calcium borates according to reaction (eq.16) at the tap temperature (1650°C) were presented in Table 20.The very negative free energies of formation of Calcium Borates suggested that the simplified reaction (eq.16) occurred. The addition of relatively high amounts of CaO in the effort to flux the formed $Al_2O_3$ inadvertently locked $B_2O_3$ into the slag phase by promoting the formation of Calcium Borates. This resulted in diminished active/free $B_2O_3$ and hence the low B recovery to the alloy. Moreover, the slag analysis results showed that significant amounts of input $B_2O_3$ reported to the slag. Unfortunately the slag analysis method (ICP-OES) used did not identify compounds or molecules present in the slag.

**Table 20: Standard free energies of formation for common calcium borates at 1650°C**

| Reaction | $\Delta G°$ at 1650°C (J/mol) |
|---|---|
| $CaO + B_2O_3 = CaB_2O_4$ | -119188 |
| $CaO + 2B_2O_3 = CaB_4O_7$ | -118562 |
| $2CaO + B_2O_3 = Ca_2B_2O_5$ | -207644 |
| $3CaO + B_2O_3 = Ca_3B_2O_6$ | -249370 |

In spite of this, the stoichiometric run (Run No.1) yielded a higher %B in the alloy as compared to the 5% excess $B_2O_3$ level. As previously discussed, the relationship between %B and %Al in the alloy was inversely proportional. This relationship was clearly defined in the $B_2O_3$ variable experimental runs (No.5-7) (Figures 32 and 33, respectively).Additionally, the %Al values in these experiments (Run. No.1-7) followed similar trends.

### 6.1.4 The influence of $B_2O_3$ volatilization

During the aluminothermic experiments (Run No.1-7) it was observed that a lot of fume which may have contained $B_2O_3$ was generated. This likely resulted in additional losses of reactant $B_2O_3$. The resultant effect was low B recovery and high Al entrainment. Incidentally, $B_2O_3$ has a wide temperature range between melting point (450℃) and boiling point (2065℃).

Lamoreaux et al (11) reported on the vaporization behaviour of $B_2O_3$ and other Boron sub-oxides. They also determined that under near atmospheric conditions, that is at 0.2bar $O_2$ partial pressure, the volatilization of oxides of boron is primarily through $B_2O_3$ evaporation. The comparison of volatilization rates of the various boron-oxygen compounds was depicted in Figure 9. The $B_2O_3$ partial pressure at and above the operating temperature (1650°C) as shown in Figure 9 was found to be above 0.01bar and increasing.

The charge size of these experiments was relatively small. Therefore, the furnace burden was too shallow to promote the reaction between Al and volatilized $B_2O_3$ or the gaseous sub-oxides of $B_2O_3$.In industrial furnaces, it is common practice that the formed gaseous and fume products are separated prior to discharging to the atmosphere. Moreover in other cases furnace design and burden characteristics allow for the reaction of gaseous products with

other charge reactants. In some instances were fume generation is unavoidable, the fume is typically recovered through various stages of dust extractions equipment. The fume can be agglomerated and recycled in the process or is despatched to industries were the fume is an input material. In the case of ferrosilicon production, the silica fume generated is typically used as an input material for cement production.

Due to the scale of the D.C. arc furnace used in the experiments, installing fume extractors and ventilation units was not found to be economically feasible. Hence, the fume generated during the reactions was not recovered for chemical analysis.

Given the high and similar $B_2O_3$ content of the slags, implementing $B_2O_3$ excess seemed to have resulted in significant loss of $B_2O_3$ to fume. That is, once the $X_{B2O3}$ value reached between 14 and 19.5 mol %, any additional or excess $B_2O_3$ was volatilized and lost to fume. The increasing $B_2O_3$ excess hence did not have a marked influence on the $X_{B2O3}$. The concomitant effect of low levels of $X_{B2O3}$ in effect reduced activity of $B_2O_3$ in the slag and thus promoted the reverse reaction (eq.8A).

### 6.1.5 Other elements

*Carbon*

The average carbon content of the alloys was found to be 0.384% which did not meet the 0.15% maximum C specification for NiB master alloy. As the experiments were undertaken in a graphite lined furnace, it was expected that carbon pick-up would occur. The temperatures reached during furnace operation could have promoted the $B_4C$ formation reaction (eq.15). Although the C specification was not met, the fact that the C content of the alloys was between 0.381-0.388% indicated the alloys were supersaturated with C. The mechanism of C pick-up could be through carbide formation and subsequent dissolution into the alloy. These mechanisms seemed to have reached maximum C pick-up capability. Therefore, increasing B recovery to the alloy would in effect dilute the alloy C content.

*Iron and Silicon*

The Fe and Si content of the alloy were proportionally due to the impure flux. The $Fe_2O_3$ and $SiO_2$ present in the calcined lime were evidently reduced to Fe and Si which were then recovered to the alloy. A chemically cleaner alloy could be achieved by using high purity input materials. However, increasing purity of common industrial materials such as fluxes typically increases costs.

Moreover, the crucible bottom was made up of self-baking bituminous carbon paste. Additional Si and Fe could have been recovered to the alloy from the carbon paste through reactions (eq.18-21).

## 6.2 Magnesiothermic Production Process

The chemical analysis results of the alloys and slag produced during the magnesiothermic investigations (Run No.8-11) were obtained by the ICP-OES method except for C, which was determined through the LECO combustion technique.
The alloy and slag chemical analysis results are presented in Tables 21 and 22, respectively.

**Table 21: Alloy composition of the magnesiothermic runs**

| Run No. | %Excess | % Ni | % B | % Al | % Fe | % Si | % C | % P | % Mg |
|---|---|---|---|---|---|---|---|---|---|
| 8 | 0 | 86.26 | 9.45 | 0.104 | 1.96 | 1.70 | 0.421 | 0.026 | 0.084 |
| 9 | 5%Mg | 84.15 | 10.94 | 0.106 | 2.37 | 1.90 | 0.442 | 0.041 | 0.048 |
| 10 | 10%Mg | 84.39 | 11.33 | 0.118 | 1.82 | 1.82 | 0.398 | 0.019 | 0.102 |
| 11 | 15%Mg | 83.95 | 11.82 | 0.154 | 1.65 | 1.63 | 0.433 | 0.035 | 0.329 |

The B content of the magnesiothermic experimental runs was found to be proportionally higher than the aluminothermic runs. The maximum B content reported was 11.82% which corresponded to 15% Mg excess. The comparison of the standard free energy changes of the magnesiothermic (eq.9) and aluminothermic (eq.8) production of NiB indicated that the magnesiothermic process was more thermodynamically feasible, hence the higher B recovery to the alloy. The Al content was orders of magnitude lower than the aluminothermic experiments. This was expected because no Al reductant was used.

The total input $B_2O_3$ used in the magnesiothermic experiments was higher than the aluminothermic processes hence the proportionally greater $B_2O_3$ content in the slag. As input $B_2O_3$ was found to have self-fluxing properties on the system, there was relatively no reported CaO in the slag. However, some $Al_2O_3$ and $SiO_2$ were reported (Table 22)

**Table 22: The magnesiothermic slag analysis results**

| Run No. | Wt. (%) | | | | |
|---|---|---|---|---|---|
| | % CaO | % $B_2O_3$ | % $Al_2O_3$ | % MgO | % $SiO_2$ |
| 8 | 0.001 | 41.44 | 3.99 | 42.48 | 3.34 |
| 9 | 0.001 | 40.45 | 2.04 | 40.96 | 6.85 |
| 10 | 0.001 | 42.86 | 1.44 | 46.20 | 3.17 |
| 11 | 0.001 | 40.70 | 2.21 | 42.33 | 3.38 |
| Run No. | Mol (%) | | | | |
| | % CaO | % $B_2O_3$ | % $Al_2O_3$ | % MgO | % $SiO_2$ |
| 8 | 0.00 | 34.13 | 2.24 | 60.44 | 3.18 |
| 9 | 0.00 | 33.56 | 1.16 | 58.70 | 6.58 |
| 10 | 0.00 | 33.66 | 0.77 | 62.68 | 2.88 |
| 11 | 0.00 | 34.13 | 1.27 | 61.32 | 3.28 |

### 6.2.1 Impact of excess Mg

The production of NiB from NiMg and supplementary Mg chips was investigated. It was calculated that NiMg fines could not yield a Ni alloy with a minimum of 15% B. Supplementary Mg chips were used to boost the B recovery to the alloy in an attempt to meet the B specification. Thus, the impact of excess reductant was investigated with Mg chips.

The influence of excess Mg was investigated between the stoichiometry requirement and 15% excess. The input $B_2O_3$ in this process accounted for the reduced oxide and the flux. Hence it was decided that given the significant quantities of $B_2O_3$ in the system, $B_2O_3$ excess investigation as in the aluminothermic runs was not necessary.

The magnesiothermic production of NiB was assumed to follow the adjusted magnesiothermic reaction (eq.11), which may be written as:

$$\frac{4.51}{2}Mg(free) + Mg(in\ Ni) + \frac{2.17}{2}B_2O_3 = \frac{6.51}{2}MgO + 2.17B(\ in\ Ni) \qquad \text{(eq.11A)}$$

Reaction (eq.11A) may be assumed to be the net reaction of the reaction of "free" Mg chips and alloyed Mg. Thus, (eq.11A) could be split into two reactions as follows:

$$Mg(in\ Ni) + \frac{1}{3}B_2O_3 = MgO + \frac{2}{3}B(\ in\ Ni) \qquad \text{(eq.11AA)}$$

$$\frac{4.51}{2}Mg(free) + \frac{4.51}{6}B_2O_3 = \frac{4.51}{2}MgO + \frac{4.51}{3}B(\ in\ Ni) \qquad \text{(eq.11AB)}$$

Mg in Ni was the Mg from the NiMg fines. The free Mg in reaction (eq.11AB) represented the Mg chips

It was found that the B content of the magnesiothermic experiments did not reach the required specification. The input materials were designed to yield at least a 15% B content alloy. The analysis results indicated that even with significant Mg and $B_2O_3$ excess, the process yielded a maximum of 11.82% B in the alloy.

#### *6.2.1.1 Mg from NiMg*

It was assumed that there were two magnesiothermic reactions where $B_2O_3$ was simultaneously reduced by the alloyed Mg and Mg chips according to reactions (eq11.AA) and (eq.11AB).

The Van't Hoff's isotherm for reaction (eq.11AA) may be represented as follows:

$$\Delta G(eq.11AA) = \Delta G°(eq.11AA) + RTln\left(\frac{(a_{B(in\ Ni)})^{2/3} \cdot (a_{MgO\ (in\ slag)})}{(a_{Mg(in\ Ni)}) \cdot (a_{B2O3\ (in\ slag)})^{1/3}}\right)$$

It can be seen from reaction (eq.11AA) that Mg was not a real variable. The relatively low Mg content of the alloys produced suggested that there was near complete consumption of alloyed Mg (Table 21).

It was evident that the reaction of NiMg with $B_2O_3$ was feasible. Thus, it was assumed that$\Delta G(eq.11AA) \leq 0$. The Van't Hoff Isotherm thus approached equilibrium and could be simplified to equilibrium conditions so that:

$$\Delta G°(eq.11AA) = -RTln\left(\frac{(a_{B(in\ Ni)})^{2/3} \cdot (a_{MgO\ (in\ slag)})}{(a_{Mg(in\ Ni)}) \cdot (a_{B2O3\ (in\ slag)})^{1/3}}\right)$$

Thus the low contamination of alloy with Mg was explained by rearranging the above equilibrium equation as follows:

$$\frac{a_{Mg\ (in\ Ni)}}{\left(a_{B\ (in\ Ni)}\right)^{\frac{2}{3}}} = \frac{\exp\left(\frac{\Delta G°(eq.11AA)}{RT}\right)}{(a_{B2O3\ (in\ slag)})^{1/3}/(a_{MgO\ (in\ slag)})}$$

The above expression followed the equation described by Gupta (41).The fixed terms in this expression were the standard free energy change($\Delta G°(eq.11AA)$) and temperature (T) as per experiments. The real variable in this expression in this equation was the $(a_{B2O3\ (in\ slag)})^{1/3}/(a_{MgO\ (in\ slag)})$ ratio.

The $a_{Mg\ (in\ Ni)}/\left(a_{B\ (in\ Ni)}\right)^{\frac{2}{3}}$ ratio expressed the extent of Mg contamination of the alloy. The Mg contamination would be minimized when $\Delta G°(eq.11AA)$ was as negative as possible and reaction temperature (T) was as low as possible. However in the experiments the standard free energy change was fixed for the magnesiothermic reduction of $B_2O_3$.The reaction temperature was effectively fixed.

Moreover, maximizing the $(a_{B2O3\ (in\ slag)})^{1/3}/(a_{MgO\ (in\ slag)})$ ratio would minimize the $a_{Mg\ (in\ Ni)}/\left(a_{B\ (in\ Ni)}\right)^{\frac{2}{3}}$ ratio and hence lower Mg contamination. Therefore, the application of Temkin's theory would suggest that when the mol fraction of $B_2O_3$ in the slag is increased (and hence increased $a_{B2O3\ (in\ slag)}$) then the $a_{Mg\ (in\ Ni)}/\left(a_{B\ (in\ Ni)}\right)^{\frac{2}{3}}$ ratio would be minimized. This scenario was obtained by utilizing additional $B_2O_3$ as flux in the process. This strategy resulted in high $B_2O_3$ content slags as compared to the aluminothermic experiments (Table 22) and minimal reductant contamination. It was also evident that to remove any trace Mg in the alloy would thus require close to even higher amounts of $B_2O_3$ in the slag.

Additionally, the contamination may be minimized by reducing the activity of $a_{MgO\ (in\ slag)}$. This could be obtained by adding an acidic oxide that would reduce the $a_{MgO\ (in\ slag)}$. $B_2O_3$ is an acidic oxide hence the additional benefit of using excess $B_2O_3$ in the process.

The fact that the alloys contain low Mg levels, which would likely have arisen from the Mg in NiMg, indicated that the reaction (eq.11AA) practically went to completion.

The Mg in reaction (eq11.AA) was limited. Thus maximum utilization of the Mg could only result in B content calculated to be 5.36% in Ni. Due to the calculated value of B through reaction (eq.11AA) supplementary Mg was therefore necessary. Mg chips were used to supplement the recovery of B to the alloy in an attempt to reach the B specification.

#### *6.2.1.2 Impact of free Mg*

Mg chips were used in conjunction with Mg in NiMg fines in an attempt to reach the alloy B specification. The input reactants were tailored to produce at least a 15% B containing alloy. The amounts of input Mg chips were designed to boost the B content of the alloy by an equivalent of 10% or more B in the alloy. Therefore the sum total of B in the alloy would equate to a minimum of 15% B. The reaction of Mg chips was assumed to follow reaction (eq.11AB).

The Van't Hoff isotherm of reaction (eq.11AB) may be written as:

$$\Delta G(eq.11AB) = \Delta G°(eq.11AB) + RTln\left(\frac{(a_{B(in\ Ni)})^{4.51/3} \cdot (a_{MgO\ (in\ slag)})^{4.51/2}}{(a_{Mg(free)}) \cdot (a_{B2O3\ (in\ slag)})^{4.51/6}}\right)$$

Two assumptions were made regarding reaction (eq.11AB) on the basis of the observed results:

The reported Mg content of the produced alloys was relatively low. Despite the low alloy Mg content, the alloy B content was not proportionally high.

1. Therefore it was assumed that the Mg dissolution rate into NiMg or Ni was significantly slower than the Mg reaction with $B_2O_3$. Therefore the activity of liquid Mg was close to unity during this reaction.
2. The characteristic Mg flaring was observed during these experiments. The flaring indicated that some free Mg was volatilized and consequently did not take part in the reduction of $B_2O_3$.

The first assumption suggested that the $a_{Mg(free)} \cong 1$. By substituting the value of $a_{Mg(free)}$ into the reaction (eq.11AB)'s Van't Hoff Isotherm, the expression was simplified to equate:

$$\Delta G(eq.11AB) = \Delta G°(eq.11AB) + RTln\left(\frac{(a_{B(in\ Ni)})^{4.51/3} \cdot (a_{MgO\ (in\ slag)})^{4.51/2}}{(a_{B2O3\ (in\ slag)})^{4.51/6}}\right)$$

This condition maximized the B formation reaction. Furthermore, the use of not only reactant $B_2O_3$ but additional $B_2O_3$ as flux also increased the $X_{B2O3}$ and thus the $a_{B2O3\,(in\,slag)}$, according to Temkin's theory.

In these experimental (magnesiothermic) runs the average $X_{B2O3}$ was reported to be 33.97% (Table 22).This value was found to be more that 10% above the $X_{B2O3}$ determined in the aluminothermic runs (Tables 19). Thus in this case where $a_{Mg(free)} \cong 1$ and an increase in the $a_{B2O3\,(in\,slag)}$ , the effect of these factors would make the *RT-term* of the above Van't Hoff Isotherm more negative. Moreover the standard free energy change of the magnesiothermic reduction of $B_2O_3$ ($\Delta G°(eq.11AB)$) may be assumed to approximate the standard free energy change of reaction (eq.9). The $\Delta G°(eq.9)$ was found to be highly negative at operating temperature considered. Therefore the reaction (eq.11.AB)'s Van't Hoff Isotherm would then become even more negative. Such a condition meant that:

$$\Delta G(eq.11AB) \ll 0$$

A more negative $\Delta G(eq.11AB)$ would promote the forward reaction (eq.11AB) resulting in increased B recovery to the alloy. This condition was proven to an extent since the B content of the magnesiothermic alloys was proportionally higher than the aluminothermic runs.

It was also shown that increasing excess Mg chips increased the B content of the alloy (Figure 35). The results of the alloys showed that reaction (eq.11AB) supplemented an equivalent amount of 4.09- 6.56% B to the alloy (Table 21). However, the excess Mg used was found to be insufficient to meet the required B specification of the alloy. The B content of the alloys showed that not all available Mg chips were utilized in reducing $B_2O_3$. It followed that the volatilized Mg resulted in the proportional loss of reductant metal. The effect of this was a lower than expected B content of the alloys.

The maximum B content of the alloy was obtained at 15% Mg excess.

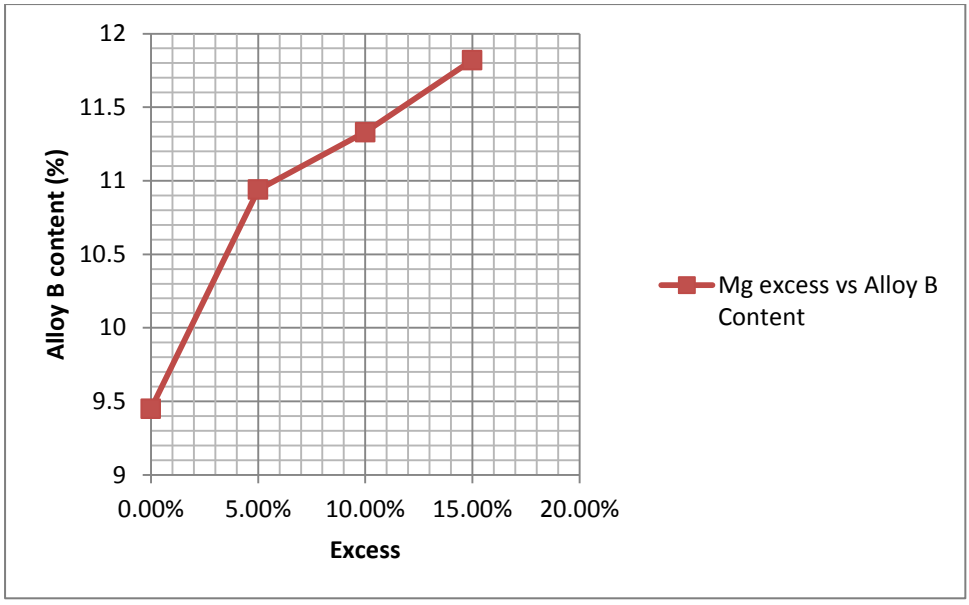


**Figure 35: Impact of excess mg of alloy b content**

### *6.2.1.3 Impact of Mg Flaring*

The fact that Mg flared during the reactions suggest that the assumption [1] was accurate. This assumption was that the rate of Mg melting and evaporating was far greater than the rate of dissolution into the dispersed NiMg alloy.

Mg flaring was represented by the reaction:

$$Mg_{(l)} = Mg_{(g)} \qquad \text{(eq.11AC)}$$

Due to the rapid temperature rise during the experiments, it was assumed that some of the Mg molten chips were volatilized. The fact that the Mg chips used were between 2-20mm meant that the surface area of the larger sized pieces was comparatively low. This meant that the reduction reaction between the larger Mg pieces was slower than the NiMg fines and the finer Mg chips. The reasons for using Mg chips instead of Mg powder were explained previously.

The Clausius-Clapeyron equation may be used to determine the impact of the rapid temperature rise on the volatilization of Mg. The Clausius-Clapeyron equation is an adaptation of the Van't Hoff's Isotherm (42).The application of the Clausius-Clapeyron equation on reaction (eq.11AC) can be represented as:

$$ln\left(\frac{p^{\circ}{}_{T}}{p^{\circ}{}_{boiling}}\right) = -\frac{L_e}{R}\left(\frac{1}{T} - \frac{1}{T_{boiling}}\right)$$

Where in this case, $p°_T$ is the vapour pressure of Mg at temperature T, and $p°_{boiling}$ is the vapour pressure of Mg at the boiling point ($T_{boiling}$), and the Latent Heat of evaporation for Mg is $L_e$. Since the vapour pressure of any liquid at its boiling equals one atmosphere ($p°_{boiling} = 1$) the Clausius-Clapeyron equation becomes:

$$ln(p°_T) = -\frac{L_e}{R}\left(\frac{1}{T} - \frac{1}{T_{boiling}}\right)$$

The Latent heat of evaporation ($L_e$) for Mg was computed to be 122938 J/mol and the boiling point of Mg is 1361K. Thus substitution of these values into the Clausius-Clapeyron yields:

$$ln\left(p°_{T,Mg}\right) = -\frac{122938}{8.314}\left(\frac{1}{T} - \frac{1}{1361}\right)$$

The anti-log of the above Clausius-Clapeyron equation yields the vapour pressure of Mg in atmospheres (atm). A plot of the vapour pressure and temperature (Figure 36) showed that significant Mg would have volatilized particularly after the reaction temperature rose above 1361K. Metallothermic reactions are known for rapid temperature rise post ignition. Hence the relatively low boiling point of Mg could have been reached and passed relatively quickly.

The vapour pressure of NiMg fines can be computed by using the vapour pressure of pure Ni and Mg and their relevant mol fractions. Moreover, it was assumed that NiMg melts to form an ideal solution as defined by Rauolt's law.

This assumption was expressed as:

$$p_{T,NiMg} = X_{Ni} \cdot p°_{Ni} + X_{Mg} \cdot p°_{Mg}$$

The mol ratio of Ni:Mg in the fines was 2.17:1, therefore the mol fraction of Ni and Mg was found to be, $X_{Ni}$ = 0.68 and $X_{Mg}$ = 0.32 .

The vapour pressure of pure Ni can be computed using the Clausius-Clapeyron equation:

$$ln\left(p°_{T,NI}\right) = -\frac{370380}{8.314}\left(\frac{1}{T} - \frac{1}{3186}\right)$$

Ni melts at 1738K and boils at 3186K. The latent heat of evaporation of Ni was found to be 370380 J/mol. The anti-log of the above expression yields the vapour pressure Ni. The sum of the vapour pressure of Ni and Mg according to Rauolt's law yields the total vapour pressure of NiMg. Vapour pressure of NiMg was determined with respect to temperature. The results of this calculation were graphically compared with the vapour pressure of Mg chips.

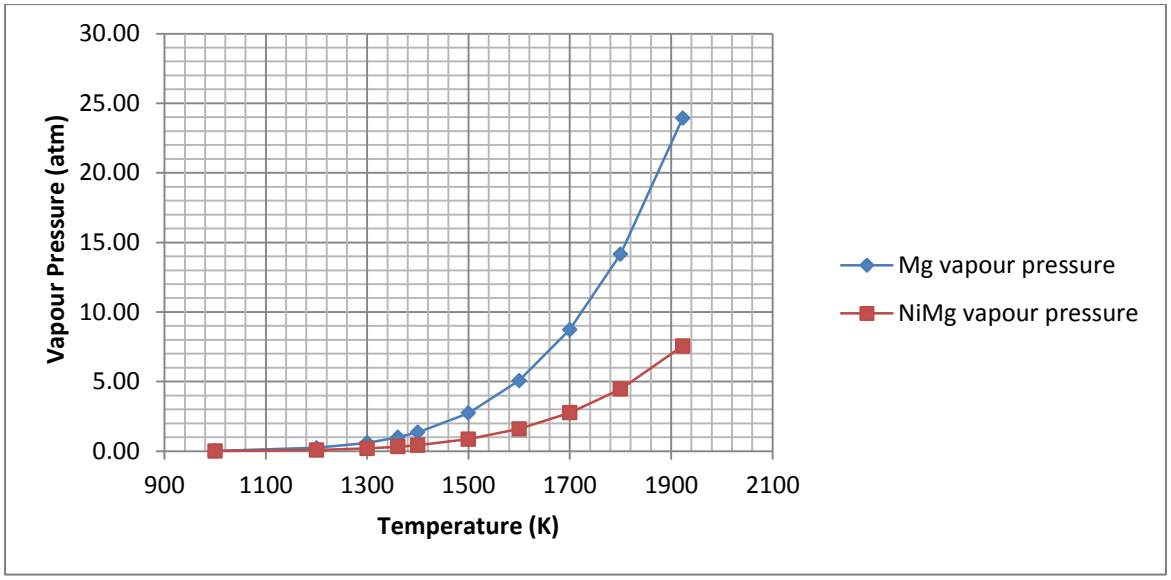


**Figure 36: Vapour pressure dependence on temperature**

The volatilized Mg could have reacted with some $B_2O_3$ if the furnace design and charge burden accommodated gaseous reactants. Unfortunately, the small scale D.C arc furnace did not allow for this process. This resulted in the loss of useful Mg which subsequently reacted with oxygen in the atmosphere. The resultant effect was the lower than expected B recovery to the alloy and minimal Mg in the alloy.

### 6.2.2 Contamination

The alloys produced in the magnesiothermic runs were contaminated with C, Fe, and Si. The Al content of the magnesiothermic alloys was found to be within the 0.2% Al specification for NiB.

*Carbon*

The alloy carbon content was reported to be between 0.398% and 0.442%. The maximum C content of NiB is 0.15%. The C content although above the required specification was consistently reported to be below 0.5%. The C in the system was from the lining and particularly the furnace bottom according to the reaction (eq.15). The surface finish of the graphite crucible was smooth and showed minimal wear or erosion. Contrarily, due to the installation of self-baking carbon paste bottom, the furnace bottom was not as smooth as the furnace wall. Additionally, the intense arcing during furnace start-up eroded the furnace bottom. The eroded material containing C could hence report to the alloy. Furthermore, the morphology of the carbon in the carbon paste is not graphitic/ planar but disordered. The

carbon particles in the paste were found to be irregular and granular with a structure similar to activated carbon. This meant that it was possible that the carbon particles were porous and thus had a high surface area. The high surface area of the exposed C in the furnace bottom could have promoted reaction (eq.15) kinetics, and hence supersaturating the formed alloy with C.

*Iron and Silicon*

There are various grades for welding and brazing alloys produced from NiB master alloys. Some of these alloys contain up to 5% iron and silicon. In some production processes, FeSi or Fe and Si metal are alloyed with NiB to yield the required Fe and Si specification in the final alloy (4) . Although the levels of Si and Fe were found to be higher than usual for metallothermic NiB, it would be possible to market an alloy with the Fe and Si content of the alloys produced. Fe and Si in this system were from the ash in the self-baking bottom. The ash was thus reduced according to reactions (eq.19 and eq.21). The products of these reactions were Fe and Si, respectively, which then contaminated the alloys.

## 6.3 Alumino-magnesiothermic Production Process

The chemical analysis results of the alumino-magnesiothermic reduction experiments are presented in Tables 23, 24, for the alloys and slags respectively.

As previously discussed, the Mg in this process not only improved the heat balance but as shown on the Ellingham Diagram (Figure 30) was more thermodynamically favourable than the aluminothermic process. Additionally, Al has a significantly higher boiling point (2519°C) than pure Mg (1088°C).Therefore the supplementary Al would effectively react with the $B_2O_3$ without volatilizing at the reaction temperatures reached. Furthermore, since only alloyed Mg was used in these experiments, it was expected that Mg flaring would be mitigated and therefore resulting in increased utilization of Mg in the reduction process.

This generated an expectation that the B recovery would be higher in these experiments than the aluminothermic and magnesiothermic experiments (Run No.1-7 and 8-11).

The B content of the alloys produced in these experimental runs (No.12-18) did not reach the minimum requirement of 15%. The maximum B content of the alloy was reported to be 10.88%, which corresponded to the 15% $B_2O_3$ excess run. The minimum %B in the alloy of 2.98% was achieved with the 5% Al excess run.

**Table 23: Alloy composition of the alumino-magnesiothermic runs**

| | | Chemical analysis of Alloy | | | | | | | |
|---|---|---|---|---|---|---|---|---|---|
| **Run No.** | **% Excess** | **% Ni** | **% B** | **% Al** | **% Fe** | **% Si** | **% C** | **% P** | **% Mg** |
| 12 | 0% | 75.23 | 3.47 | 0.286 | 4.57 | 15.75 | 0.628 | 0.011 | 0.053 |
| 13 | 5% Al | 65.92 | 2.98 | 0.280 | 4.01 | 26.02 | 0.724 | 0.010 | 0.052 |
| 14 | 10% Al | 73.19 | 4.53 | 0.417 | 3.84 | 17.26 | 0.661 | 0.029 | 0.076 |
| 15 | 15% Al | 74.19 | 4.21 | 0.501 | 4.56 | 15.72 | 0.721 | 0.015 | 0.083 |
| 16 | 5% $B_2O_3$ | 74.66 | 5.31 | 0.578 | 1.82 | 16.72 | 0.776 | 0.042 | 0.091 |
| 17 | 10% $B_2O_3$ | 80.36 | 3.36 | 0.260 | 4.20 | 11.02 | 0.698 | 0.022 | 0.075 |
| 18 | 15% $B_2O_3$ | 84.12 | 10.88 | 0.385 | 1.80 | 2.26 | 0.436 | 0.030 | 0.091 |

As expected, due to replacing a fraction of Al with Mg, the reported Al in the alumino-magnesiothermic results was reported to be lower than the aluminothermic process (Run No.1-7). It was also noted that although the Al content of the alloy was low, there was significant alloy contamination with Si and Fe. Consequently, the alloys produced did not reach the required NiB specification.

**Table 24: Slag composition of the alumino-magnesiothermic runs**

| | Wt. % | | | | |
|---|---|---|---|---|---|
| Run No. | % CaO | % $B_2O_3$ | % $Al_2O_3$ | % MgO | % $SiO_2$ |
| 12 | 0.00 | 23.02 | 33.82 | 20.94 | 19.72 |
| 13 | 0.00 | 15.59 | 37.09 | 23.65 | 4.15 |
| 14 | 0.00 | 22.12 | 33.50 | 20.76 | 20.37 |
| 15 | 0.00 | 18.26 | 28.10 | 16.47 | 20.71 |
| 16 | 0.00 | 19.10 | 35.26 | 17.69 | 20.39 |
| 17 | 0.00 | 20.93 | 36.83 | 19.83 | 15.96 |
| 18 | 0.00 | 21.51 | 33.31 | 19.14 | 22.48 |

**Table 25: Slag composition of the alumino-magnesiothermic experiments (mol %)**

| Run No. | Mol % | | | | |
|---|---|---|---|---|---|
| | % CaO | % $B_2O_3$ | % $Al_2O_3$ | % MgO | % $SiO_2$ |
| 12 | 0.00 | 21.90 | 21.96 | 34.41 | 21.73 |
| 13 | 0.00 | 18.00 | 29.25 | 47.19 | 5.55 |
| 14 | 0.00 | 21.18 | 21.90 | 34.33 | 22.59 |
| 15 | 0.00 | 20.31 | 21.34 | 31.65 | 26.70 |
| 16 | 0.00 | 19.61 | 24.73 | 31.39 | 24.26 |
| 17 | 0.00 | 21.18 | 25.44 | 34.67 | 18.71 |
| 18 | 0.00 | 20.81 | 22.00 | 31.98 | 25.20 |

The results of these experiments were discussed on the basis of slag metal interaction and the application of the Van't Hoff's isotherm on the adjusted reaction (eq.13). Reaction (eq.13) was assumed to be the net reaction of the magnesiothermic and aluminothermic reactions.

The magnesiothermic reaction:

$$Mg_{(in\ Ni)} + \frac{1}{3}B_2O_{3(in\ slag)} = MgO_{(in\ slag)} + \frac{2}{3}B_{(in\ Ni)} \qquad \text{(eq.13A)}$$

The Van't Hoff Isotherm for reaction (eq.13A) can be written as:

$$\Delta G(eq.13A) = \Delta G°(eq.13A) + RTln\left(\frac{(a_{B(in\ Ni)})^{2/3} \cdot (a_{MgO\ (in\ slag)})}{(a_{Mg(in\ Ni)}) \cdot (a_{B2O3\ (in\ slag)})^{1/3}}\right)$$

It can be seen that $\Delta G(eq.13A) = \Delta G(eq.11AA)$

The aluminothermic reaction per mol of Al:

$$Al_{(in\ Ni)} + \frac{1}{2}B_2O_{3(in\ slag)} = \frac{1}{2}Al_2O_{3(in\ slag)} + B_{(in\ Ni)} \qquad \text{(eq.13B)}$$

The reactions (eq.13B) stoichiometry can be multiplied by $\frac{4.51}{3.00}$mols to yield the aluminothermic reaction that supplements the B yield of reaction (eq.13).

The Van't Hoff isotherm for reaction (eq13.B) is equivalent to the Van't Hoff isotherm for reaction (eq.8A).

$$\Delta G(eq.13B) = \Delta G(eq.8A)$$

Then,

$$\Delta G(eq.13B) = \Delta G°(eq.8A) + RTln\left(\frac{(a_{B(in\,Ni)}) \cdot (a_{Al2O3\,(in\,slag)})^{1/2}}{(a_{Al(in\,Ni)}) \cdot (a_{B2O3\,(in\,slag)})^{1/2}}\right)$$

The Van't Hoff isotherms for both the magnesiothermic and aluminothermic reactions were discussed in their relevant experiments.

### 6.3.1 Impact of Mg on the Alloy

The analysis results for the alloys produced by the dual reaction process suggest that practically all the input Mg was oxidized. This was evidenced by the low Mg content of the alloy. It was discussed under the *Magnesiothermic Production Process* section that the ratio of the activities of Mg and B in the alloy affects the Mg and B content of the alloys. This ratio was expressed as:

$$\frac{a_{Mg\,(in\,Ni)}}{\left(a_{B\,(in\,Ni)}\right)^{\frac{2}{3}}} = \frac{\exp\left(\frac{\Delta G°(eq.13AA)}{RT}\right)}{(a_{B2O3\,(in\,slag)})^{1/3}/(a_{MgO\,(in\,slag)})}$$

This expression similarly applies for reaction (eq.13A) given that reaction (eq.13A) is equivalent to reaction (eq.11AA). It was explained that this ratio is minimized when the standard free of reaction is minimized. In comparison, the standard free energy change for the reduction of $B_2O_3$ with Mg is more negative than the aluminothermic reaction.

Additionally, this ratio may be minimized by increasing the activity of $B_2O_3$ and reducing the activity of the MgO. Since the effective Mg in the experiments was fixed in the NiMg alloy, the $a_{Mg(in\,Ni)}$, could not be adjusted by varying the input Mg. Therefore, the influence of $a_{Mg(in\,Ni)}$ on the $\Delta G(eq.13A)$ was not investigated. However, the interaction of MgO, a product of reaction (eq.13A) with other slag components is discussed in later sections of this work.

The amount of input NiMg was tailored to yield a minimum of 5.36% B in the alloy. Therefore the complete magnesiothermic reduction of $B_2O_3$ would yield a minimum of 5.36% B in the alloy. The alloy analysis indicated that the input Mg was practically consumed, however, the B content of the alloy did not correspond to available input Mg. Moreover, the reported Si content of the alloys was significantly higher than expected.

#### *6.3.1.1 Mg interaction with $SiO_2$ Flux*

The alloys produced in the experimental runs (No. 12-18) contained up to 26.02% Si. Since Si was introduced into the process through $SiO_2$, it was evident that $SiO_2$ was reduced along with $B_2O_3$. Since the B content of the alloys did not reach the theoretical 5.36% B through the magnesiothermic reaction (eq.13.AA). It was evident that Mg reduced $SiO_2$ according to reaction (eq.21) although $SiO_2$ in this case was from the flux and or slag.

The silica reduction reaction may be written as:

$$Mg_{(in\ Ni)} + \frac{1}{2}SiO_{2(in\ slag)} = MgO_{(in\ slag)} + \frac{1}{2}Si_{(in\ Ni)} \qquad \text{(eq.21A)}$$

The Van't Hoff isotherm for this reaction is:

$$\Delta G(eq.21A) = \Delta G°(eq.21A) + RTln\left(\frac{(a_{Si(in\ Ni)}) \cdot (a_{MgO\ (in\ slag)})^2}{(a_{Mg(in\ Ni)})^2 \cdot (a_{SiO2\ (in\ slag)})}\right)$$

The preferential magnesiothermic reduction of $SiO_2$ instead of $B_2O_3$ would require that the free energy change of reaction (eq.21A) be more negative than free energy change of reaction (eq.13A). This condition may be written as:

$$\Delta G(eq.21A) < \Delta G(eq.13A)$$

The standard free energy change for the magnesiothermic reduction of $B_2O_3$ was shown to be more negative than the $SiO_2$ reduction process. These reactions may be written as:

$$Mg + \frac{1}{3}B_2O_3 = MgO + \frac{2}{3}B \qquad \text{(eq.13AA)}$$

$$\Delta G°(eq.13AA) = -319992 + 134.0T \quad J/mol$$

$$Mg + \frac{1}{2}SiO_2 = MgO + \frac{1}{2}Si \qquad \text{(eq.21AA)}$$

$$\Delta G°(eq.21AA) = -281479 + 118.7T \quad J/mol$$

Due to insufficient thermochemical data for the alloy system discussed, it was assumed that the $\Delta G°(eq.13AA) \cong \Delta G°(eq.13A)$ and $\Delta G°(eq.21AA) = \Delta G°(eq.21A)$. The standard free energy changes for these reactions were computed from the data presented in Table 12.

A plot of the standard free energy changes with respect to temperature for the reactions (eq.13AA) and (eq.21AA) (Figure 37) showed that $\Delta G°(eq.13AA) < \Delta G°(eq.21AA)$. However, difference between the standard free energy changes of the reactions (eq.13AA) and (eq.21AA) approaches zero at temperatures above 1900K.

Therefore when $\Delta G°(eq.13AA) - \Delta G°(eq.21AA) \approx 0$; the magnesium may react with $B_2O_3$ and or $SiO_2$. This means that the preferential reduction of $B_2O_3$would thus be minimized at

high temperatures recorded in the experimental runs (No.12-18) It was explained previously that once a metallothermic reaction ignites, it would be difficult to control the temperature rise.

The minimum recorded temperature reached at the end of the 30 minutes reaction time for the alumino-magnesiothermic reactions was 2027K (1754°C). This temperature reading was obtained in Run No.16. The standard free energy change for the competing reactions at that temperature was computed substituting the 2027K into the relevant equation. The values of the standard free energy change for the reactions at 2027K were found to be $\Delta G°(eq.13AA) = -48734 \quad J/mol$ and $\Delta G°(eq.21AA) = -40874 \quad J/mol.$

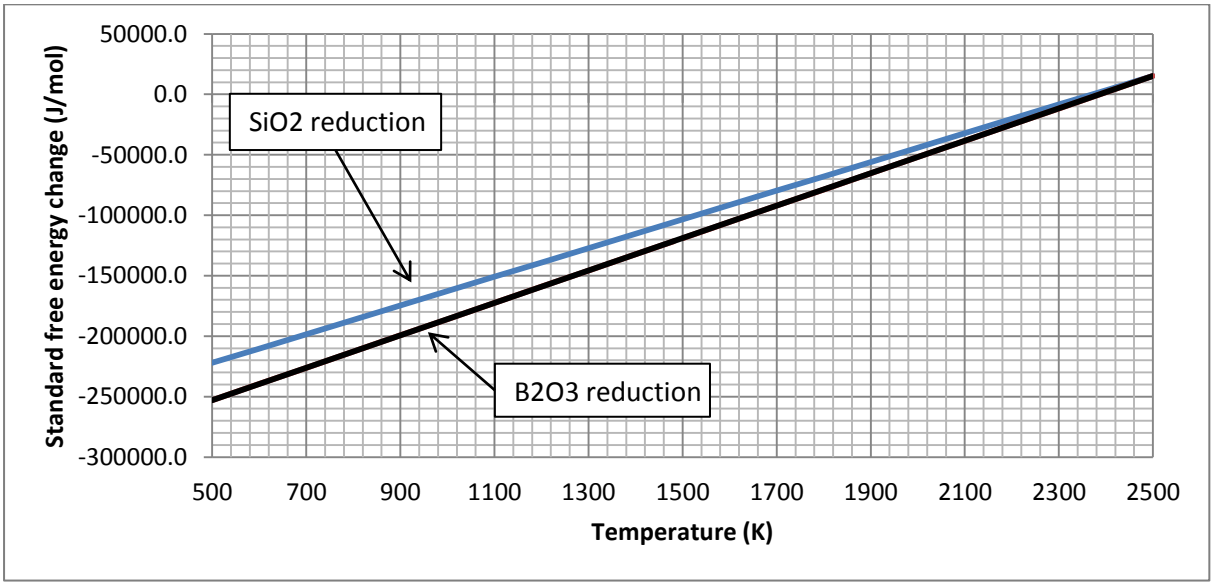


**Figure 37: Standard free energy change of the magnesiothermic reduction of $B_2O_3$ and $SiO_2$**

However, even at the temperatures reached during these runs, the standard free energy change for $B_2O_3$ is more negative than the $SiO_2$ reduction. The fact that the reported Si content in the alloy was more than the B content suggests that *RT-term* in the $\Delta G(eq.21A)$ was more negative than the *RT-term* in $\Delta G(eq.13A)$.

This condition can be attained by increasing the activity of $SiO_2$ in the slag and simultaneously reducing the activity of $B_2O_3$ in the slag.

MgO was found to be a common product of the magnesiothermic reactions (eq.13AB and eq.21A). MgO is a basic oxide, whereas both $B_2O_3$ and $SiO_2$ are acidic oxide. Therefore,

MgO could react with both $B_2O_3$ and $SiO_2$ and effectively reduce their respective $a_{B2O3\ (in\ slag)}$ and $a_{SiO2\ (in\ slag)}$.

The magnesiothermic reduction of $B_2O_3$ reaction (eq.13A) consumes more mols of $B_2O_3$ as compared to the $SiO_2$ reduction reaction (eq.21A). The mol ratio of $B_2O_3$ to $SiO_2$ is 1.5:1 in the competing reaction (eq.13A) and (eq.21A). Additionally, the standard free energy change of the magnesiothermic reduction of $B_2O_3$ was found to be more negative than the reduction of $SiO_2$. However, the amount of input $SiO_2$ was greater than the amount of input $B_2O_3$.The amount of input $B_2O_3$ in these runs was increased from 5.04 kg to 5.80kg, corresponding to the stoichiometric requirement and 15% excess. The amount of input $SiO_2$ was kept constant at 7.81kg.

Therefore, it would follow that the mol fraction of $B_2O_3$ *($X_{B2O3}$)* in the slag would consistently be lower than the mol fraction of $SiO_2$ *($X_{SiO2}$)*. However the slag analysis results presented in Table 24 showed that the unreduced $B_2O_3$ reported to the slag. Additionally there was no significant difference in $X_{B2O3}$ and $X_{SiO2}$ with the exception for Run No.13. Therefore; it was postulated that the reaction of basic MgO (that was produced in reactions (eq.13A and eq.21A)) and acidic $B_2O_3$ was more pronounced than anticipated. The results also indicated that this MgO-$B_2O_3$ interaction was more noticeable than the MgO-$SiO_2$ interaction. The effect of this acidic oxide-basic oxide interaction would thus have minimized the activity of $B_2O_3$ in the slag. Minimizing $a_{B2O3\ (in\ slag)}$ has the effect of making the *RT-term* in $\Delta G(eq.13A)$ less negative. Despite the fact that $\Delta G°(eq.13AA) < \Delta G°(eq.21AA)$ in the temperatures reached, it was evident from the slag and metal analysis results that *RT-term* in $\Delta G(eq.13A)$ was less negative than the *RT-term* in$\Delta G(eq.21A)$. Therefore, such a case could be represented as:

$$RTln\left(\frac{(a_{B(in\ Ni)})^{2/3}\cdot(a_{MgO\ (in\ slag)})}{(a_{Mg(in\ Ni)})\cdot(a_{B2O3\ (in\ slag)})^{1/3}}\right) > RTln\left(\frac{(a_{Si(in\ Ni)})\cdot(a_{MgO\ (in\ slag)})^{2}}{(a_{Mg(in\ Ni)})^{2}\cdot(a_{SiO2\ (in\ slag)})}\right)$$

The result of this condition on the Van't Hoff Isotherms for the reactions considered may be written as:

$$\Delta G(eq.13A) > \Delta G(eq.21A)$$

The average B and Si content of the alloys was found to be 4.96 and 14.97% respectively. The relatively high Si content of the alloys showed that the free energy change of the magnesiothermic reduction of $SiO_2$ (reaction (eq.21A) was more favourable than the $B_2O_3$ reaction (eq.13A), as proposed in the above expression. Since, B was recovered to the alloy; the above condition was not true throughout the whole process. Therefore, in addition to the reasons considered, it could be postulated that at lower temperatures, the B formation reaction was more feasible than the Si formation reaction. However since reaction temperatures rose rapidly; it was evident that $SiO_2$ reduction was favoured at higher reaction temperatures.

The magnesiothermic reduction of $SiO_2$ could yield a maximum possible 9.91% Si content of the alloy if all Mg reacted with $SiO_2$ and no B was formed. This would have required 2.01kg of $SiO_2$. However, the average Si content was higher than the maximum possible alloy Si content. Thus, the additional Si in the alloy was due to the aluminothermic reduction of $SiO_2$.

### 6.3.2 Impact of Excess Al on %B, %Al and %Si of the Alloy

The variation of Al from the stoichiometric requirement to 15% excess in the alumino-magnesiothermic reactions did not result in a target specification alloy. The maximum B content (4.53%) of the Al-variable experiments was obtained at 10% Al excess. There was no discernible trend of B content with respect to Al excess (as depicted in Figure 38).

The Al content of the alloys was found to be between 0.260 and 0.578% in the alumino-magnesiothermic experiments.

The low Al content of the alloys indicated that most of the input Al was oxidized. This has significant implications on reaction (eq.13B)'s Van't Hoff's Isotherm. It was assumed that Al obeys Rauolt's law in Ni. Thus the activity of Al in Ni was assumed to be proportional to the composition. The input $B_2O_3$ was fixed in Run No.12-15. It was also assumed that since input $B_2O_3$ was fixed, the $B_2O_3$ content of the slag did not vary significantly. The slag analysis results showed that the $B_2O_3$ mol fraction in slags for Run No. 12-15 varied between 18.00 and 21.90 mol %. Moreover it was assumed that Temkin's theory on slags was applicable.

According to Rauolt's law, increasing mol fraction of Al in Ni, would proportionally increase the $a_{Al(in\ Ni)}$. The increase in $a_{Al(in\ Ni)}$ in the $\Delta G(eq.13B)$ expression makes the $RT$-term more negative. This has the effect of making the overall $\Delta G(eq.13B)$ more negative. A

more negative $\Delta G(eq.13B)$ promoted the reaction (eq.13B) and consequently an increase in B recovery to the alloy. The alloy analysis results showed that increasing Al excess from 0% to 15%, and hence $a_{Al(in\ Ni)}$, increased the B content of the alloy from 3.47% and 4.21%, respectively. Contrarily, the minimum B content of the alloy (2.98%) was reported at 5% Al excess and the maximum B content was obtained at the 10% Al excess.

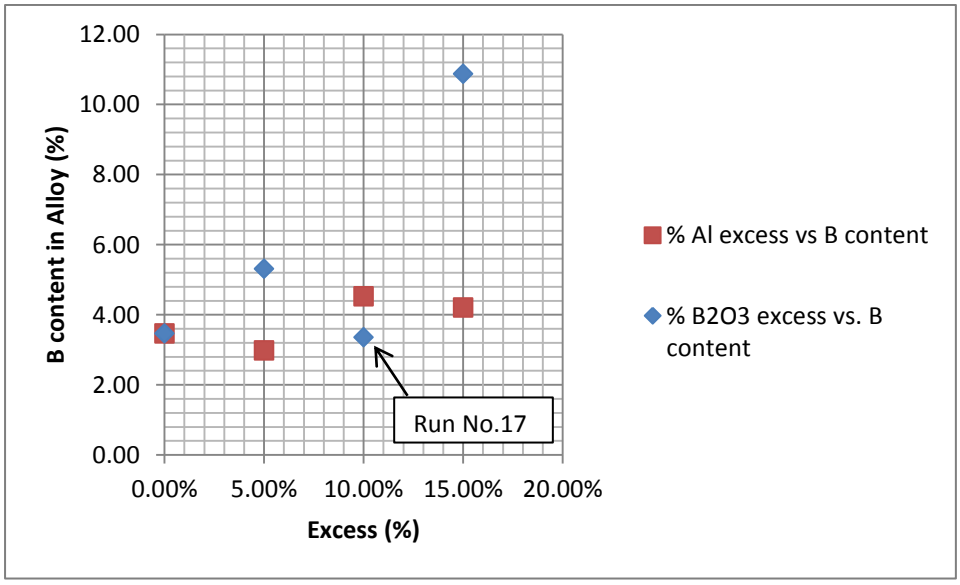


**Figure 38: Impact of Al and $B_2O_3$ Excess on %B in the alloy (alumino-magnesiothermic runs)**

The input Al used for $B_2O_3$ reduction was designed to yield a minimum of 10% alloy B content in an attempt to supplement the magnesiothermic reactions. However, relatively high Si content of the alloy was reported. As mentioned previously, the magnesiothermic reduction of $SiO_2$ could only produce 9.91% Si content of the alloy. Moreover, the input $SiO_2$ of (7.81kg) was 5.80kg in excess when compared the potential magnesiothermic reduction of silica.

From the stoichiometric level, the B content decreased with increasing excess up to 5% Al excess. Thereafter, the B content increased proportionally to the excess amount. Due to the proportionally lower input Al in the alumino-magnesiothermic reactions, the Al entrained in the alloys produced (Run No.12-18) was up to an order of magnitude lower than aluminothermic reactions.

The increase in Al excess had the effect of increasing Al content of the alloy because once all the reducible oxides are reduced, any excess or unreacted Al reported to the alloy. Due to input $B_2O_3$ and $SiO_2$ content being fixed for Al-variable experiments, the Al entrained in the alloy increased with increasing Al excess (Figure 39). Moreover, high Al excess did not significantly increase %B values in the alloy. Thus, operating at high Al excesses resulted in higher Al entrainment with insignificant increase in B yield. The results indicated that Al did not have a significant impact on the B recovery to warrant the potential Al contamination beyond 15% Al excess.

The D.C. arc furnace operation was found to be a quiescent operation. That is, after ignition, the liquid slag and metal phases remained well separated without any discernible turbulence and consequent mixing. Dynamic metal movement is typical in some A.C. arc furnace and coreless induction furnace processes. However this was not observed in the small-scale D.C. arc furnace used. The liquid metal phase did not display significant dynamic flow induced by the electrical current flow .This meant that the slag and metal phases did not adequately mix. Poor mixing of the liquid slag and metal phase typically results in slag metal interaction only at the interface. Since the interface area was limited by the top surface area of the metal pool, the slag metal reaction kinetics were likewise limited. This meant that extended residence time was required to establish slag metal equilibrium and eventually minimize the Al content of the alloy. The residence times for these experiments were fixed at fixed at 30 minutes. The high Al contamination of the alloy and relatively high $B_2O_3$ content of the slag indicated that the residence time selected was insufficient to establish equilibrium. This consequently yielded Al contamination.

The use of $SiO_2$ flux in the process introduced the Si into the alloy. The Si contamination has already been discussed with respect to the magnesiothermic reaction. Moreover, it was found that the amount of input $SiO_2$ in the process was in excess with respect to the same reaction. Moreover the relatively high Si content of the alloys indicated that the silica flux was reduced. This reduction reaction may be written as:

$$Al_{(in\ Ni)} + \frac{3}{4}SiO_{2(in\ slag)} = \frac{1}{2}Al_2O_{3_{(in\ slag)}} + \frac{3}{4}Si_{(in\ Ni)} \qquad \text{(eq.22)}$$

The free energy change of the aluminothermic reduction of $SiO_2$ is thus:

$$\Delta G(eq.22) = \Delta G°(eq.22) + RTln\left(\frac{(a_{Si(in\ Ni)})^{3/4} \cdot (a_{Al2O3(in\ slag)})^{1/2}}{(a_{Al(in\ Ni)})^2 \cdot (a_{SiO2\ (in\ slag)})^{3/4}}\right)$$

The increase in Al excess resulted in the increase in $a_{Al(in\ Ni)}$ (Rauolt's law). The corresponding effect would be a more negative *RT-term* and hence a more negative $\Delta G(eq.22)$ . A more negative $\Delta G(eq.22)$ would promote the consumption of Al.

The Al contamination in the alloy may be expressed as:

$$\frac{a_{Al\ (in\ Ni)}}{\left(a_{Si\ (in\ Ni)}\right)^{\frac{2}{3}}} = \frac{\exp\left(\frac{\Delta G°(eq.22)}{RT}\right)}{(a_{SiO2\ (in\ slag)})^{3/4}/(a_{Al2O3(in\ slag)})^{1/2}}$$

This expression suggested that increasing the $(a_{SiO2\ (in\ slag)})^{3/4}/(a_{Al2O3(in\ slag)})^{1/2}$ ratio decreases the $a_{Al\ (in\ Ni)}$ and hence the proportional decrease %Al in the alloy when Rauolt's law was obeyed in the alloy. But, when the required reactant oxide, $B_2O_3$ and or $SiO_2$,was completely consumed, increasing Al excess would result in the increase of Al contamination.

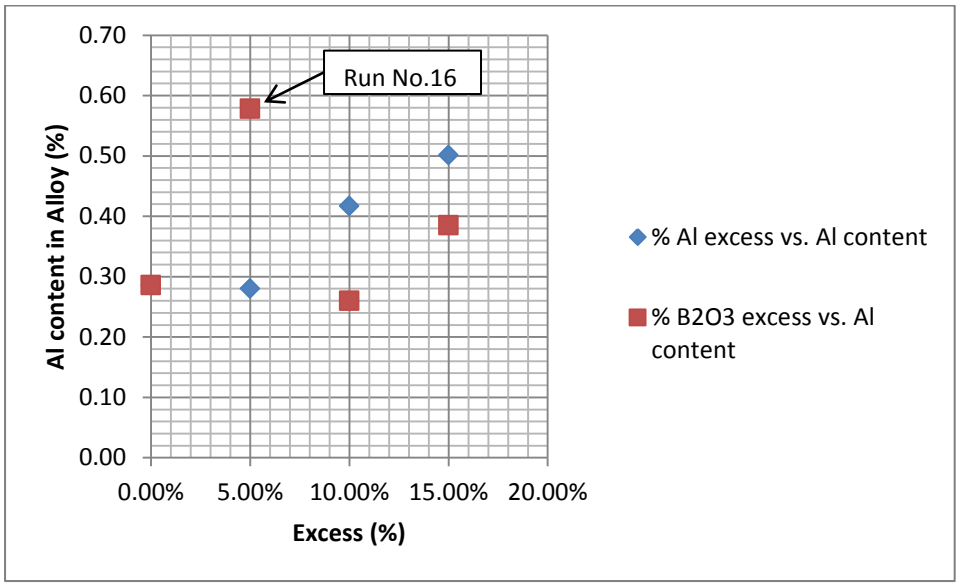


**Figure 39: Impact of Al and $B_2O_3$ Excess on %Al in the Alloy (Alumino-magnesiothermic Runs)**

However, the Al content of the alloys was found to be significantly lower than the Si content of the alloys. It was mentioned that Al contamination may be minimized by increasing $(a_{SiO2\ (in\ slag)})^{3/4}/(a_{Al2O3(in\ slag)})^{1/2}$ . The use of $SiO_2$ flux increased the mol fraction of $SiO_2$ in the slag as opposed to the non-use of $SiO_2$ flux. According to Temkin's theory, the resultant effect would was an increase in $a_{SiO2\ (in\ slag)}$. Increasing the $a_{SiO2\ (in\ slag)}$ thus increased the $(a_{SiO2\ (in\ slag)})^{3/4}/(a_{Al2O3(in\ slag)})^{1/2}$ ratio. The overall effect was a low Al content alloy. However it can be seen from reaction (eq.22) that minimizing Al content of the

alloy would result in increased Si production. The produced Si reported to and contaminated the alloy.

The Al excess considered resulted relatively high Si content of the alloys. However, the variance in Si content due to increasing Al excess was not significant. The maximum Si content of the alloy was obtained at the 5% Al excess level as depicted in Figure 40.

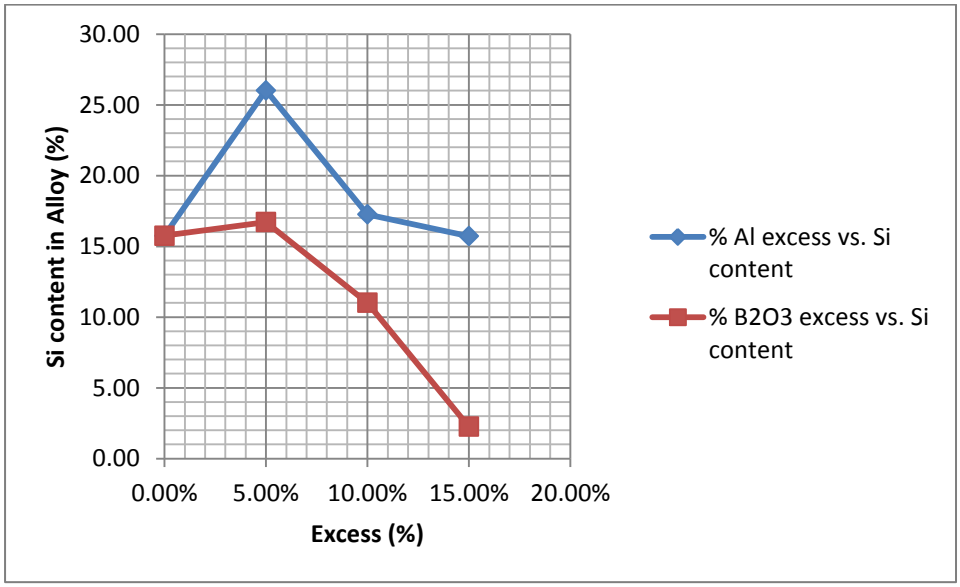


**Figure 40: Impact of Al and $B_2O_3$ excess on %Si content of alloy**

### 6.3.3 Impact of $B_2O_3$ Excess on %B, %Al and %Si of the Alloy

The maximum % B content (10.88%) of the alloy was obtained at 15% $B_2O_3$ excess. An increase in %B values was observed from the stoichiometric level up to 15% $B_2O_3$ excess, with the exception of a lower %B content of the alloy at the 10% $B_2O_3$ excess (Figure 38). The Fe content of Run No. 16 and 18 was reported to be 1.82% and 1.80%, respectively. Run No.17 Fe content was found to be 4.20%. The increased Fe content (as compared to Run No.16 and 18) indicated that Fe pick-up from the chill mold was higher during that particular run. Fe recovery to the produced alloy effectively diluted the poured alloy. This resulted in proportionally lower than anticipated amounts of alloying elements, including B. An increase in $B_2O_3$ excess was expected to increase the yield of B and lower %Al in the alloy. The 5% and 15% excess $B_2O_3$ reported values higher than the stoichiometric level (Figure 38). It was notable that the maximum alloy B content of these runs (No.16-18) was obtained at 15%

$B_2O_3$ excess. Furthermore, the Si content of this run was found to be the lowest at 2.26% (Table 23).

The impact of increasing $B_2O_3$ excess resulted in the Al content varying from 0.260% to 0.385%. This is tolerable due to unaccounted feed losses upon ignition. Therefore, some of the low density $B_2O_3$ powder was lost dust upon ignition. Efforts were taken to replicate ignition conditions as closely as possible; however, slight variations in attempting to strike an arc and differences in furnace burden density resulted in variations of the amount of remaining input materials upon ignition. Thus it was feasible that under violent or explosive ignition conditions the low density $B_2O_3$ may be blown off. This would result in lower available $B_2O_3$ for the reaction and thus consequently increasing the Al content above the required stoichiometry. Further some cross-contamination of experiments may occur due to insufficient cleaning of the furnace from products of previous experiments. The reaction products may affect the chemistry of the alloy produced in the subsequent experiments. Run No.15 used 15% excess Al. The remaining metallic products of this run posed a risk due to the high Al excess. It can be deduced from the anomalous result of 0.578% Al of the subsequent Run No. 16, (which was obtained at 5% $B_2O_3$) may be attributable to cross-contamination from the residual products of Run No.15 (Figure 39) .

The detrimental effect of adding $SiO_2$ flux to the process has been discussed. The impact of increasing $B_2O_3$ excess resulted in the subsequent decrease in Si content of the alloys (Figure 40). Additionally, the B content of the alloys peaked at 15% $B_2O_3$ excess (Figure 38).The observations made suggested that at high $B_2O_3$ excess, the activity of $B_2O_3$ increased. According to the Van't Hoff isotherm for the magnesiothermic and aluminothermic reduction of $B_2O_3$, $\Delta G(eq.13A)$ and $\Delta G(eq.13B)$, increasing $a_{B2O3\,(in\,slag)}$ makes the corresponding *RT-terms* more negative. Moreover, more negative *RT-terms* proportionally make the $\Delta G(eq.13A)$ and $\Delta G(eq.13B)$ more negative. The forward reactions of (eq.13A and eq.13B) would be promoted, and thus increasing the B yields to the alloy.

At the 15% $B_2O_3$ excess, the resultant increase in B content of the alloy indicated that the $SiO_2$ reduction reactions (eq.21A and eq.22) were becoming less favoured. This can be expressed as:

for the magnesiothermic reactions:

$$\Delta G(eq.13A) < \Delta G(eq.21A)$$

and for the aluminothermic reactions it may be written as:

$$\Delta G(eq.13B) < \Delta G(eq.22)$$

### 6.3.4 Fe Contamination

It was noted that the cast iron chill moulds used in the alumino-magnesiothermic experiments showed signs of erosion. This indicated that the Fe content of these alloys was attributable to the Fe from the chill moulds.

## 6.4 Practical Considerations

The experiments were undertaken at a production plant and data obtained from these experiments can be utilized in production and economic feasibility studies.

### 6.4.1 Ni Recovery (Aluminothermic Process)

Post the 2008 financial crisis, the Ni price fluctuated between 13-25 US$/kg. The pricing of Ni therefore required careful metal accounting. Also, even if the required chemical specification of the alloy was not reached, the recovery of metal was critical due to the high Ni content. Therefore, the relationship between the reactant % excess and Ni recovered was fundamental for economic considerations.

As depicted, the trends described by the graphs show a successive increase in Ni recovery with increase in excess amounts. The Ni recovery peaked at 10% excess in both the Al and $B_2O_3$ variable experiments. Similarly, the Ni recovery decreased with increasing excess amounts after the 10% excess level. The 10% excess is shown to be the most optimum operating parameter for increased Ni recovery (Figure 41). Across the percentage excess range under consideration, the Al variable experiments (Run No, 2-4) had higher Ni recovery than the $B_2O_3$ variable experiments (Run No.5-7).

Although the 10% excess resulted in the highest Ni recovery, the results can be assumed optimum when the B content of the alloy is maximized at that particular percentage excess.

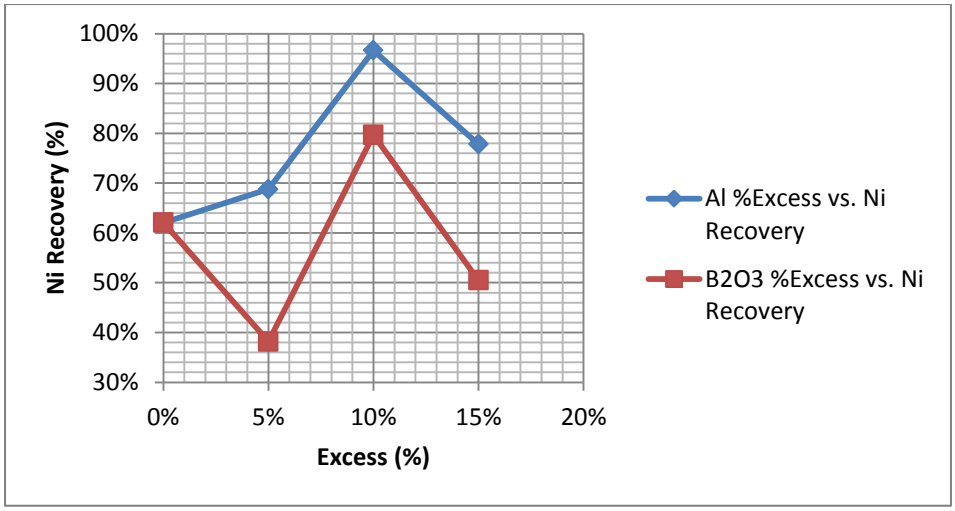


**Figure 41 : Impact excess on Ni recovery in aluminothermic processes**

### 6.4.2 Ni Recovery (Magnesiothermic)

The alloys produced in the magnesiothermic showed increased recovery with increased Mg excess. Since maximum B content was obtained at 5%Mg excess, financial calculations would need to be investigated to determine the cost trade-off between B recovery and Ni recovery.

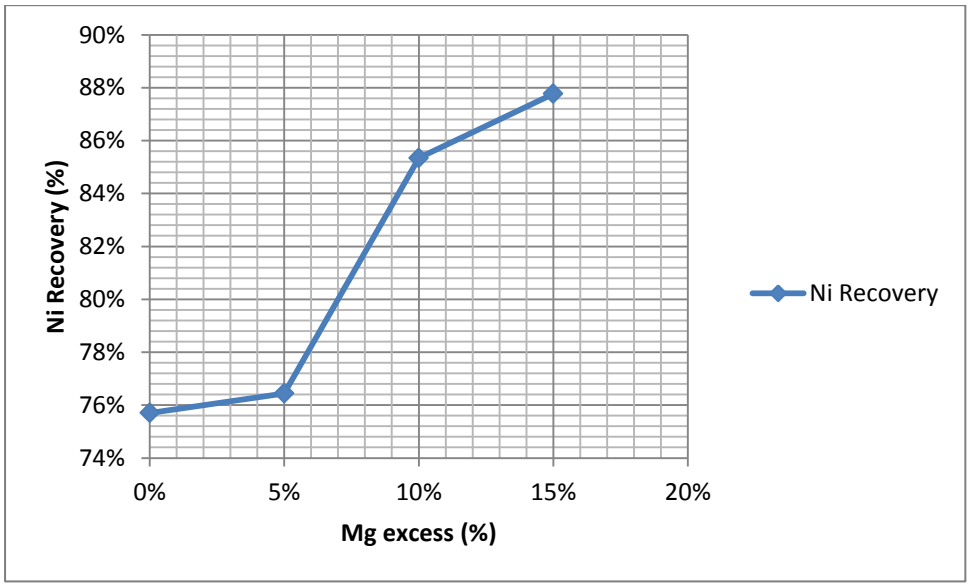


**Figure 42: Ni recovery dependence on Mg excess**

### 6.4.3 Ni Recovery (Alumino-magnesiothermic Process)

The consideration of recovery of Ni is important. Given that NiB contains approximately 85% of high value Ni, even off specification alloys are of relatively high value. Increasing the

excess amounts of Al resulted in a sharp decline in Ni recovery. The Ni recovery dropped from 99% at the stoichiometric level, as the Al excess was increased (Figure 43).

The impact of $B_2O_3$ excess was less drastic in comparison to the Al-variable experiments. Apart from the 10% excess $B_2O_3$ level, the Ni recovery was relatively constant. The 10% excess $B_2O_3$ stoichiometry level reported the highest Ni recovery at 82%.

Beyond the 10% excess level, a decreasing Ni recovery trend was observed for both Al- and $B_2O_3$-variable experiments

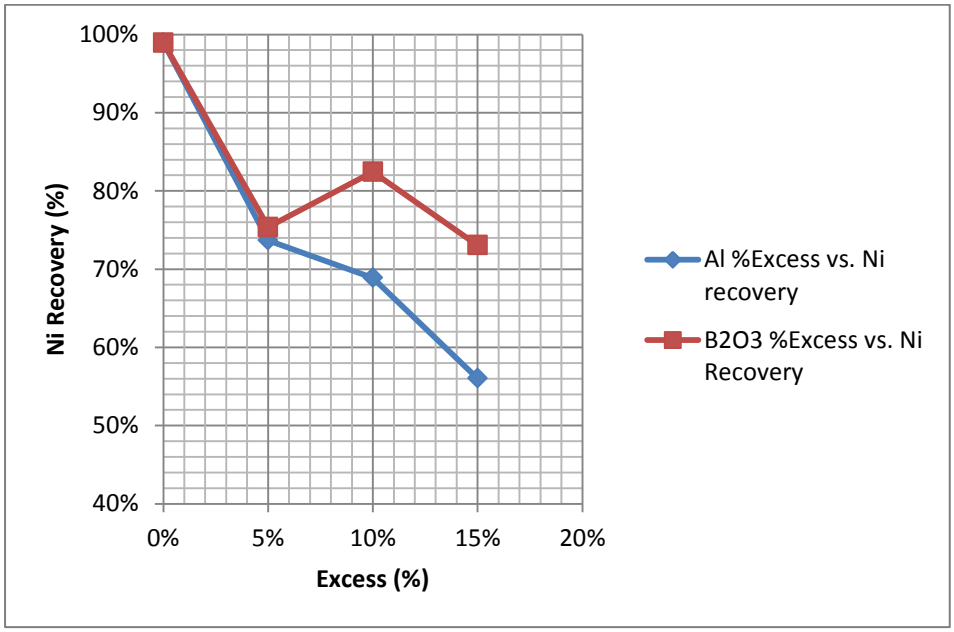


**Figure 43: Impact of excess on Ni recovery in alumino-magnesiothermic experiments**

### 6.4.4 Hazards Associated with Pyrometallurgical Experiments

Metallothermic reduction reaction kinetics are generally increased with the use of high surface area reactants. Thus the reactants were all powder/fines form with particle size less than 2mm with the exception of the Mg chips. The high surface area presents handling

hazards, as Ca, Mg and to a lesser extent Al and Si, will readily react with water or water vapour. When Ca and Mg react with moisture or water, the products include highly flammable hydrogen gas. Ca, Mg and Si present potential fire hazards. The oxidation of Al in contrast to Ca and Mg forms a passivating $Al_2O_3$ layer, therefore preventing further oxidation. This film reduces the Al reactivity and thus the likelihood of ignition, but it is noteworthy that in powder form it poses similar hazards as the other reductants under consideration.

### 6.4.5 Temperature Hazards

Pyrometallurgical experiments are inherently hazardous. Due to high temperatures reached, run-away reaction resulting in excessive heat generation can cause furnace burn-through. This occurs when the furnace contents are superheated to sufficiently high temperature to cause the lining to fail and material to breach the furnace shell.

Because of these risks, it is important to determine the final species formed and their tapping temperature. This also allows for proper planning for downstream materials handling processes.

The heat and material balance also yields information on whether additional heat or cooling is required for the system to ensure safe and effective operating conditions.

### 6.4.6 Additional Heat for Self-propagation

The aluminothermic reduction reaction (eq.9) requires additional energy for self-propagation. There are various methods to provide additional heat energy. Common practice includes using auxiliary chemical reactions producing high heat output, commonly known as booster reactions, and pre-heating of reactants pre-ignition. Hall (27) that the latter is less favoured as it presents a challenge to pre-heat generally low thermal conductivity charge. Also, premature ignition of the preheated charge presents a significant safety hazard.

As mentioned earlier, the NiB production charge was made up of reactants of powder $B_2O_3$ and less than 2mm discrete metallic particles except for the Mg chips. The charge was well mixed, resulting in well distributed high thermal conductivity metallics among the low thermal conductivity $B_2O_3$ matrix; and therefore the overall thermal conductivity of the charge was low.

The use of booster chemical reactions mitigates most of the hazards involved with charge pre-heating. Additionally, booster chemical reactants can be more economical than pre-heating of reactants. It is advantageous to use a booster reaction that does not affect the chemical specification of the final alloy. For example, in the aluminothermic production of Ferro-vanadium (FeV) from $V_2O_3$, the aluminothermic reduction of $V_2O_5$ is used as a booster reaction.

Booster reactants such as potassium perchlorate, sodium nitrates, barium oxide and sodium and potassium chromates and other highly reactive compounds are common. The products of these reactants can contaminate the produced alloy. Also; in the case of some chromates they are highly toxic.

# 7 CONCLUSION

The production of NiB by the aluminothermic, magnesiothermic and alumino-magnesiothermic reduction of $B_2O_3$ is an exothermic process. The use of Al and Mg as reductants promoted the feasibility of $B_2O_3$ reduction. The use of dissolved Mg in NiMg minimized the volatility of Mg at high temperatures. It was the objective of this investigation to determine the thermodynamic possibility of the reduction process by plotting an Ellingham diagram. It was shown that the Al and Mg can reduce $B_2O_3$ according to the Ellingham Diagram.

It was also required to determine if the reactions were autothermic. The heat requirement guideline purported that the aluminothermic and alumino-magnesiothermic processes were not likely to be autothermic. In contrast, the magnesiothermic experiments were calculated to be autothermic; however that was not the case in practice.

## 7.1 Results of the Aluminothermic Experiments

In order to convert the non-autothermic aluminothermic experiments to provide fluid metal and slag supplementary energy from the furnace was required. This enabled good metal and slag separation.

The alloys produced by the aluminothermic process contained less than 15% B content which was the required specification. In order to increase the B content of the final alloy, Al excess was increased proportionally. This resulted in higher Al content in the metal. Increasing B content in the alloy required that some $B_2O_3$ be allowed to pass to the slag. This consequently increased the proportion of $B_2O_3$ in the slag. As compared to the variation of Al excess, it was observed that increasing $B_2O_3$ excess resulted in proportionally higher B yield. Moreover such an increase in $B_2O_3$ excess reduced the Al content of the alloy.

It can be suggested that the low %B and high Al contamination in the alloy was due to a number of factors. These could have included insufficient reaction time to maximize reductant and oxide interaction. Also, the high temperatures achieved could have promoted $B_2O_3$ volatilization and $B_2O_3$ losses to fume. Therefore; temperature-time interrelation of the aluminothermic production of NiB could be important.

Additionally, the furnace design and charge burden should promote the reaction of volatilized $B_2O_3$ or its gaseous sub-oxides with Al.

In the aluminothermic reactions (Run No.1-7), it was determined that lime (CaO) had a significant fluxing impact on alumina ($Al_2O_3$). Therefore metallurgical lime was chosen as flux for the aluminothermic production of NiB experiments. The lime requirement was adjusted to form an $Al_2O_3$-CaO eutectic. Contrarily, the basic lime also reduced the activity of acidic $B_2O_3$ in the slag and locked $B_2O_3$ in the slag. This resulted in poor B recovery to the alloy. Moreover, the resultant low activity of $B_2O_3$ contributed to the significant Al contamination of the alloy. The maximum B content of these runs (7.59% B) was obtained at 15% $B_2O_3$ excess.

The results presented showed that the aluminothermic production of NiB would require high $B_2O_3$ excesses to fully utilize the remaining Al. Increasing the reaction time may also contribute in improving B yields. Furthermore, increased experimental scale may allow for furnace burden design and thus improve B yields.

## 7.2 Results of the Magnesiothermic Experiments

Additional input $B_2O_3$ was used as flux in the magnesiothermic experiments. (Run No.8-11). Relatively clean alloys were produced however not to the required B specification. The slags invariably contained high levels of expensive $B_2O_3$. The maximum B content of the alloys in these runs was reported to be 11.82% corresponding to Run No.11.

A significant proportion of Mg chips flared during the reactions. This flaring resulted in the loss of Mg as MgO to fume.

## 7.3 Results of Alumino-magnesiothermic Experiments

The 1.0kg alloy and 10.0kg metal producing experiments of the alumino-magnesiothermic reduction proved that the reactions were not autothermic. When compared to the general hematite thermite, poor slag metal separation was observed in the 1.0kg alloy producing alumino-magnesiothermic experiment. The slag produced through the alumino-magnesiothermic ($Al_2O_3$-MgO) was a high temperature slag. From the small-scale experiments, it was evident that fluxes for $Al_2O_3$-MgO slags were required to improve slag metal separation.

The binary slag phase diagram of the $Al_2O_3$-MgO system showed that the slag produced by the alumino-magnesiothermic production of NiB would fall in the spinel region. Relatively inexpensive and available silica ($SiO_2$) was selected as a flux for the alumino-magnesiothermic experiments. The cordierite region of the $Al_2O_3$-MgO-$SiO_2$ ternary liquidus slag phase diagram was selected for the alumino-magnesiothermic production of NiB. The use of $SiO_2$ flux introduced unexpected Si contamination due to the preferential reduction of $SiO_2$ at high temperatures

The low Mg and Al content of the alloys produced indicated that Mg and Al utilization was high. Notwithstanding the aforesaid, the target alloy B specification was not achieved. The maximum %B content of the alloy was reported at 10.88% corresponding to 15%$B_2O_3$ excess.

The produced alloys were highly contaminated with Si; up to 26.02% Si was reported. The high Si contamination was due to excessive reduction of $SiO_2$ flux. The use of $SiO_2$ flux minimized the activity of $B_2O_3$ in the slag. This resulted in B loss to the slag. Furthermore, $SiO_2$ addition to the process increased the activity of $SiO_2$ in the slag and hence and increase in Si contamination of the alloy.

In this system, B yields were improved at high $B_2O_3$ excess with the resultant decrease in Si contamination.

Out of the two variables Al and $B_2O_3$, both the aluminothermic and alumino-magnesiothermic experiments proved that $B_2O_3$ excess resulted in higher B contents of the alloys.

The objective of this work was to determine the possible pyrometallurgical process route for NiB production. Due to the overall low B recovery in the experiments, the possible pyrometallurgical production of NiB would require high $B_2O_3$ excess and chemically inert fluxes. Moreover, high purity input materials should be used so as to mitigate contamination risks.

The small-scale 200KVA D.C. arc furnace was found to be suitable for pilot-scale production.

# 8 RECOMMENDATIONS

The research highlighted that the production of NiB by the aluminothermic, magnesiothermic and alumino-magnesiothermic processes requires careful control of reactant species, fluxes and furnace environment.

- The chemical specification of NiB master alloy requires that higher purity raw materials should be used to minimize contamination of the alloy.
- In the aluminothermic experiments, an $Al_2O_3$ flux that does not reduce the activity of $B_2O_3$ needs to be investigated.
- In the magnesiothermic experiments, it would be necessary to use alloyed Mg in an attempt to mitigate Mg flaring and maximum the magnesiothermic reduction of $B_2O_3$.
- Alumino-magnesiothermic reaction kinetics should be studied in order to promote B formation and suppress $SiO_2$ reduction.
- It was evident from the results of the alumino-magnesiothermic production process that $SiO_2$ and $B_2O_3$ reaction competition was high, resulting in Si contamination. An inert $Al_2O_3$-MgO flux should be investigated in order to mitigate Si contamination.
- Inert chill moulds should be used to minimize alloy contamination.
- An alternative furnace bottom material would need to be investigated in order to minimize introduction of ash into the system.

# 9 REFERENCES


1. **Baudis, U and Fichte, R.** Boron and Boron Alloys. *Ullmann's Encyclopeadia of Industrial Chemistry.* 2000, pp. 281-293.
2. **Liao, P K and Spear, K E.** B-Ni. [ed.] H Baker. *ASM Handbook Alloy Phase Diagrams.* Ohio, USA : ASM International, 1992, p. 83.
3. **Massachusetts Institute of Technology .** MIT. [Online] 2014. [Cited: 27 08 2014.] http://web.mit.edu/2.813/www/readings/Ellingham_diagrams.pdf.
4. **Communication, Private.** 2011.
5. **Enviromental Protection Agency, USA.** EPA. [Online] 2014. [Cited: 28 08 2014.] http://www.epa.gov/ttnchie1/ap42/ch12/final/c12s04.pdf.
6. **Goel, R.P.** *Thermodynamic Considerations in the Production of Bulk Ferro Alloys (Fe-Mn, Fe-Cr and Fe-Si).* Jamedepur : National Metallurgical Library, 1994.
7. *Oxidation Behaviour of Boron Carbide Powder.* **Li, Y.Q. and Qui, T.** 444, 2007, Materials Science and Engineering A, pp. 184-191.
8. **Tasyurek K, Alkan M, Yucel O.** *Development of NiCkel Boron Alloys for Brazing Materials.* Instanbul Technical University, Faculty of Chemical and Metallurgical Engineering. Istanbul : The Minerals, Metals &Materials Society, 2013.
9. *Mechanism of Ferroboron Formation in a DC Electric Arc Furnace.* **Yucel, O., et al., et al.** Trondheim, Norway : FFF, 1995. Vol. 7, pp. 647-654.
10. *Activity of Boron in Ni-B-C Melts Saturated with Carbon.* **Yukinobo, M., Ogawa, O. and S.Goto.** 1990, Metallurgical Transactions B, Vol. 21, pp. 791-793.
11. **Lamoreaux, R.H., Hildebrand, D.L. and Brewer, L.** Oxides of Be,Mg,Ca,Sr,Ba,B,Al,Ga,In,Tl,Si,Ge,Sn,Pb,Zn,Cd and Hg. *High Temperature Vaporization Behavior of Oxides II.* 28 November 1986, pp. 420-443.
12. **Dautzenberg, W.** *Metallurgie der Ferrolegierungen.* [ed.] R Durrer. 2nd. New York : Springer Verlag,Berlin-Gottingen-HHeidelberg, 1972.
13. **Gupta, C K and Krishnamurthy, N.** Extractive Metallurgy of Vanadium. *Process Metallurgy.* 8, 1992, pp. 475-500.
14. *The Preparation of Chromium Metal by a Sealed, Cold-Hearth, Plasma-Assisted Aluminothermic Method.* **Nelson, L.R.** 1996, The Journal of The South African Institute of Mining and Metallurgy, pp. 135-144.
15. *The Aluminothermic Production of Extra Low Carbon Ferrochromium from Low Grade Chromite Ore.* **Eissa, M.M., et al., et al.** Helsinki : International Ferroalloys Congress, 2010.
16. **Alcock, C.B.** *Principles of Pyrometallurgy.* London : Academic Press, 1976.
17. *Preparation of NiB allloys from spent NiAl catalysts by induction furnace.* **Zhan-Gou, F and Chang-ye, L.** 436, 2007, Journal of Alloys and Compounds, pp. 178-180.
18. **Andrieux, J L, Grenoble and Peffen, R.** *Aluminothermic process of making Boron, Boron compounds and alloys.* 1956. Patent 3016288.
19. **Nash, P, Singleton, M F and Murray, J L.** Al-Ni. [ed.] H Baker. *ASM Handbook Alloy Phase Diagram.* Ohio, USA : ASM International , 1991, p. 49.
20. **Factsage.** Factsage. [Online] 2014. [Cited: 23 January 2014.] http://www.crct.polymtl.ca/fact/documentation/TDNucl/B-O.jpg.
21. **Nayeb-Hashemi, A A and Clark, J B.** Mg-Ni. [ed.] H Baker. *ASM Handbook Alloy Phase Diagram.* Ohio, USA : ASM International, 1992, p. 281.
22. **Murray, J L.** Al-Mg. [ed.] Baker H. *ASM Handbook Alloy Phase Diagrams.* Ohio, USA : ASM International, 1992, p. 49.

23. **Wriedt, et al., et al.** Al-O. [ed.] Verein Deutscher Eisenhuttenleute. *Slag Atlas.* 2nd. Dusseldorf,Germany : Verlag Stahleisen GmbH, 1995, p. 30.
24. **Wriedt, et al., et al.** Mg-O. [ed.] Verein Deutscher Eisenhuttenleute. *Slag Atlas.* 2nd. Dusseldorf, Germany : Verlag Stahleisen GmbH, 1995, p. 34.
25. **Neumann J, P, Zhong, T and Chang, Y,A.** Ni-O. [ed.] H Baker. *Alloy Phase Diagram.* Ohio, USA : ASM International, 1992, p. 312.
26. **Factsage.** B-O. [Online] 2014. [Cited: 21 January 2014.] http://www.crct.polymtl.ca/fact/documentation/TDNucl/B-O.jpg.
27. **Hall, W F.** Aluminothermic Processes. [ed.] F Ullmann. *Ullman's Encyclopedia of Industrial Processes.* Rotherham,UK : Wiley-VCH, 2000, pp. 447-457.
28. **Klug, et al., et al.** Al2O3-SiO2. [ed.] Verein Deutscher Eisenhuttenleute. *Slag Atlas.* Dusseldorf,Germany : Verlag Stahleisen GmbH, 1995, p. 47.
29. **Factsage TM.** FACT oxide database. [Online] 2010. [Cited: 1 August 2013.] http://www.crct.polymtl.ca/FACT/phase_diagram.php?file=Al-B-O_B2O3-Al2O3.jpg&dir=FToxid.
30. **Schafer, U L and Kuzel, H I.** Al2O3-B2O3-CaO. [ed.] Verein Deutscher Eisenhuttenleute. *Slag Atlas.* 2nd. Dusseldorf, Germany : Verlag Stahleisen GmbH, 1995, p. 99.
31. **Gielisse, P J and Foster, W R.** Al2O3-B2O3-SiO2. [ed.] Verein Deutscher Eisenhuttenleute. *Slag Atlas.* 2nd. Dusseldorf,Germany : Verlag Stahleisen GmbH, 1995, p. 99.
32. **Miyaga, S., Mirano, S. and S.Somiya.** B2O3-MgO. *Slag Atlas.* Dusseldorf : Verlag Stahleisen GmbH, 1995.
33. **Rankin, Merwin and Alper.** Al2O3-MgO. [ed.] Verein Deutscher Eisebhuttenleute. *Slag Atlas.* 2nd. Dusseldorf,Germany : Verlag Stahleisen GmbH, 1995, p. 44.
34. *Vitrification and devitrification phenomena in the ternary MgO-Al2O3-B2O3 system.* **Esmat, M A, Hamzawy and Darwish, H.** 34, 2008, Ceramics International, pp. 1965-1969.
*35. **Kiss, S, J, Kostic, E and Boskovic, S.** The influence of B2O3 on spinel formation in the Al2O3-MgO-B2O3 system. *Science of Ceramics.* 23-30 June 1984, Vol. 12, pp. 195-199.
36. *Synthesis and properties of flux-cast refractories in the Al2O3-MgO-B2O3 sytem.* **Sokolov, V,A, et al., et al.** 2, 2008, Refractories and Industrial Ceramics, Vol. 49, pp. 161-163.
37. **Rankin, et al., et al.** Al2O3-CaO-MgO. [ed.] Verein Deutscher Eisenhuttenleute. *Slag Atlas.* 2nd. Dusseldorf,Germany : Verlag Stahleisen GmbH, 1995, p. 104.
38. **Osborn, E F and Maun, A.** Al2O3-MgO-SiO2. [ed.] Verein Deutscher Eisenhuttenleute. *Slag Atlas.* 2nd. Dusseldorf, Germany : Verlag Stahleisen GmbH, 1995, p. 113.
39. **Schoukens, A.** Metallurgical Design. *Lecture Notes* . 2009.
40. **Turkdogan, E.T.** *Physical Chemistry of High Temperature Technology.* Monroeville : Academic Press, 1980. ISBN 012704650X.
41. **Gupta, C.K.** *Chemical Metallurgy: Principles and Practice.* Weinheim : Wiley VCH Verkag GmbH &Co., 2003. 3527303766.
42. **Moore, J.J.** *Chemical Metallurgy 2nd Edition.* Bodmin, Cornwall : Butterworth Heinemann Ltd, 1990. 0750616466.
43. **Factsage TM.** Factoxid Database. [Online] 2010. [Cited: 1 8 2013.] http://www.crct.polymtl.ca/fact../phase_diagram.php?file=Al-Mg-O_MgO-Al2O3.jpg&dir=FToxid.

# APPENDIX

## Raw Material Chemical Analyses

The chemical analyses of the $B_2O_3$ and Particle Size Distribution

| Compound | Typical Analysis (%) |
|---|---|
| $B_2O_3$ | 98.8 min. |
| $SiO_2$ | 0.1 max. |
| Na | 0.02 max. |
| $Al_2O_3$ | 0.005 max. |
| $Fe_2O_3$ | 0.005 max. |
| CaO | 0.01 max. |

$B_2O_3$ PSD

| mesh | μm | % Passing |
|---|---|---|
| 30 | 600 | 0-0 |
| 50 | 300 | 0-20 |
| 100 | 150 | 50-80 |
| 200 | 75 | X |
| 270 | 53 | X |
| PAN(retained value) | | 1-10 |

Typical chemical analyses of Al used.

| Element | Typical Analysis (%) |
|---|---|
| Al | min.96 |
| Cu | 1.0 max |
| Mg | 1.0 max |
| Fe | <0.25 |
| Si | <0.2 |
| Zn | 1.0 max |

Al Powder PSD

| Size (μm) | % Retained (Cumulative) |
|---|---|
| +425 | 0-5 |
| +180 | 10-35 |
| +90 | 45-80 |
| +45 | 75-95 |

Ni used was from London Metal Exchange Deliverable Grade

| **Elements** | **Analysis (%)** |
|---|---|
| Ni | 99.9 |
| Cu | 0.001 |
| Fe | 0.007 |
| Co | 0.07 |
| Pb | <0.0009 |
| As | 0.0002 |
| Bi | 0.0003 |
| Sb | 0.0004 |
| Sn | <0.001 |
| Si | 0.0001 |
| Zn | 0.001 |
| P | 0.0004 |
| Mn | 0.0009 |
| S | 0.003 |
| C | 0.012 |

The chemical analysis of the NiMg alloy

| **Elements** | **Analysis (%)** |
|---|---|
| Ni | balance |
| Mg | 16.14 |
| Si | 0.014 |
| C | 0.012 |
| Fe | 0.038 |
| Cu | 0.005 |
| Al | 0.002 |

Mg supplier specification analysis

| **Element** | **%** |
|---|---|
| Mg | 99.98 |
| Ca | 0.0028 |
| Cl | 0.003 |
| Sn | 0.01 |

Typical chemical analysis of CaO

| **Compound** | **Typical Analysis (%)** |
|---|---|
| CaO | 92 min |
| MgO | 7 max. |
| $Fe_2O_3$ | 2.0 max. |
| MnO | 0.4 max. |
| $TiO_2$ | 0.2 max. |
| $SiO_2$ | 2.0 max. |

CaO PSD

| Size (μm) | % Retained |
|---|---|
| 2000 | 0 |
| 1000 | 60 |
| 500 | 18 |
| 250 | 9 |
| 150 | 5 |
| -150 | 8 |

Silica Flux Typical analysis

| **Compound** | **Typical Analysis (%)** |
|---|---|
| $SiO_2$ | 99.4 |
| $Al_2O_3$ | 0.5 |
| $Fe_2O_3$ | 0.05 |

$SiO_2$ PSD

| Size (μm) | % Retained |
|---|---|
| 1700 | 3.4 |
| 1400 | 7.18 |
| 1000 | 30.7 |
| 710 | 73.76 |
| 425 | 97.91 |
| 125 | 99.89 |
| PAN | 100 |